

Dissertation

Microsystems for particle analysis

ausgeführt zum Zwecke der Erlangung des akademischen
Grades eines Doktors der technischen Wissenschaften

eingereicht an der Technischen Universität Wien
Fakultät für Elektrotechnik und Informationstechnik
von

Dipl.Ing. Jeroen H. Nieuwenhuis
23. 07. 1977, Bergen op Zoom

begutachtet von

Prof. M.J. Vellekoop
Prof. P. Telleman

Wien, am 28. Jänner 2005

.....

Kurzfassung

Die vorliegende Arbeit beschreibt die Entwicklung von vier neuartigen Mikrosystemen zur Analyse von Kleinstpartikeln mit Durchmessern zwischen 5 und 50 μm . Die Mikrosysteme wurden konzipiert um spezifische, im Mikrometerbereich auftretende physikalische Effekte zu nutzen. Zur Herstellung der auf der Plattform Silizium-Glas basierenden Systeme wurden Standard-IC-Technologien eingesetzt.

Um die zu analysierende Probenflüssigkeit den Sensoren zuverlässig und reproduzierbar zuführen zu können, wurden zwei integrierte Durchflusszellen entwickelt. Diese Durchflusszellen ermöglichen sowohl die Generierung einer koaxialen als auch einer nicht-koaxialen Schichtströmung. Voneinander unabhängige Steuerungsmechanismen erlauben dadurch die adaptive Einstellung des Probenflusses bezüglich räumlicher Ausdehnung und Position und bieten somit die Möglichkeit das Strömungsprofil für den entsprechenden Sensortyp zu optimieren. Aufgrund des relativ einfachen Herstellungsprozesses können die konzipierten Durchflusszellen problemlos mit anderen Mikrosystemen kombiniert werden.

Um die praktische Funktionsweise zu verifizieren, wurde mit einer der beiden Durchflusszellen eine Reihe von Messungen durchgeführt. Die Gegenüberstellung der Simulationsresultate mit den experimentell ermittelten Daten zeigt, dass die Durchflusszellen mit hoher Genauigkeit modelliert werden können. Die Steuerungsmechanismen mit deren Hilfe die räumliche Ausdehnung des Probenflusses eingestellt werden kann funktionieren gut und ermöglichen die Variation des Probenflusses über einen großen Bereich. Diese Steuerungsmechanismen sorgen dafür, dass die Durchflusszellen auch für alternative Anwendungen wie beispielsweise Probenteilung oder -umlenkung eingesetzt werden können, was deren vielseitigen Charakter beweist.

Um die Größe von Partikeln erfassen zu können wurde ein integrierter 'Coulter Counter' entwickelt. Das System besteht aus einer Durchflusszelle in der mit Hilfe einer elektrisch leitfähigen Probenflüssigkeit und einer nicht-leitfähigen Flüssigkeit, welche erstere umschließt, eine flüssige Apertur gebildet wird. Im Gegensatz zur klassischen fixen Apertur zeichnet sich die flüssige Apertur durch zwei entscheidende Vorteile aus: Durch die Entkopplung der elektrischen Größe der Coulter-Apertur von den physikalischen Ausdehnung des Flüssigkeitskanals weist das System eine deutlich höhere Empfindlichkeit verglichen mit dem traditionellen 'Coulter Counter' auf. Als weiteren Vorteil ermöglicht der entwickelte 'Coulter Counter' die dynamische Veränderung der (flüssigen) Apertur ohne das Austauschen mechanischer Komponenten. Aus diesem Grund kann das System zur Größenerfassung von Partikeln in einem verhältnismäßig breiten Bereich eingesetzt werden.

Experimentelle Untersuchungen zeigen, dass der entwickelte 'Coulter Counter' Partikel die um 20% im Durchmesser voneinander abweichen deutlich unterscheiden kann. Die Messergebnisse stimmen gut mit den Spezifikationen der Partikel überein, was das Potential des Systems für die quantitative Größenanalyse aufzeigt. Wie auch beim konventionellen 'Coulter Counter' können sowohl elektrisch leitfähige als auch elektrisch nicht-leitfähige Partikel detektiert werden.

Um einerseits die Form von Mikropartikeln bestimmen zu können und andererseits Informationen über deren optische Eigenschaften zu gewinnen wurde ein Projektions-Zytometer konzipiert. Durch die Integration des optischen Sensors in den transparenten Strömungskanal ergibt sich ein extrem kleiner Projektionsabstand. Dies hat zur Folge, dass das Nahfeld der optischen Projektion ohne den Einsatz von Linsen oder anderen optischen Komponenten erfasst werden kann.

Zu diesem Zweck wurden zwei, sich hinsichtlich Einsatzflexibilität und Benutzerfreundlichkeit deutlich unterscheidende, optische Sensoren eingesetzt: ein 'Array-Sensor' und ein 'Linien-Sensor'. Quasi-statische Messungen zeigen, dass beide Sensortypen in der Lage sind, ein hochpräzises Bild eines Miniatur-Objektes zu erfassen. Mit Hilfe eines auf einem 'Linien-Sensor' basierenden integrierten Projektions-Zytometer konnten zwei verschiedene Arten von Partikeln vergleichbarer Größe anhand der optischen Eigenschaften deutlich voneinander unterschieden werden. Darüber hinaus zeigen die Messergebnisse nicht nur zusätzliche optische Details der Partikel, sondern weisen auch eine hohe Wiederholgenauigkeit auf.

Als viertes und letztes Mikrosystem, das im Rahmen der vorliegenden Arbeit konzipiert wurde, wurde ein Aktuator zur Sortierung von Partikeln entwickelt. Ziel war es, einen Durchfluss-Sortierer zu entwickeln, der Partikel abhängig von bestimmten Eigenschaften in einen definierten Kanalzweig lenkt. Die entwickelte Sortiereinheit basiert auf einem elektrischen Aktuationsprinzip – der so genannten Dielektrophorese. Dies hat den Vorteil, dass ein solches System problemlos mit anderen Mikrosystemen kombiniert werden kann.

Im Rahmen der Designoptimierung wurde die Elektrodenkonfiguration in einer zweidimensionalen Fläche orthogonal zur Flußrichtung analysiert. Eine qualitative Analyse, die durch eine komplette Simulation des Systems bestätigt wurde, resultierte in der Erkenntnis, dass Sortierer mit Elektroden auf gegenüberliegenden Seiten des Kanals eine deutlich höhere Leistung aufweisen verglichen mit Sortierern, die lediglich Elektroden auf einer Seite des Kanals aufweisen.

In einem weiteren Optimierungsschritt wurden zwei neue Elektrodenanordnungen erarbeitet: die 'Switching Electrode Topology' und die 'Focusing Electrode Topology' die jeweils für maximale Durchflussgeschwindigkeit beziehungsweise maximale Umschaltgeschwindigkeit optimiert wurden. Darüber hinaus konnte anhand eines Sortier-Systems mit 3 Kanalzweigen gezeigt werden, dass durch die Erhöhung der Anzahl der Kanalzweige die Leistung deutlich gesteigert werden kann. Verglichen mit klassischen Systemen weisen die optimierten Sortierer einen Leistungsanstieg von mehr als 200% auf, wobei sogar Potential für weitere Verbesserungen detektiert wurde.

Abgeschlossen wird die vorliegende Arbeit durch einen Ausblick, in dem viel versprechende Ideen für zukünftige Forschungsaspekte kurz diskutiert werden.

Summary

This thesis discusses the development of four new microsystems for the analysis of small particles (diameter 5-50 μm). The microsystems have been designed to take advantage of the unique physics found at the micro-scale. IC-technology has been used to fabricate the microsystems on a common silicon-glass platform.

Two integrated flow cells have been developed to create a flow profile that transports the sample to the sensors in a reliable and reproducible manner. The flow cells can be used to create non-coaxial and coaxial sheath flows. Orthogonal control mechanisms allow to control the dimensions and the position of the sample flow, so that the flow profile can be optimised to the type of sensors. The fabrication of the flow cells is very simple, so that they can be easily integrated with other microsystems.

Experiments have been carried out with one of the flow cells and a comparison of the experimental results with simulation results shows that the flow cell can be modelled very accurately. The mechanisms to control the horizontal and vertical dimensions of the sample flow work well and allow to adapt the sample flow over a large range. The control ports make the flow cells very versatile so that they can also be used for other applications such as sample splitting and flow switching.

An integrated Coulter counter has been developed to measure particle size. The Coulter counter features a liquid aperture, which is defined by a sheath flow in which a conductive sample liquid is surrounded by a non-conductive sheath liquid. The liquid aperture has two main advantages over the classical fixed aperture. By decoupling the electrical dimensions of the Coulter aperture from the physical dimensions of the channel the Coulter counter can be operated at a much higher sensitivity than the traditional Coulter counter. A second advantage is that the liquid aperture can be dynamically adapted, without the need to exchange parts. Therefore, the instrument can be used to size particles over a relatively large size range.

Particle sizing experiments have been performed with the integrated Coulter counter and the measurement results demonstrate that particles differing 20% in diameter can be clearly discriminated. The measurements match well with the specification of the particles, which demonstrates the potential of the instrument for quantitative particle analysis. Just like in the conventional Coulter counter both conductive and non-conductive particles can be detected.

To measure the shape of particles and to obtain information on their optical properties an optical projection cytometer has been developed. By integrating the optical sensor into a transparent flow-channel a very small projection distance has been achieved. As a result the near-field of the optical projection can be registered without the need for lenses or any other optical components.

Two different optical sensors, an 'array sensor' and a 'strip sensor', are introduced that differ in versatility and ease of use. Quasi-static measurements prove that with both of the sensors an image of a small object can be accurately obtained. An integrated projection cytometer has been fabricated based on the strip sensor. Two types of particles of comparable size could be clearly distinguished based on their optical properties. The measurement signals show optical details of the particles and demonstrate very good repeatability.

The last microsystem that has been worked on is an actuator to sort particles. The analysis is focused on sorters of the flow-through type, which send the particles either to one channel branch or to the other. The sorters are based on dielectrophoresis, which is an electrical actuation principle. The main advantage of using electric actuation is that the sorters are very suitable for integration with other microsystems.

The design of the sorter has been optimised. Firstly the electrode configuration was analysed in a 2D plane, orthogonal to the direction of flow. Qualitative analysis, confirmed by a full simulation of the sorter, lead to the conclusion that sorters having electrodes on opposing sides of the channel show significantly higher performance than sorters with electrodes only on one side of the channel.

In a second step the layout of the actuators was optimised. Two new electrode topologies have been presented, the 'switching electrode topology' and the 'focusing electrode topology', optimised for a general increase in flow-rate or to maximise switching speed, respectively. By increasing the number of channel branches the performance can be increased significantly. This has been experimentally verified for a topology with three outlets. The optimised sorters show a performance increase of more than 200% over the classical sorter design and the new topologies show the potential for an even larger increase.

The thesis is concluded with a brief outlook in which some promising ideas for future research are briefly discussed.

Table of contents

Kurzfassung	ii
Summary	iv
Chapter 1	1
1.1. Historical context	2
1.2. Advantages of miniaturisation	4
1.3. Microsystems for particle analysis.....	4
1.4. Overview of particle analysis techniques.....	5
1.4.1. Sieving	5
1.4.2. Electrical zone sensing.....	6
1.4.3. Light scattering methods.....	6
1.4.4. Sedimentation.....	7
1.4.5. Permeametry	7
1.4.6. Microscopy.....	8
1.4.7. Tomography	8
1.5. Selection of particle analysis techniques.....	9
1.6. Thesis outline	9
1.7. References	10
Chapter 2	12
2.1. Introduction	13
2.2. Substrate material.....	13
2.3. Micro-channel technology	13
2.4. Bonding technology	15
2.5. Process flows.....	15
2.6. Device holder	18
2.7. References	19
Chapter 3	20
3.1. Introduction	21
3.2. Theory	23
3.3. Design considerations	24

Table of contents

3.4. Non-coaxial sheath flow cell.....	24
3.5. Coaxial sheath flow cell.....	26
3.6. Experimental verification.....	27
3.6.1. Sample diffusion	29
3.6.2. Vertical control of sample flow dimensions	30
3.6.3. Horizontal control of sample flow dimensions	31
3.7. Sample flow splitting and switching.....	33
3.8. Conclusions.....	34
3.9. References.....	34
Chapter 4.....	12
4.1. Introduction.....	37
4.2. Aperture control	38
4.3. Device simulation.....	40
4.4. Device fabrication	43
4.5. Experimental	44
4.6. Improved Coulter counter	46
4.7. Discussion	48
4.8. Conclusions.....	49
4.9. References.....	49
Chapter 5.....	51
5.1. Introduction.....	52
5.2. Operation principle.....	53
5.3. Diffraction.....	53
5.4. Sensor design	56
5.5. Sensor characterisation.....	59
5.6. Integrated cytometer.....	63
5.7. SU-8 based cytometer	66
5.8. Discussion	69
5.9. Conclusions.....	69
5.10. References.....	70

Table of contents

Chapter 6	71
6.1. Introduction	72
6.2. Theory	73
6.3. Critical flow speed	74
6.4. Design variables	75
6.5. Electrode configuration	76
6.5.1. Configuration I	77
6.5.2. Configuration II	78
6.5.3. Configuration III	78
6.5.4. Configuration IV	78
6.6. Simulation of electrode configuration	79
6.7. Electrode shape	81
6.8. Sorter topology	82
6.8.1. Switching electrode topology	82
6.8.2. Focusing electrode topology	83
6.8.3. Sorter selection	84
6.9. Simulation of electrode topology	85
6.10. Sorter experiments	86
6.11. Results and discussion	87
6.12. Joule heating	88
6.13. Conclusions	89
6.14. References	90
Chapter 7	92
7.1. Introduction	93
7.2. Flow cell	93
7.3. Coulter counter	93
7.4. Integrated projection cytometer	94
7.5. Particle sorter	94
7.6. Low-cost version	94
7.7. References	95

Table of contents

Acknowledgements.....	96
Publications.....	97
About the author.....	99

Chapter 1

Introduction

1.1. Historical context

This thesis deals with the development of microsystems for the analysis of small particles (diameter 5-50 μm). These microsystems can be combined with other components to form a device that has become to be known as a lab-on-a-chip. To explain what a lab-on-a-chip is, to understand what the main motivations were for its development and to outline the fundamental differences between a lab-on-a-chip and apparently similar concepts such as chemical sensors, a brief description is given of the technological advancements that lead to the development of the lab-on-a-chip.

The transistor was invented at Bell Telephone Laboratories in 1947 [1, 2] by Shockley, Bardeen and Brattain. This invention started the development of the micro-electronics technology. Important milestones in the evolution of this technology were the development of the first integrated circuit (IC) at Texas Instruments in 1958 by Kilby, using germanium devices, and the development of a planar silicon IC a few months later at Fairchild Semiconductor by Noyce. Since 1970 the complexity of IC's has doubled every 18 months, resulting in very complex devices containing more than 100 million transistors on a single chip. During this evolution the fabrication technologies continuously improved, reducing the minimum dimension of manufactured devices and ICs from 20 μm to the sub-micron levels of today.

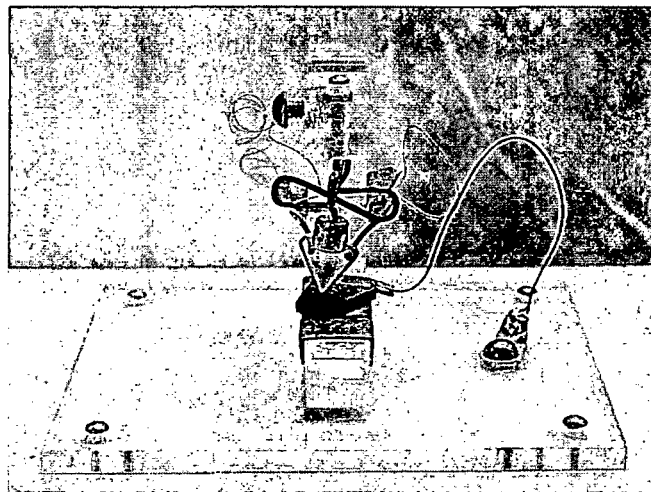


Figure 1-1. Model of the first point-contact transistor as built by Brattain.

These highly refined fabrication tools, allowing fabrication of devices with an unprecedented geometrical accuracy, were mainly reserved for the fabrication of IC's. This changed when Peterson of IBM published a paper in 1982 entitled 'Silicon as a Mechanical Material' [3]. In this paper he noted that silicon has remarkable mechanical properties including a hardness and tensile yield strength similar to stainless steel. The combination of the excellent mechanical properties and the available infrastructure for silicon sparked the rapid development of a new field that became known as MEMS (Micro-Electro-Mechanical Systems). It is worth noting though, that it was not until 1987 that the term MEMS was first introduced during a series of workshops.

MEMS are small integrated devices or systems that combine electrical and mechanical components. These components range in size from the sub-micrometer level to the millimetre level, and there can be any number, from only a few to millions, in a single device. Although,

there were some developments on silicon strain-gauges in the late 1960's and on silicon pressure sensors in the 1970's at Kulite Semiconductor Products and Honeywell among others [4], 1982 is seen as the starting point where the development of the MEMS field really took off. In the beginning the mechanical components in MEMS were restricted to rigid structures such as cantilevers, bridges and diaphragms, which only contain bending joints. In 1987-1988 an important break-through was achieved with the introduction of movable micromechanical structures such as rotatable joints, sliding and translating members and energy storage elements [5]. Since then a variety of MEMS-based sensors has been developed for measuring position, velocity, acceleration, pressure, force, torque, flow, magnetic field, temperature, gas, humidity, pH and ionic concentration. Quite a few of these sensors have made it into series-production as a result of their favourable properties such as small dimensions, high reliability and low costs.

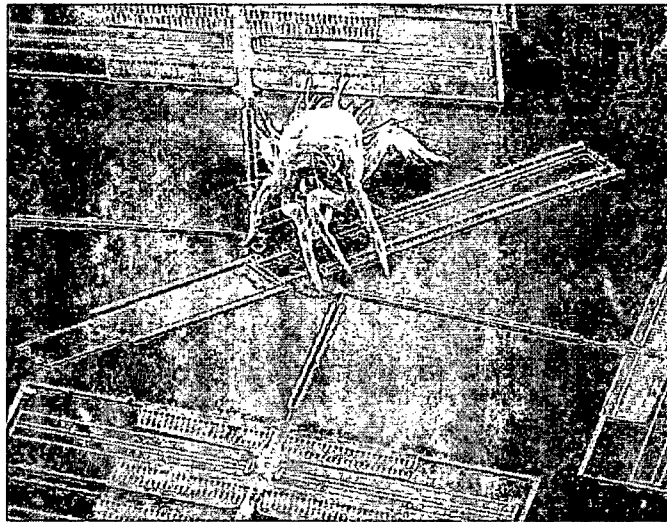


Figure 1-2. Photograph of spider mite on mirror assembly, Courtesy Sandia National Laboratories, SUMMiT™ Technologies, www.mems.sandia.gov.

Although many MEMS-based sensors proved successful, especially in the mechanical and magnetic domain, this was not necessarily so in the chemical and biological domain. These sensors typically rely on a chemical or biochemical interface that consists of a selective, chemically sensitive layer that is influenced by the presence of the species of interest. The development of this chemical interface appears to be the bottleneck in (bio)chemical sensors. The chemical interfaces lack stability, durability, selectivity or sensitivity and are hard to manufacture in a reproducible manner [6]. Furthermore the interfaces are very sensitive to contamination and for every specific application a new interface is required.

A novel approach to the application of IC-technology for (bio)chemical measurements was introduced in 1990 with the concept of the miniaturised total chemical analysis system (μ TAS) by Mantz and co-workers [7]. A μ TAS is a chemical analysis system integrated on a miniaturised chip-like platform. Chemical information is transformed into electrical information by sampling, sample transport, separation, any necessary chemical reactions and separations, as well as detection. Initially, the main reason for miniaturisation was to enhance the analytical performance of the device rather than to reduce its size [8]. However, it was also recognized that a small size presented the advantages of a smaller sample and reagent consumption. In a μ TAS the problematic chemically sensitive interface is not needed, since

the selectivity is achieved by the integrated analytical techniques. Furthermore, the total chemical analysis system scheme provides an integration of separation techniques that enables the monitoring of many components within a single device, which is a large advantage over the 'classical' chemical sensors. Because of the highly integrated functionality of the total analysis system the concept has also become to be known under the name lab-on-a-chip; both names are used interchangeably.

1.2. Advantages of miniaturisation

There are a number of reasons why miniaturisation of fluidics systems is of interest for chemical and biological applications. Some of the main advantages are summarised in Table 1-1. As mentioned in the previous paragraph enhanced performance and the reduced consumption of sample and reagent were the main reasons to start the downscaling of microfluidics systems in the first place. But there are additional advantages that come with these small systems. The reduced dimensions of the microsystems result in much smaller analytical instruments. In combination with the reduced power requirement this opens the door to portable devices. Portable analysis system would mean a great step forward, since samples do no longer have to be sent to a laboratory for analysis, but can be analysed on-site. Another advantage of their small dimensions is that microsystems can be placed directly in a process stream, or in restricted spaces like boreholes or pipes.

Table 1-1. Advantages of miniaturisation.

Property	Advantage
Small liquid volumes	Small amount of sample required Reduced reagent costs
Small dimensions	Portable devices Integration in process stream
Based on IC technology	Parallel fabrication Relatively low fabrication costs
Fast response times	Chemical analysis can be applied as sensors

The miniaturised devices are often made using IC-technology, which allows to manufacture many devices in a single batch, resulting in relatively modest costs per device. The high complexity that can be realised with these fabrication technologies can be used to make large parallel arrays; this is particularly useful for applications like drug screening. Finally, due to the large surface to volume ratio in microsystems, many processes take place much faster than in comparable macro-instruments. This allows performing quasi real-time measurement with these miniaturised systems, so that they can be used as sensors.

1.3. Microsystems for particle analysis

In many industries particulate materials play an important role, both as a substrate material and in the final product. The behaviour and properties of particulate materials, such as pigment capacity, adsorbing power, texture and flow properties, largely depend on particle shape, particle size and the size distribution of the particles [9]. Therefore, there is an industrial need to measure these particle properties. Also in biology and medicine it is of interest to measure properties of small particles, where the particles are frequently cells. Here the goal is often to identify particles based on their shape, size and optical properties.

Miniaturisation of systems for particle analysis is very interesting, since microsystems can be fabricated that have features in the same order of size as the particles to be analysed. This has the advantage that no intermediate stages are required to bridge the gap between the size of the particles and the size of the sensors and actuators of the instrument. This leads to more direct measurements methods and simpler, more elegant sensors and actuators. Another advantage of particle analysis with a microsystem is that the way the particles are exposed to the sensors can be well controlled, which has a great potential for very repeatable measurements.

The goal of this thesis is to develop generic microsystems for the analysis of particles. To make the systems suitable for in-line measurements it should be possible to operate them continuously. The design of the microsystems should be such that it is possible to separate particles of interest from the sample flow so that they can be further analysed.

1.4. Overview of particle analysis techniques

There are many macro-instruments available for the analysis of particles, based on a variety of techniques. The most common techniques for particle analysis will be briefly discussed below. The techniques are quickly analysed for their potential to be integrated in a microsystem for particle analysis to yield information on particle shape, particle size and the optical properties of the particles.

1.4.1. Sieving

The introduction of sieves for size analysis is often attributed to Von Rittinger [10]. The characterisation of the examined particles is usually done by letting it pass through a stack of sieves, where the size of the holes decreases from one sieve to the other. When the sieving process is done, the amount of powder remaining in each of the sieves is determined by weighing or by chemical procedures. Particles that have a cross-sectional area that is smaller than the sieve aperture are able to pass the sieve. Sieving sorts particles according based on two dimensions, the third dimension of the particle can have any size and can be much larger than the other two.

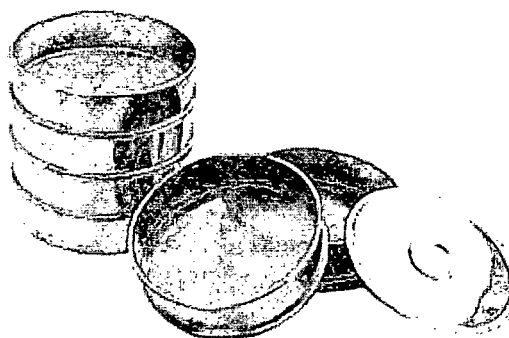


Figure 1-3. A set of sieves for particle size analysis.

Although IC-technology is very suitable to fabricate sieves with reproducible holes, the miniaturisation potential of sieving is limited. Sieving is typically performed on a batch basis, where the analysed particles are stored inside the instrument. Due to the very small dimensions of the system, the storage capacity inside the device is very limited. This might be solved, however, if a way is found to operate sieving in a continuous way. The second

problem is more severe. The very fine holes required for such small particles easily get blocked. It will be very difficult to make the system reliable for continuous operation. Finally, particles are only sorted according to their second dimension, which for some kinds of particles can be too severe a limitation.

1.4.2. Electrical zone sensing

The electrical zone sensing method [10], also known as the Coulter principle, was developed by Wallace H. Coulter in the late 1940s under contract to the United States Navy as a method of counting blood cells rapidly. The operation principle of a Coulter counter is as follows. Particles suspended in an electrolyte are forced through an orifice, where on either side an electrode is immersed. The electrical impedance over the aperture is measured and when a particle passes through the orifice the changes proportional to the volume of the particle.

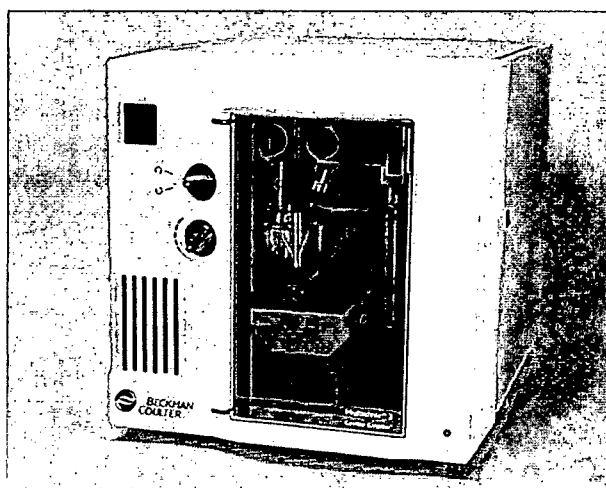


Figure 1-4. A modern Coulter counter: the Beckman Coulter Multisizer™ 3.

The Coulter counter measures particle volume, which is a good measure of particle size. The measurements are performed electrically, requiring only an orifice and a set of electrodes. These are easy to fabricate in IC-technology. In contrast to the sieving the orifice is typically a few times larger than the size of the particle, so blocking of the orifice is far less problematic. Particles are analysed on an individual basis, so there is the potential to sort out individual particles of interest.

1.4.3. Light scattering methods

When a beam of light passes through a suspension containing particle, the particles scatter some of the light in all directions. When the particles are very small compared with the wavelength of the light, the intensity of the scattered light is uniform in all directions (Rayleigh scattering); for larger particles, above approximately 250 nm diameter, the intensity is angle dependent (Mie scattering).

For larger particles the intensity of the scattered light in any particular direction can be correlated with particle size. The main problem with this method is the complexity of the calculations, which are often approximate or iterative. This causes different manufacturers to use different algorithms, which leads to different results on the same sample [9].

For small particles fluctuations in intensity of the scattered light can be used to calculate particle size. Movement of the particles due to Brownian motion causes rapid fluctuations in

scattering intensity. These intensity fluctuations depend on particle size. The calculated correlation function results in a diffusion coefficient for a given temperature and viscosity, which can be converted to particle size. This method is known as dynamic light scattering.

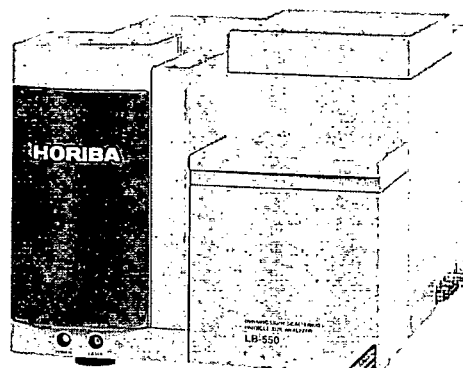


Figure 1-5. The Horiba LB 550 particle sizer is an instrument for particle size analysis based on dynamic light scattering.

For the particle size range of interest Mie scattering is the technique that would be of interest. Due to the small dimensions and the planar nature of microsystem it might be difficult to measure the intensity of the scattered light at a certain angle accurately, since the propagation distance would be very small.

1.4.4. Sedimentation

The sedimentation of particles gives information about their size properties. A measurement starts with a uniform distribution of particles and the sedimentation of the particles is monitored by optical absorption at a certain vertical position. The suspension should be dilute so that there is no particle interaction. Furthermore it is assumed that the motion of the particles obeys Stokes' law and that the particles rapidly accelerate to their terminal velocity [11]. Under these assumptions a cumulative size distribution of the particle sample can be obtained.

The potential for miniaturisation of sedimentation is limited. The small dimensions of a microsystem limit the sedimentation distance and particle interaction is likely. Furthermore the method inherently operates on a batch basis and only yields a cumulative size distribution instead of information on the individual particles.

1.4.5. Permeametry

Permeametry is a particle analysis method based on fluid flow through a packed bed of particles. The pressure drop through a randomly packed bed of uniformly sized particles can be related to particle size with the Carman-Kozeny equation. When particles of different sizes are used, the arithmetic mean is calculated. This is probably the main drawback of permeametry for particle measurements: only the mean size can be determined.

Permeametry is not suitable for single particle analysis. This makes it practically impossible to sort out individual particles for further analysis. Furthermore permeametry works on a batch basis and requires reasonably large quantities of particles to be stored.

1.4.6. Microscopy

Microscopy is a very popular analysis technique, because it yields an image of the particles analysed. Based on this image detailed particle properties can be extracted, such as shape and size. Even some of the internal properties of the particles can be analysed, since most particles are at least partially transparent. However, since microscopy only yield a two-dimensional projection of the particle, its size in the third dimension is not known.

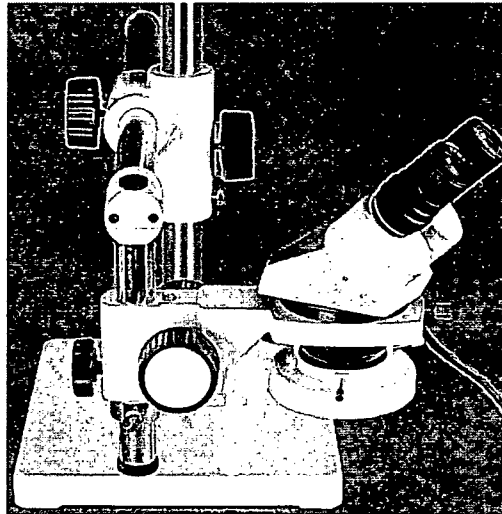


Figure 1-6. Microscopy is an analysis technique that yields detailed information on particle shape and size.

Microscopy yields detailed particle information and the size and shape of individual particles can be accurately measured in two dimensions. Microscopy is typically operated on a batch basis, where the particles to be analysed are confined between two glass slides to keep all particles in focus. If a way is found to operate microscopy on a continuous basis it could be an interesting technique.

1.4.7. Tomography

Many different tomography techniques exist (e.g. optical, electrical, X-ray, ultrasonic tomography systems), but the basic idea is always the same. A number of sensors are installed on the periphery of the area that is to be examined. From different positions an actuator is activated and its signal interacts with the matter. The sensors register this interaction and a computer is used to reconstruct an image of the cross-section observed by the sensors. By stacking several of these two-dimensional distributions it is possible to build up a three-dimensional image of the particle, including the internal composition. The main drawback is that the very detailed information comes at a very high computational cost, which makes real-times operation relatively slow.

The planar nature of IC fabrication technology makes integration of tomography in a microsystem complicated. Tomography is suitable for the analysis of individual particles, but the throughput is low because of the large number of measurements required.

1.5. Selection of particle analysis techniques

The different techniques are compared in Table 1-2. Particle shape can only be measured using microscopy and tomography, since these techniques yield an image of the particle. In light-scattering, sedimentation and permeametry the particle size measurement is influenced by particles shape; when the particle shape is not known accurate size measurements are not possible. Tomography yields the most complete information on a particle, however the disadvantages associated with tomography are considered too severe. Besides the difficulties to integrate tomography into a microsystem another large problem is that real-time application is very hard due to the large number of measurements required and the computationally intensive data processing. The image obtained with microscopy is a two-dimensional projection of the particle; information about the third dimension is not available. To supplement the information obtained with microscopy a second analysis technique is required.

Table 1-2. Comparison of the different particle analysis techniques.

	Particle size	Particle shape	Continuous operation	Compatible fabrication
Sieving	v ¹	-	-	v
Electrical zone sensing	v	-	v	v
Light scattering	v ²	-	v	-
Sedimentation	v ²	-	-	-
Permeametry	v ²	-	-	-
Microscopy	v ¹	v	v	v
Tomography	v	v	v	-

¹ Only 2-dimensional particle size measurement

² Under the assumption of a spherical particle

Both sieving and electrical zone sensing are relatively easy to integrate in a microsystem. Sieving only yields two-dimensional particle size information and furthermore it seems very difficult to make sieving reliable. Electrical zone sensing yields particle volume information, it is suitable for continuous operation and is compatible with integration into a microsystem. Based on these considerations electrical zone sensing seems the most suitable measurement technique to supplement microscopy. The two techniques nicely complement each other. Electrical zone sensing yields size information on the particles, where microscopy allows differentiating between particles of comparable size having different shapes or different optical properties.

1.6. Thesis outline

This thesis deals with the development of microsystems for the handling, analysing and sorting of small particles (5-50 μm). The general philosophy employed in this thesis is that the unique physics resulting from the downscaling should be used as an advantage; this in contrast to taking macro-systems and just making them smaller, while trying to cope with the different physics. Below follows a brief outline of the thesis with a short description how this philosophy on miniaturisation is brought into practice for each microsystem.

Before discussing the individual microsystems in detail, some fabrication technologies are introduced in chapter 2. Based on these technologies a universal platform is selected that is used as the basis for all the microsystems that are developed in the subsequent chapters.

The first microsystem that will be discussed is a component that ensures reliable delivery of the particles to the sensors. Chapter 3 presents the development of a new flow cell that creates a flow profile, which prevents clogging and makes the particles pass the integrated sensors in a reliable and repeatable way. The operation of the flow cell is based on the laminar flow conditions that are typical for fluidics in a microsystem.

In chapter 4 an integrated Coulter counter is discussed. The limited interaction between flowing liquids in a microsystem has been used to define a liquid Coulter aperture. This aperture combines the reliability of a large physical aperture with the high sensitivity associated with an aperture having much smaller dimensions. As a result measurements with the integrated Coulter counter can be performed at a much higher sensitivity than would be possible with a traditional Coulter counter having a fixed aperture.

An integrated optical sensor based on optical projection is the topic of chapter 5. The sensor registers detailed optical properties of the particle without the application of lenses or any other optical components. This has been realised by the extremely small projection distance that can be realised in a microsystem in combination with the application of components that have dimensions substantially smaller than the particles to be imaged.

The functionality of a microsystem can be greatly extended by including a component to sort out particles of interest based on the readings of the sensors. In chapter 6 flow-through sorters based on dielectrophoresis are discussed. The small dimensions of the electrodes generate very strong field gradients only obtainable in a microsystem. Based on a thorough analysis the sorters are optimised so that they can handle much higher flow-rates.

The thesis is concluded with an outlook in chapter 7. Some promising ideas for further developments of the microsystems are presented. Also a possible first step towards a commercially viable realisation of the microsystems is briefly discussed.

1.7. References

- [1] J. Bardeen and W. H. Brattain, "The Transistor, a Semiconductor Triode," *Phys. Rev.*, vol. 74, pp. 230, 1948.
- [2] W. Shockley, J. Bardeen, and W. H. Brattain, "Electronic Theory of the Transistor," *Science*, vol. 108, pp. 678-679, 1948.
- [3] K. Petersen, "Silicon as a Mechanical Material," *Proc. of IEEE*, vol. 70, pp. 420-457, 1982.
- [4] H. Helvajian, *Microengineering Aerospace Systems*: AIAA, 1999.
- [5] L.-S. Fan, Y.-C. Tai, and R. S. Muller, "Integrated movable micromechanical structures for sensors and actuators," *IEEE Transactions on Electron Devices*, vol. 35, pp. 724-730, 1988.
- [6] M. J. Vellekoop, "The emerging of physical chemosensors and biosensors," presented at Transducers '01, Munich, Germany, 2001.
- [7] A. Manz, N. Graber, and H. M. Widmer, "Miniaturized Total Chemical Analysis Systems: a Novel Concept for Chemical Sensing," *Sensors and Actuators B*, vol. 1, pp. 244-248, 1990.
- [8] D. R. Reyes, D. Iossifidis, P.-A. Auroux, and A. Manz, "Micro Total Analysis Systems. 1. Introduction, Theory, and Technology," *Analytical Chemistry*, vol. 74, 2002.

- [9] C. Washington, *Particle size analysis in pharmaceuticals and other industries, theory and practice*, 1st ed. ed. Chichester: Taylor & Francis Ltd, 1992.
- [10] T. Allen, *Particle size measurement.*, vol. 1. Powder sampling and particle size measurement, 5th ed. London: Chapman and Hall, 1997.
- [11] M. Rhodes, *Introduction to particle technology*, 1st ed. ed. Chichester: John Wiley & Sons Ltd, 1998.

Chapter 2

Fabrication technology

2.1. Introduction

The platform for the microsystem has to be carefully selected, since it has far-reaching consequences for the functionality that can be integrated into the system. The focus in this thesis is on the development of microsystems for particle analysis on the system level. To ensure that sufficient attention can be allocated to this focus, proven fabrication technologies are used whenever possible to prevent unnecessary technological obstacles.

Further considerations in selecting the platform are versatility, compatibility and local availability. The platform should be versatile so that different sensors and actuators can be supported, based on a large range of actuation principles. Compatibility with standard IC-processing is required to ensure that the IC-infrastructure can be utilised for the fabrication of the devices. The importance of local availability of the fabrication technologies should also not be underestimated. Especially in the research phase, close interaction with the people who actually fabricate the devices results in additional flexibility and valuable feedback.

2.2. Substrate material

Silicon has been selected as the main substrate, since it has many favourable properties for the fabrication of microfluidics/analytical devices [1]. Silicon is an extremely well-characterised material with an incredibly large ‘toolbox’ full of technologies developed by researchers in the electronics industry. As a result it is possible to fabricate a certain geometrical structure very precisely in silicon. Other reasons are its mechanical properties (hard, strong) and its easy coverage by a chemically well-known and relatively inert layer of silicon dioxide. Because of these favourable properties a large range of sensors and actuators have been developed that can be integrated into a microsystem.

An additional advantage of using a silicon substrate is that it allows for equipping the microsystems with signal conditioning electronics, which can greatly improve the quality of the signals that are measured on the chip. In theory it is even possible to integrate the complete signal processing into the microsystem itself, although from a commercial point of view this is not always attractive.

2.3. Micro-channel technology

One of the key requirements to make a microsystem for the analysis of particles is to have some integrated channel to contain and transport the sample. There are different ways to realise this [2]:

1. Micro-channels etched in silicon using either wet- or dry-etching process [3, 4]; the main advantages of etching channels in silicon is that the dimensions and shape of the channel can be accurately controlled.
2. Micro-channels etched in glass or quartz [5]; these channels are transparent, and chemically inert.
3. Ground plate supported insulating channels (GPSICs) [6], which are formed by etching a channel in a silicon wafer that is then coated with silicon-oxide or silicon nitride. The wafer is bonded to a substrate after which the silicon is etched away. The remaining channels consist of a thin layer of silicon-oxide or silicon-nitride and are optically transparent, electrically insulating and demonstrate very efficient heat dissipation, but are also very fragile.
4. Buried micro-channels [6] that are formed in the bulk of a silicon substrate by a combination of anisotropic etching, surface passivation and isotropic etching. These

channels require only a single wafer, but it is very complicated to integrate any functionality into the channels.

5. Micro-channels by replication in polymers; here a (silicon) master is used and the geometry is transferred by either casting a liquid polymer onto the master that is then cured (e.g. PDMS [7]) or by hot-embossing channels in hard plastic materials like polymethylmethacrylate (PMMA [8]) at temperatures close to the softening point of the plastic. The main advantage of this approach is that once you have made one master it is relatively easy to fabricate large volumes.
6. Micro-channels formed by photolithography of thick polymers such as e.g. SU-8 [9].

A transparent channel is required to allow for visual inspection of the microsystem. This means that channels buried in the silicon cannot be used. Furthermore it will be very difficult to integrate any additional components with this technology. A transparent channel can be formed by etching it into the silicon and covering it with a transparent lid. However, this requires modifications to the processing of the silicon wafer that forms the sensors and actuators, which might cause major technological hurdles. This makes etching the channel into the silicon substrate not an option. The complicated processing and the fragility of the resulting channels make the GPSICs not a very attractive option either.

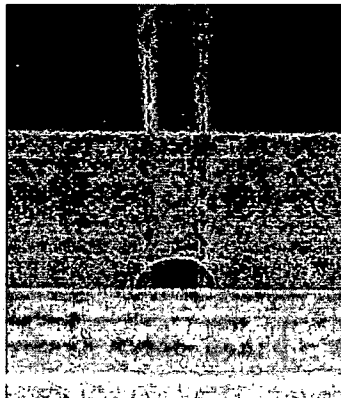


Figure 2-1. Photograph of the cross-section of a micro-channel formed by wet- etching in glass (width 200 μm) and bonding to a silicon wafer.

Since the channel has to be formed in a transparent material the choice is between plastics and glass technology. At the start of the project there was no experience with plastics technologies, but there was a vast amount of experience with glass technology in the laboratory. Therefore, it was decided to fabricate the micro-channels on a glass substrate. Initially this was achieved by etching a groove in the glass wafer, later in the project it was decided to use SU-8 on glass to define the micro-channels. The reason for this change will be discussed in detail in chapters 4 and 5.

To keep the glass part of the device free for optical inspection the inlets for the liquid are made through the silicon part of the device. Another motivation for this choice is based on technological considerations. It is much easier to etch through-holes in the silicon wafer than in the glass wafer, because of the anisotropic etching behaviour of silicon (as a consequence of its lattice structure).

2.4. Bonding technology

Closed channels are formed when the glass wafer and the silicon wafer are bonded together, completing the devices. There are four main bonding techniques [10]:

1. Adhesive bonding; an intermediate glue, polymer or glass layer is used for adhesion of the two wafers. The adhesive bonding techniques are fairly insensitive to wafer roughness and particle contamination.
2. Eutectic bonding; in the most elementary form eutectic bonding involves bringing a silicon surface in contact with a gold plated substrate. Applying a contact force and increasing the temperature beyond the Au-Si eutectic temperature of 363 °C results in diffusion of silicon into the gold and the formation of a eutectic compound at the interface; at cool-down a eutectic bond is formed [11].
3. Anodic bonding; a glass wafer and a silicon wafer are brought into contact and at a temperature of 250-450 °C a voltage of 500-1000 V is applied. The high electric field creates a strong electrostatic force that pulls the two surfaces together forming an intimate contact. Additionally in the glass Na⁺-ions start drifting to the negative electrode, creating depletion zone adjacent to the silicon. During this charging process, the electric field is high enough to allow a drift of oxygen to the positive electrode reacting with silicon and creating Si-O bond [10].
4. Fusion bonding; the bonding relies on the tendency for both very smooth and flat surfaces to adhere. An annealing step at 700-1000 °C forms a strong and irreversible bonding.

Adhesive bonding techniques have the main disadvantage that they cannot be used on wafers having trenches, because spinning the adhesive onto the wafer will result in an uneven application. The glass wafer contains a large recess that forms the flow channel, so applying the adhesive to the glass wafer is not an option. Applying the adhesive to the silicon wafer is not very attractive either, since it would cover all sensor interfaces and the adhesive would locally have to be removed to uncover them. Eutectic bonding is typically used when an electric contact needs to be formed between the two parts that are bonded. In the case of the micro-channel an electrical contact is not favourable since it shorts the metal wires that connect the sensors inside the channel, which need to cross a bonded area. Additionally it is difficult to get a completely bonded area with eutectic bonding [10], which might lead to leakages. For these reasons eutectic bonding does not seem to be the right choice. Fusion bonding requires an extremely flat surface, which is not available on the silicon wafer, since it has been processed to fabricate integrated sensors.

Based on the considerations above anodic bonding seems to be the most suitable technique to bond the two wafers together. It is suitable to bond a glass and a silicon wafer together without the requirement for any intermediate layers. Furthermore, the flatness requirements are not as strict as with the fusion bonding process. However, when anodic bonding is used special techniques may be required to protect the components on the silicon wafer from the strong electric field [12].

2.5. Process flows

This paragraph briefly discusses the fabrication processes based on the design decisions described above. The process flow that uses anodic bonding to join the two wafers is schematically depicted in Figure 2-2. A silicon wafer is used as a substrate (I), which is processed to fabricate any sensors and actuators (II). As a post-processing step through-holes

are made by etching in KOH (potassium hydroxide) to form the inlets and the outlet for the liquid (III). A glass wafer forms the other part of the device (IV). By wet-etching in HF (hydrofluoric acid) a channel is formed (V). To complete the devices, the glass wafer and the silicon wafer are aligned and joined (VI) using anodic bonding [10].

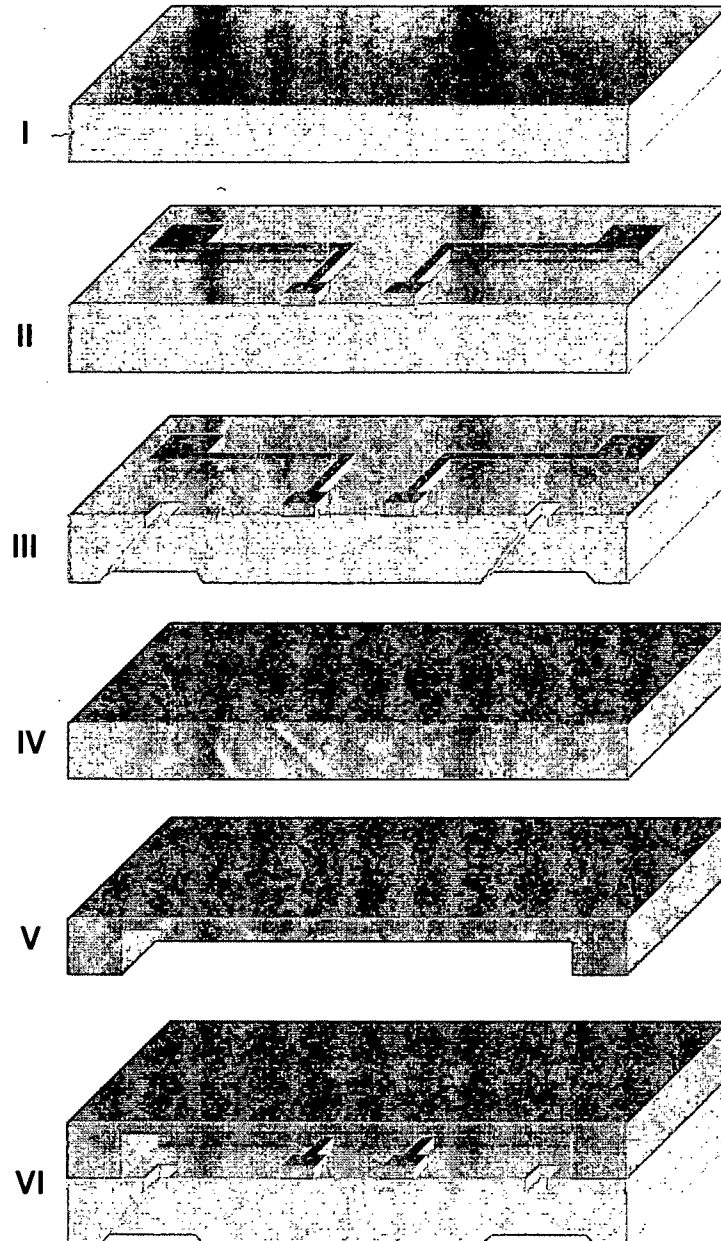


Figure 2-2. Schematic overview of the device fabrication based on etching the channels in the glass and anodic bonding.

Later in the project the process flow was slightly altered. A new two-step SU-8 process had become available [13], where the SU-8 is used to define the channels and also to bond the two wafers together. This means that the adhesive bonding can now be used with a wafer having a trench. Other advantages of this process are that it is very tolerant to surface roughness and it does not require a high voltage to be applied. Furthermore, the tedious wet-etching of the

channels into the glass wafer is no longer needed. The process flow based on the SU-8 process is illustrated in Figure 2-3.

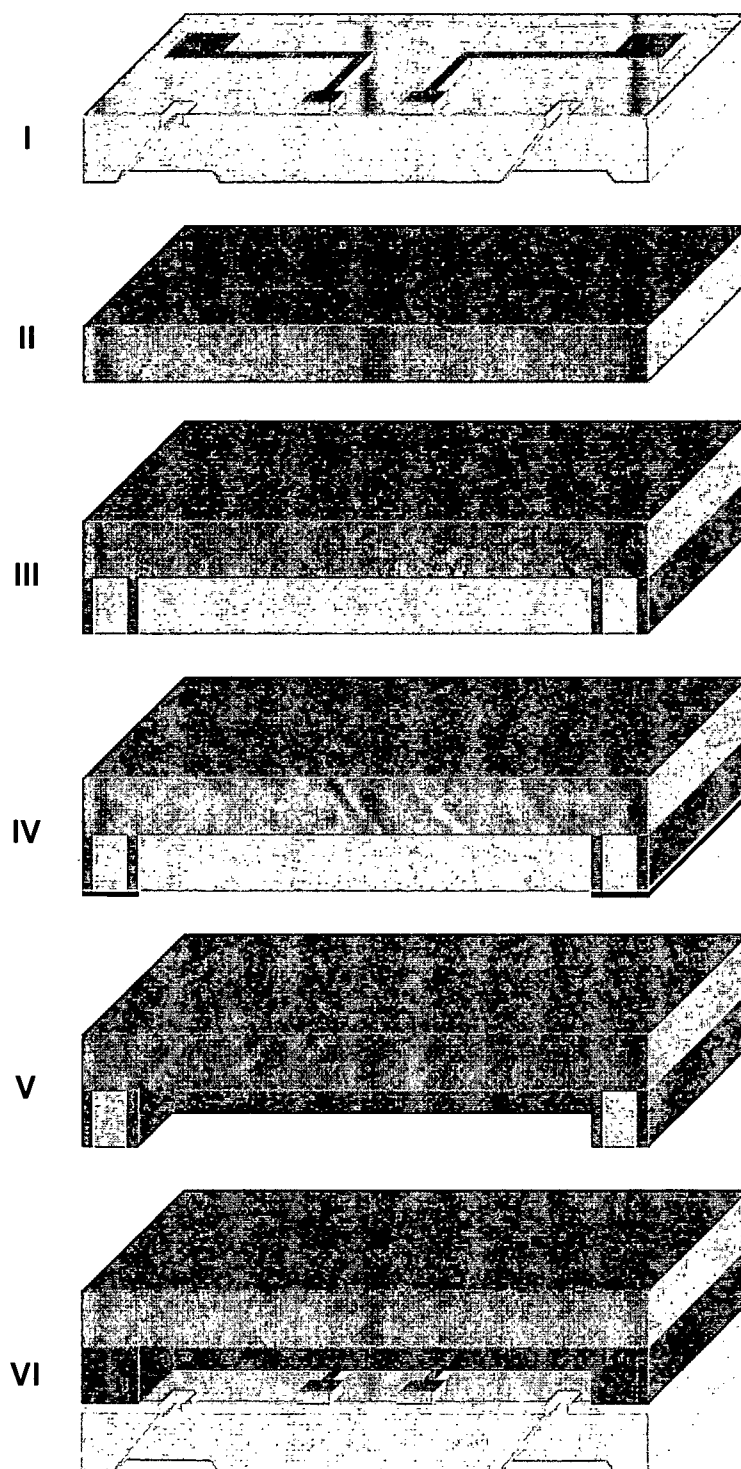


Figure 2-3. Schematic overview of the device fabrication based on defining the channels in SU-8 and using SU-8 to bond the two wafers together.

The silicon wafer is fabricated in the same manner as in the old process (I). A glass wafer is again used as the other half of the device (II), but now a thick layer of SU-8 is applied onto the glass wafer and this SU-8 is selectively exposed (III, the exposed SU-8 is marked with the darker colour). Next, a sacrificial silver layer is applied that covers some of the unexposed SU-8 (IV). The SU-8 is developed, where the unexposed SU-8 that is not covered by the silver is dissolved, after which the silver layer is removed (V). The two wafers are aligned and pressed together. The unexposed SU-8 is still plastic, so it fills up all of the small holes sealing the channel. At a temperature of 200 °C the unexposed SU-8 now also cross-links, forming a strong bond between the two wafers (VI).

All of the devices described in this thesis are fabricated based on one of the two process flows described above. The impact of the selected fabrication technology on the performance of the devices will be discussed in detail in the relevant chapters.

2.6. Device holder

A custom device holder was developed to form the interface to the chip. The main considerations in the development of the holder were ease of use and reliability. The holder consists of three main components. The liquid interface block (see Figure 2-4 middle) forms the liquid connections to the chip. The connections are established by O-rings, which have the advantage that they form a liquid-tight seal directly to the silicon. The O-rings are located in a recess that automatically aligns the inlets of the chip with the O-rings on the holder. A Perspex plate (see Figure 2-4 left) fixates the chip and is used to press it against the O-rings to seal the connections.

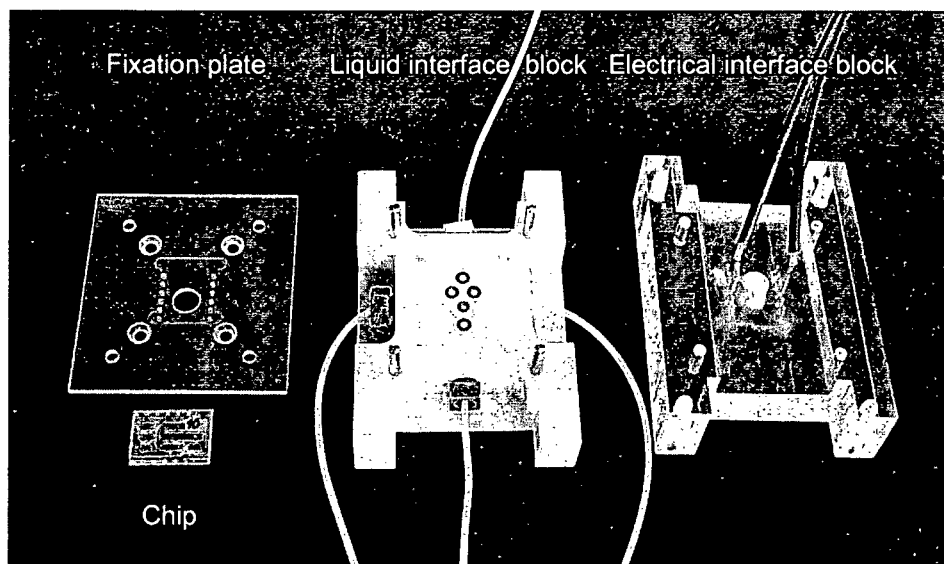


Figure 2-4. A photograph of three main components of the custom chip holder.

The electrical connections are established using spring pins. Twelve spring pins can be fitted into the electrical interface block (see Figure 2-4 right) at the same time. The electrical connections are established by simply putting the electrical interface block on top of the liquid interface block and sliding it down the guide pins. The spring pins are then aligned with the contact surfaces on the chip. A large hole in the electrical contact block, located between the

two rows of contact pins, allows for visual inspection of the chip during electrical measurements.

The holder proved to be very easy to use. The relatively large O-rings (thickness 1 mm) formed a leakage-free connection up to very high flow-speeds and accompanying pressures. Changing of the chips between measurements was quick and only required removing the two other pieces from the liquid interface block, dropping in another chip and sliding the pieces back together.

2.7. References

- [1] A. v. d. Berg, "Integrated micro- and nanofluidics: silicon revisited," presented at MicroTAS, Monterey, California, USA, 2001.
- [2] E. Verpoorte and N. F. D. Rooij, "Microfluidics meets MEMS," *Proceedings of the IEEE*, vol. 91, pp. 930-953, 2003.
- [3] G. T. A. Kovacs, *Micromachined Transducers Sourcebook*. New York: McGraw-Hill, 1998.
- [4] M. Madou, *Fundamentals of Microfabrication*, 1st ed. ed. Boca Raton, FL: CRC Press, 1997.
- [5] M. A. Grétilat, F. Paoletti, P. Thiébaud, S. Roth, M. Koudelka-Hep, and N. F. d. Rooij, "A new fabrication method for borosilicate glass capillary tubes with lateral inlets and outlets," *Sensors and Actuators A*, vol. 60, pp. 219-222, 1997.
- [6] Y. Fintschenko and A. v. d. Berg, "Silicon microtechnology and microstructures in separation science," *J. Chromatogr. A*, vol. 819, pp. 3-12, 1998.
- [7] J. C. McDonald, D. C. Duffy, J. R. Anderson, H. W. D. T. Chiu, O. J. A. Schueller, and G. M. Whitesides, "Fabrication of microfluidic systems in poly(dimethylsiloxane)," *Electrophoresis*, vol. 21, pp. 27-40, 2000.
- [8] L. Martynova, L. E. Locascio, M. Gaitan, G. W. Kramer, R. G. Christensen, and W. A. MacCrehan, "Fabrication of plastic microfluid channels by imprinting methods," *Anal. Chem.*, vol. 69, pp. 4783-4789, 1997.
- [9] H. Lorenz, M. Despont, N. Fahrni, N. LaBianca, P. Renaud, and P. Vettiger, "SU-8: a low-cost negative resist for MEMS," *J. Micromech. Microeng.*, vol. 7, pp. 121-124, 1997.
- [10] A. Berthold, "Low-temperature wafer-to-wafer bonding for microchemical systems," in *DIMES*. Delft: Delft University of Technology, 2001, pp. 119.
- [11] R. F. Wolffenbuttel, "Low-temperature intermediate Au-Si wafer bonding; eutectic or silicide bond," *Sensors and Actuators A*, vol. 62, pp. 680-686, 1997.
- [12] A. V. Chavan and K. D. Wise, "A monolithic fully-integrated vacuum-sealed CMOS pressure sensor," *Electron Devices, IEEE Transactions on*, vol. 49, pp. 164 - 169, 2002.
- [13] P. Svasek, E. Svasek, B. Lendl, and M. Vellekoop, "Fabrication of miniaturized fluidic devices using SU-8 based lithography and low temperature wafer bonding," *Sensors and Actuators A*, vol. 115, pp. 591-599, 2004.

Chapter 3

Integrated flow cell

3.1. Introduction

The first function that has to be fulfilled in a microsystem for particle analysis is reliable transportation of the particles through the system. Typically the particles are suspended in a liquid, which is pumped through tiny channels to move the particles. The main problem with channels having a small diameter is that they easily get blocked, especially when dealing with particulate samples. A straightforward solution to achieve reliable transport is to increase the diameter of the channels, but without taking any additional measures some of the advantages of miniaturisation would be lost. High reliability with a narrow stream of sample liquid can be realised with the application of a sheath flow, which decouples the physical dimensions of the flow-channel from the dimensions of the sample flow.

A sheath flow is a combined flow-profile that consists of the flow of multiple liquids within a single channel (see Figure 3-1). The first liquid is the sample liquid that contains the matter to be analysed. The second liquid, the so-called sheath liquid, has the function to focus the sample liquid into a narrow stream and to fix the position of the sample liquid with respect to the sensor interface. Focusing the particles into a very narrow stream causes the particles in the sample liquid to line up, so that each particle can be analysed individually. The small diameter of the sample flow and its accurate positioning by the sheath liquid make all particles pass the sensor in exactly the same manner, which allows for very repeatable measurements.

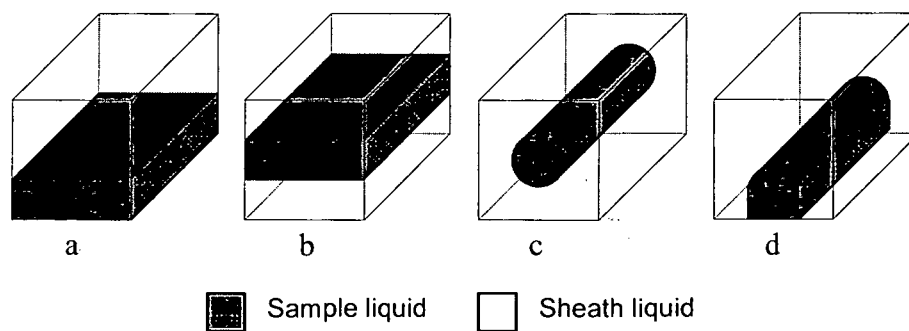


Figure 3-1. Four different types of sheath flow: single layered (a), double layered (b), coaxial (c) and non-coaxial (d).

A sheath flow can be considered to combine the advantages of a large diameter channel with those of a small diameter channel (see Table 3-1): due to the small dimensions of the sample flow the high sensitivity, modest sample consumption and accurate sample positioning of a small channel device can be achieved; at the same time the larger physical dimensions of the channel alleviate many problems such as clogging, air bubbles and strict fabrication tolerances.

Most of these advantages are obvious, but the final advantage might need some further explanation. The imperfections in the channel wall are smoothed out by the sheath liquid, which is in direct contact with the wall. The sample flow, which is screened from the wall by the sheath liquid (except for the bottom of the channel for a non-coaxial sheath flow) will not be disturbed as much. Therefore, the imperfections of the channel are not as critical as without the application of a sheath flow.

Table 3-1. Advantages of small and large diameter channels.

Channel	Advantages
Small	High sensitivity
	Modest sample consumption
	Accurate sample positioning
Large	No clogging problems
	No problems with air bubbles
	Less strict fabrication tolerances

A number of realisations of sheath flow on a chip have been presented in literature. In the simplest form a sheath flow is formed by a layered flow configuration, where the sample liquid is confined in one dimension by the sheath liquid and the channel wall (see Figure 3-1a). In [1] a microsystem is presented, fabricated in PDMS, that was designed for application to evanescent wave biosensors. It comprises a 20 μm deep micro-channel system with sample inlet, open sensing area and outlet in the bottom layer and a sheath flow inlet in the top layer. In [2] a layered flow is used for hydrodynamic addressing, in which a flow is directed to different parts of the flow cell. The concept is designed and implemented for bio-molecular interaction analysis, where the ability to distinguish multiple detection spots in the same flow cell provides improved signal quality and time resolution of the analyses.

In literature also systems have been presented where a layered flow is applied in which the sample liquid is sandwiched between two or more layers of sheath liquid (see Figure 3-1b). In [3] a flow cell is discussed where five layers of liquid are stacked. A flow of conductive sample liquid is sheathed firstly by a flow of electrolyte and secondly by a poorly conducting sheath liquid. The flow cell was designed for particle sizing based on impedance measurements. The system described in [4] applies a sheath flow to focus particles with the purpose to queue them and to ensure that the particles move through the middle of an interrogation zone for size analysis. Another interesting application of a layered sheath flow is found in [5], where a layered flow is used to switch a stream of sample liquid between different outlet branches.

In the flow cells described above only one dimension of the sample liquid is confined by the sheath liquid, in the other dimension the sample flow is fixed by the physical dimensions of the channel. These are not sheath flows in the classical sense, where the sheath liquid surrounds the sample flow on all sides. Only a few flow cells have been presented where a classical, coaxial sheath flow (see Figure 3-1c) was realised on chip. One of the first realisations consists of a miniaturised cytometer configuration [6]. The resulting flow cell is rather complex to fabricate, consisting of a stack of three metal plates sandwiched between two glass plates. Another early device featuring a three-dimensional sheath flow is described in [7]. It consists of a sandwich of four silicon wafers and features silicon nitride windows for optical measurements. More recently less complicated devices were demonstrated where a special 'U-shaped' sample inlet [8] or a circular 'chimney-shaped' sample inlet [9] was used to lift the sample liquid from the bottom of the channel. In these flow cells the shape of the sample flow is fixed by the geometry of the flow cell and therefore these flow cells offer little control over the sample flow dimensions.

All the flow cells described above use a sheath liquid to confine the sample liquid, but also a rare example is known where a gas is used to confine the sample flow [10]. When a gas is used to sheath the sample liquid it is quite difficult to maintain a stable flow, since the surface tension forces tend to break up the sample flow. In the paper mentioned above a stable layered flow was achieved by controlling the surface properties of the channel walls.

In this chapter two new flow cells are presented that are designed for integration in a microfluidics system. These flow cells distinguish themselves from the flow cells found in literature by their versatility. By means of multiple sheath inlets the width, the height and the horizontal position of the sample flow can be controlled individually. One of the flow cells additionally offers control over the position of the sample flow in the vertical dimension. With this high degree of control over the flow profile it is possible to create an optimal sample flow for many different applications. Another attractive property of the flow cells presented here is that they are very simple to fabricate. The flow cells consist of a two-layer structure and the processing is compatible to standard IC-processes, which makes it easy to integrate the flow cells with other components into larger systems.

3.2. Theory

Laminar flow conditions are a prerequisite to have a stable sheath flow. The flow conditions inside a channel are determined by the Reynolds number:

$$Re = \frac{\rho}{\mu} vD \quad (\text{Formula 3-1})$$

In this formula ρ is the density of the liquid, μ is the dynamic viscosity, v is the velocity and D is the diameter of the channel. For channels having a non-circular cross-section the diameter is not well-defined. This is solved by the introduction of the hydraulic equivalent diameter:

$$D_h = 4 \frac{\text{cross - sectional area}}{\text{perimeter}} \quad (\text{Formula 3-2})$$

For a Reynolds number >2300 the flow is typically assumed to be turbulent [11], where for lower values the flow regime is laminar. Due to the small dimensions found in a microsystem the Reynolds number is typically much smaller than 2300 so that these systems show a laminar flow behaviour.

The channel dimensions found in microsystems that apply a sheath flow are typically larger than in devices in which only the sample liquid is present. The larger dimensions increase the Reynolds number for microsystems with a sheath flow somewhat, but the Reynolds number found in practical systems is still quite low. For a channel having a diameter of 500 μm (which is considered very large for a micro-channel) and a watery liquid flowing at 1 m/s, (which is considered a very high speed) the Reynolds number is only 500. So it is safe to say that typically only laminar flow conditions will be encountered in a microsystem.

In the laminar flow regime the main interaction between liquids is by diffusion [12], which is a relative slow process. The laminar flow behaviour and the limited interaction between the sample liquid and the sheath liquid make a sheath flow very suitable to be used with microsystems.

3.3. Design considerations

The classical coaxial sheath-flow is typically formed by a pair of concentric tubes [13]. In the outer tube the sheath-liquid is flowing and by means of the inner tube the sample liquid is injected into the middle of the flow of sheath liquid. Although it is possible to mimic this kind of structure in IC-technology, this leads to quite complex structures like the five-layer device in [6]. This is not attractive because of the large number of processing steps involved and associated costs; an even more fundamental problem is that this kind of complex structures is difficult to integrate with other components in a complete system.

One of the main design considerations for the flow cells developed in this chapter is to make its fabrication compatible to the planar nature of standard IC-processes. A second important design consideration is versatility; the flow cell should be able to create a sheath-flow profile that is suitable for different sensing principles. For example, for an optical evanescent wave sensor the sample flow should ideally have a small height, positioned at the wall of the channel on the same side as the sensor interface [1], while for fluorescence measurements the accurate position of the sample flow is critical.

The design-process was performed based on finite-element simulations. The physics involved under the laminar flow regime is well known and therefore different designs can be accurately simulated. Studying the behaviour of different designs in software has large advantages. Firstly, the simulations save considerable time, since many designs can be studied in a short period of time, where the time required for a design cycle is in the order of hours. In contrast the time of a design cycle to make a real device is typically in the order of months, because of the complicated nature of IC-processes. Secondly, the result of a software simulation allows access to 'internal data'. Parameters such as flow-speed and flow directions of every point inside the structure are readily available. Advanced visualisation techniques such as contour plots and stream-line plots allow insights that are difficult to obtain from experiment. So, simulation allows achieving a higher level of optimisation than would be possible based on measurements alone. Finally, much money can be saved, since fewer processing cycles are required, which are typically very expensive.

3.4. Non-coaxial sheath flow cell

The first flow cell that has been developed generates a non-coaxial sheath flow with dynamic control of the sample flow dimensions (see Figure 3-2). In this flow cell the sheath flow is formed by orthogonally injecting a sample liquid into a channel through which sheath liquid is flowing. Hydrodynamic focussing forms a smooth flow of sample liquid that still touches the bottom of the channel. A focussing section brings the channel width down from 625 μm to a width of 160 μm . The application of such a focussing section allows the use of fairly large inlets which prevents clogging by particles. The less critical alignment of the inlets and the lower pressure drop over the wider section are additional advantages. The dimensions of the sample flow can dynamically be adapted by two orthogonal control mechanisms.

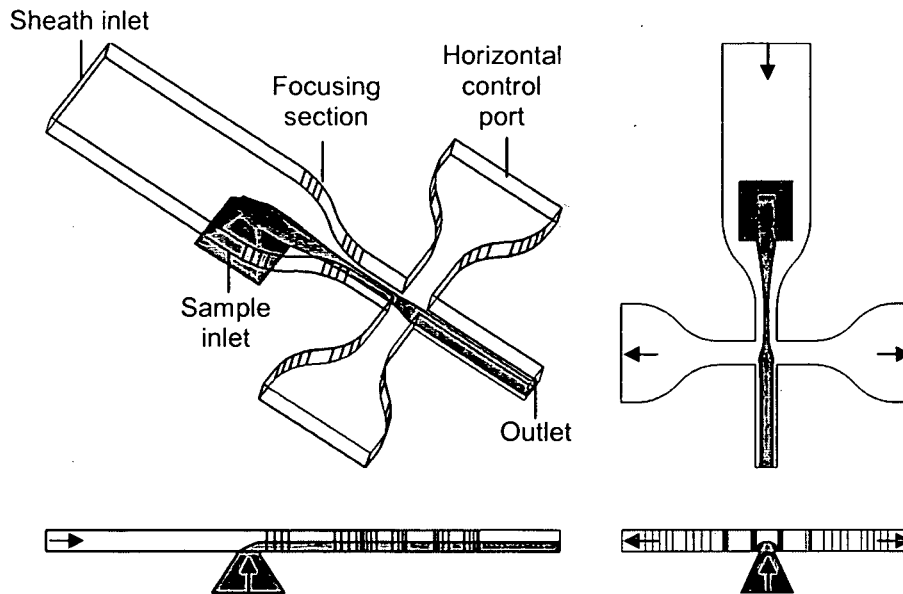


Figure 3-2. Non-coaxial sheath flow cell I: this flow cell creates a non-coaxial sheath flow and allows controlling the sample flow dimensions; here the control ports are used to widen the sample flow.

The vertical dimensions of the sample flow are controlled by the relative flow-rate at which the sample liquid is injected into the sheath liquid. At higher relative flow-rates the sample liquid penetrates further into the sheath liquid, thereby increasing the height of the sample flow. Lowering the relative flow-rate of the sample liquid will result in a sample flow with less height. In Figure 3-3 simulation results are shown, that were obtained using the model shown in Figure 3-2. In the pictures from top to bottom the vertical sample flow control is shown.

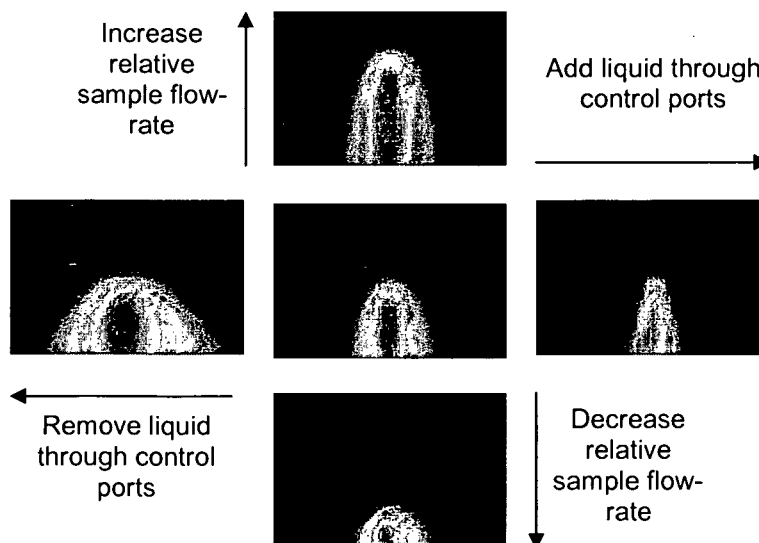


Figure 3-3. Overview of simulation results on the control of the sample flow dimensions in a cross-section of the channel with the non-coaxial sheath flow cell.

The horizontal dimensions of the sample flow are controlled by two horizontal control ports that are located on the sides of the flow-channel, downstream of the sample inlet (see Figure 3-2). By adding or removing sheath liquid through these control ports at an equal rate the already present sheath flow is horizontally compressed or expanded respectively which leads to a narrower or wider sample flow. In Figure 3-3 from left to right this effect is shown. Notice that the height of the sample flow is not affected by this control mechanism. By adding sheath liquid to one of the control ports and removing it at the same rate from the other control port the position of the sample flow can be controlled in the horizontal plane.

3.5. Coaxial sheath flow cell

The coaxial sheath flow cell looks quite similar to the non-coaxial sheath flow cell, but there is one large difference: the coaxial sheath flow cell has an additional inlet, located in between the focussing section and the sample inlet (see Figure 3-4). This additional inlet gives flow cell II the added functionality to freely position the sample flow anywhere inside the flow-channel. Two control mechanisms are in place to achieve this.

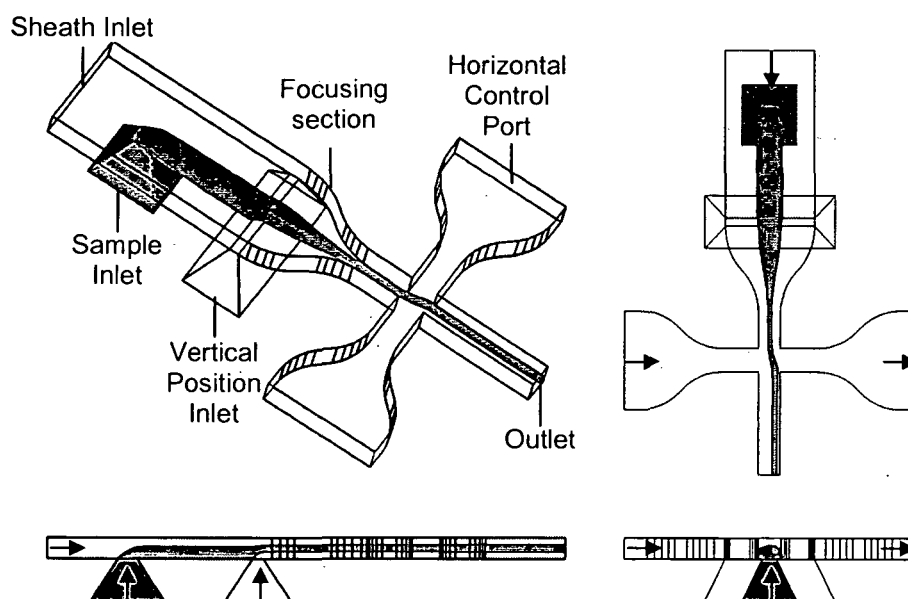


Figure 3-4. Coaxial sheath flow cell: the additional vertical position inlet of this flow cell also allows positioning of the sample flow in the channel; here the control ports are used to position the sample flow vertically in the centre of the channel with a horizontal off-set.

The vertical position of the sample flow is controlled by the additional vertical control inlet. When sheath liquid is added through this inlet the entire sheath flow in the channel is lifted up from the channel bottom. As a result a coaxial sheath flow is formed that no longer has any contact with the channel bottom. The relative amount of liquid that is added through this inlet determines the vertical position of the sample flow. The vertical position control inlet has a narrow shape ($625\ \mu\text{m} \times 50\ \mu\text{m}$) to create a flow profile through the inlet that is as uniform as possible. This ensures that the shape of the sample flow is hardly influenced by the vertical position control, except for some vertical compression. Vertical position control of the sample flow is demonstrated in Figure 3-5 in the pictures from top to bottom.

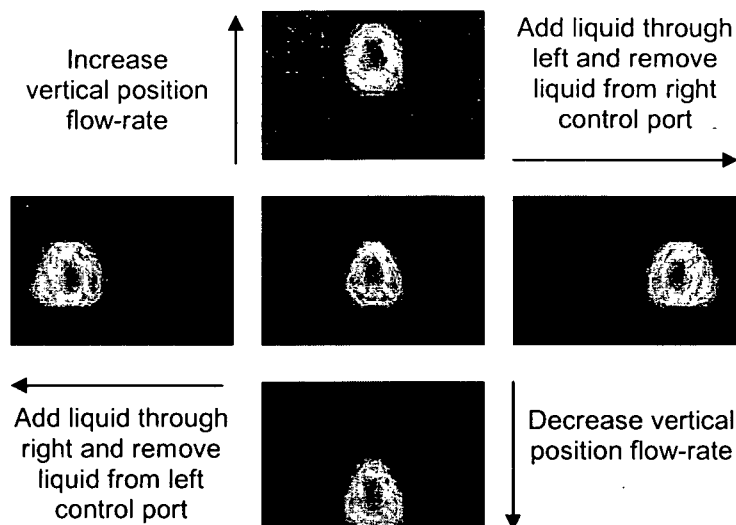


Figure 3-5. Overview of simulation results on the position control of the sample flow in a cross-section of the channel.

Just like in the non-coaxial sheath flow cell the horizontal control ports can also be used to control its horizontal position. In this type of operation the direction of flow through both inlets is opposite. By adding sheath liquid through one of the control ports and removing it from the other control port at the same flow-rate, the sample flow is shifted in the horizontal plane. This is depicted in Figure 3-5 in the pictures from left to right.

Apart from the additional inlet, the configuration of the inlets of the coaxial sheath flow cell is similar to that of the non-coaxial sheath flow cell; therefore the sample dimension control mechanisms described for that flow cell will work for coaxial sheath flow cell as well.

3.6. Experimental verification

Flow cell chips were fabricated based on the process flow that uses wet-etching of glass to form the channels and anodic bonding to join the two wafers, discussed in the previous chapter. A series of experiments has been carried out with the flow cell chips to verify the simulation results presented above. The measurement setup is shown in Figure 3-6. The flow cell chip is placed in a custom holder, which forms an interface between the chip and the tubing. The holder is described in more detail in paragraph 2.6.

Two syringe pumps (kdScientific model 200 series) are used to control the flow-rates at the inlets. Both the sheath liquid and the sample liquid are purified water, where a red dye (standard plotter dye) was added to the sample liquid to visualise the sample flow. The flow cell is positioned underneath a microscope (Zeiss Stemi SV11) that is coupled to a digital still camera (Sony Cybershot DSC-75). The camera captures images of the flow cell for quantitative analysis and comparison with the simulation results.

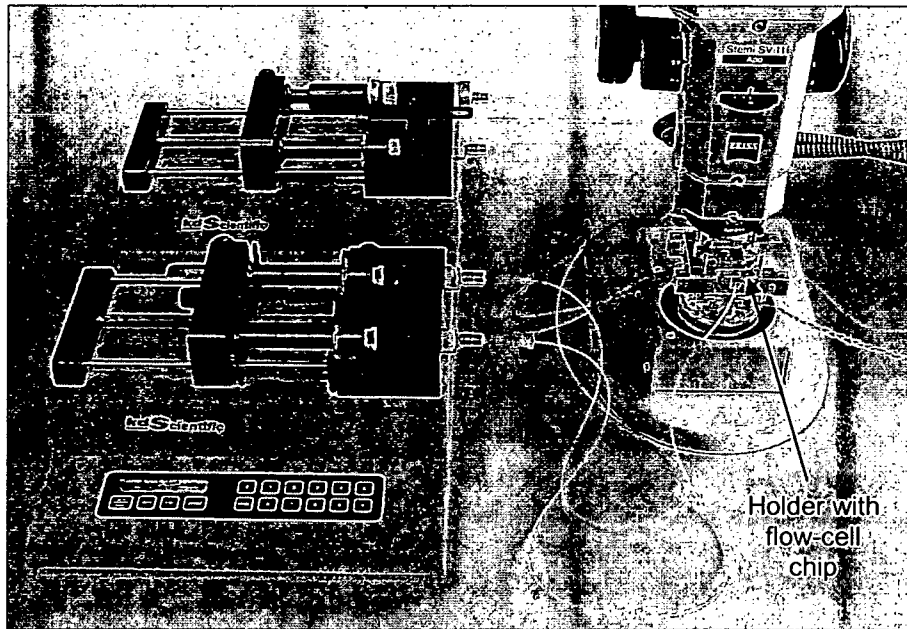


Figure 3-6. Overview of the experiment set-up.

Due to the planar nature of the device it is only possible to analyse it from the top. Performing measurements on the width of the sample flow is straightforward in this configuration, but analysing the vertical dimensions of the sample flow is more complicated. However, by analysing the intensity of the dye, also quantitative information about the sample height can be obtained. Before each series of experiments, photographs were taken of the channel without any dye present and photographs were taken when the channel was completely filled with the dye. After the experiment the height of the sample flow was calculated by regression between these two references. To obtain a reliable result each measurement point was taken from the average of three photographs. The noise was reduced by averaging the intensity of the dye over 100 adjacent image lines. The area of the photographs that was used in the experiments is marked with the dotted white squares in Figures 3-7, 3-9 and 3-11. Unfortunately, analysing the vertical position of the sample flow from the top is not possible with this method; therefore it was decided to base the experiments only on the non-coaxial sheath flow cell.

Simulations were performed using the *Netflow* module of the finite element package *Coventorware 2001.3*. Detailed models of up to 100,000 elements with a well designed grid were required to obtain a sufficiently high accuracy. Besides the geometry of the model and the flow-rates also the diffusion constant of the dye was included in the simulations. From the simulation results the height of the sample flow could easily be obtained by just summing the concentrations of the sample distribution along the vertical axis for all data points in the measurement area. The experimental results and the simulation results are compared by plotting them in the same graph.

3.6.1. Sample diffusion

A reference experiment was carried out to determine the influence of diffusion and to see how well it can be modelled. In this experiment the ratios of the flow-rate of the sample liquid, the flow-rate through the control ports and the flow-rate of the sheath-liquid were kept constant at 1:5:10. During the experiment the total flow-rate was varied from 1-50 $\mu\text{l}/\text{min}$. The intensity of the dye was measured in the wider section following the narrow section (see Figure 3-7), since in this location the visible area is not blocked so much by the rounded corners of the isotropic etching of the channel. A detailed finite element model similar to the one in Figure 3-2 was made, but the model used here mimics the experimental device by having a wide section following the narrow section so that the quantitative data from the simulations can be obtained in the same location as in the experiment. In Figure 3-7 some illustrative results of the experiments are shown.

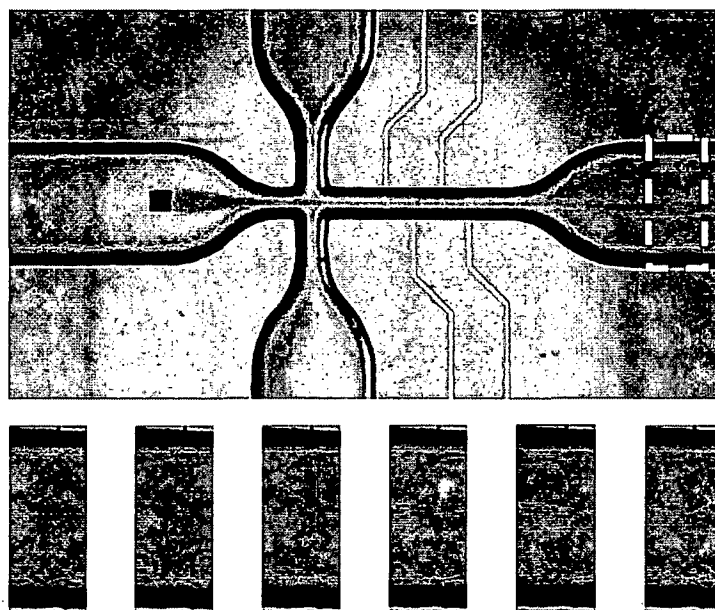


Figure 3-7. Illustrative results from the diffusion experiment.

Figure 3-8 compares the quantitative results of simulation and the experiment. The two sets of curves match well and clearly show the influence of diffusion. At higher flow-rates a narrow, high concentration sample flow is formed, while at lower flow-rates the sample flow broadens and gets diluted.

In the following paragraphs the control mechanisms for the height and the width of the sample flow will be analysed. The measurements have been carried out at a flow-rate above 10 $\mu\text{l}/\text{s}$ to prevent the diffusion from obscuring the effects of the control mechanisms.

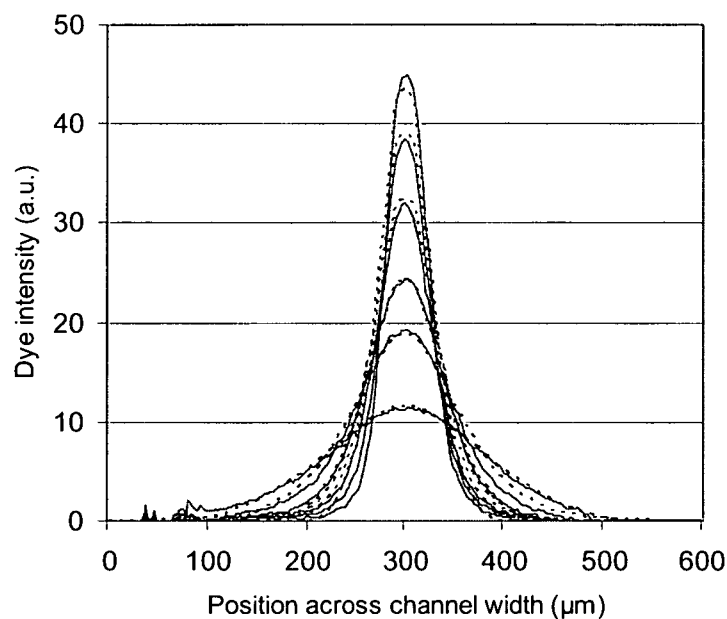


Figure 3-8. Quantitative comparison of the simulation results (dashed) and the experimental results (solid) for the diffusion experiment.

3.6.2. Vertical control of sample flow dimensions

A series of measurements was performed in which the vertical dimensions of the sample flow were controlled. Since for this measurement the width control of the sample was not necessary, a device without horizontal control ports was used which is for the rest similar to flow cell I. During the experiment the flow-rate of the sheath liquid was kept constant at 10 $\mu\text{l}/\text{min}$ and the sample liquid was injected at six different flow-rates in a range from 0.05 to 2 $\mu\text{l}/\text{min}$, which corresponds to a relative sample flow-rate of 0.5% to 20% of the sheath flow-rate.

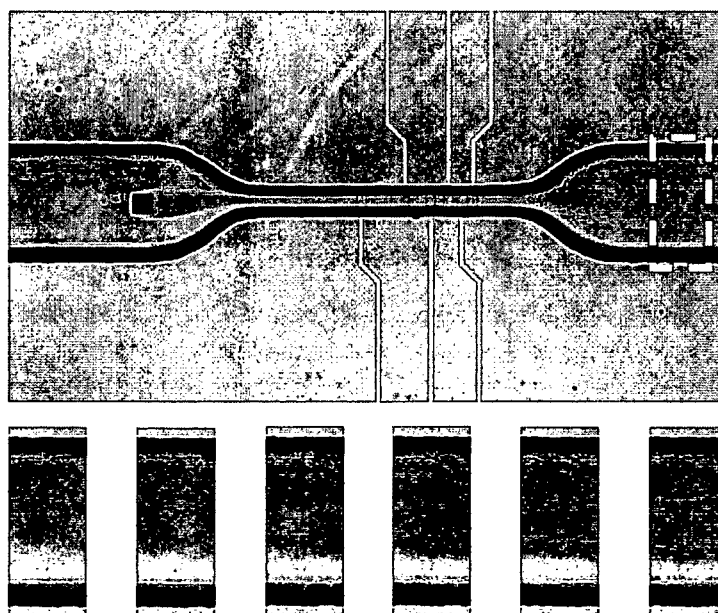


Figure 3-9. Illustrative results from the sample height control experiment.

The intensity of the dye was measured at the same location: in the wide section of the channel, downstream of the narrow section. Some illustrative results are depicted in Figure 3-9. Figure 3-10 shows the quantitative results obtained in this experiment. The height of the sample can be controlled over a wide range. For the relative flow-rates used in the experiment the height of the sample flow can be controlled in a range from 3 to 60 μm in a channel with a depth of 100 μm . In it can be seen that the width of the sample is constant for the smaller flow-rates, only at the highest flow-rate the sample flow becomes slightly wider. For the height control of the sample flow there is a good match between the finite element simulations and the experimental results. The slight mismatch at the highest vertical dimension is due to saturation of the camera for the red colour.

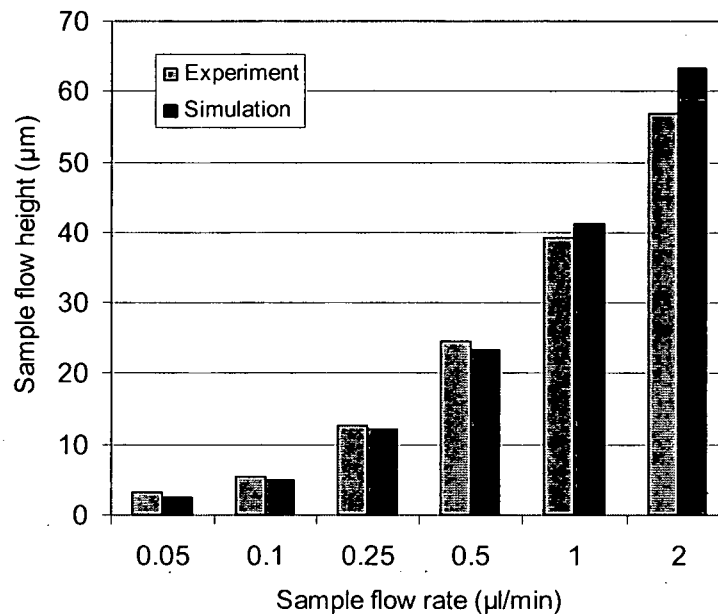


Figure 3-10. Comparison of the simulation results and the experimental results for the sample height control experiment.

3.6.3. Horizontal control of sample flow dimensions

Next a series of measurements was performed in which the horizontal dimensions of the sample flow were controlled. During this experiment the sheath liquid and sample liquid flow-rates were kept constant at 10 $\mu\text{l}/\text{min}$ and 1 $\mu\text{l}/\text{min}$ respectively. The flow-rate through each control port was varied from -3 to +25 $\mu\text{l}/\text{min}$. The dye was measured at the same location as in the previous experiments; here it was even more important to have a visible area that is maximally wide. Some illustrative results are depicted in Figure 3-11, where the size of the arrows indicates the flow-rate.

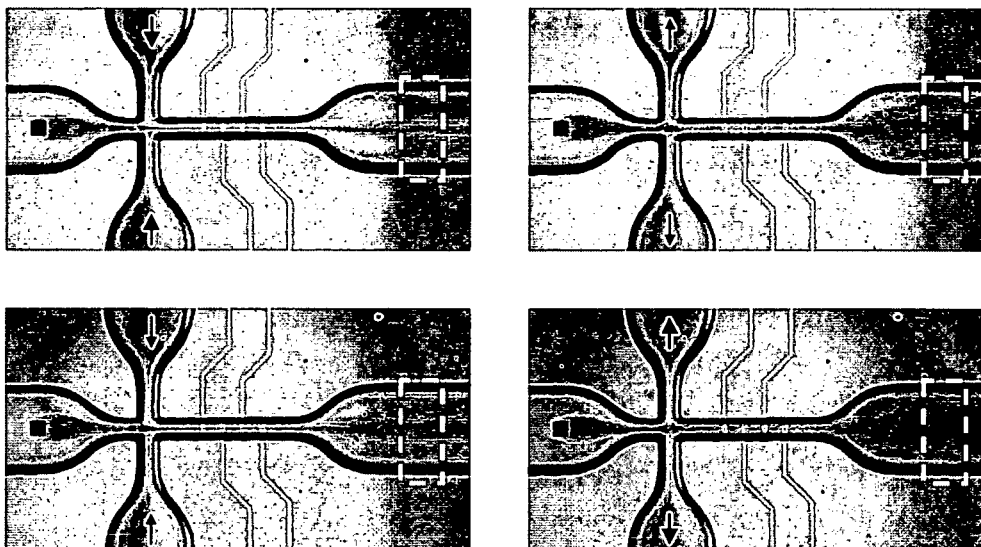


Figure 3-11. Illustrative results from the sample width control experiment.

The quantitative results in Figure 3-12 show that the width of the sample flow can be controlled over a wide range: for the flow-rates used in the experiment the width of the sample flow varies from 40 to 292 μm in the wide part of the channel, which has a width of 625 μm . As a result the width of the sample flow in the narrow section where the sensor should be positioned (width 160 μm) is varied in the range from 10 to 73 μm . The width of the sample flow is defined here as the width of the sample at 50% of the maximum dye intensity. Also for the horizontal control of the sample flow dimension the results show a good match between simulation and experimental results.

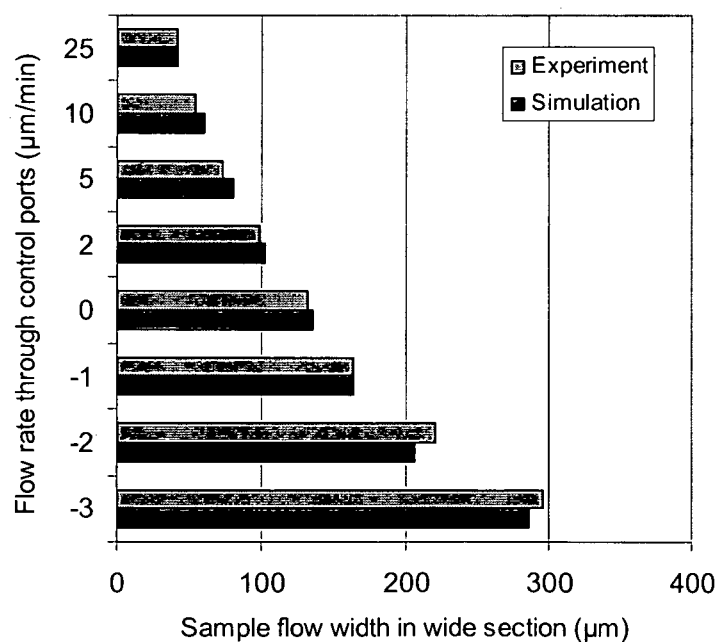


Figure 3-12. Comparison of the simulation results and the experimental results for the sample width control experiment.

3.7. Sample flow splitting and switching

The flow cell used in the experiment turned out to be a very versatile device. Besides the horizontal and vertical control of the sample also other useful functions can be realised. The first example is sample splitting. For this application only one control port is used. Through this inlet 50% of the total flow of liquid is removed. The result is an equal splitting of the sample (see Figure 3-13). By removing more or less liquid through the control port an unequal splitting of the sample is also possible of course.

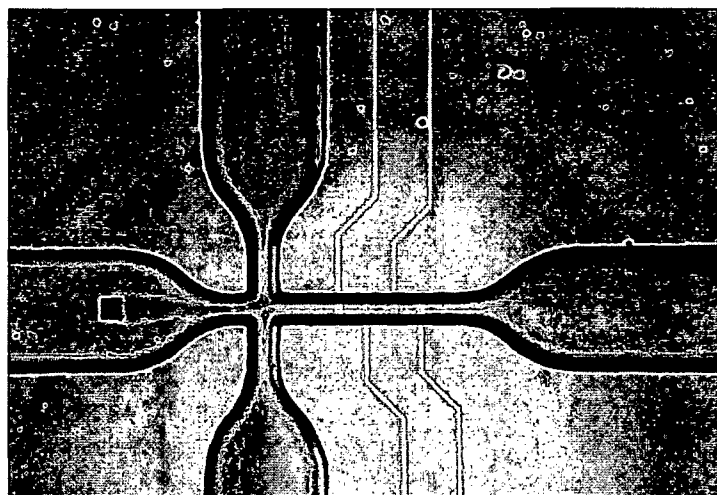


Figure 3-13. The flow cell applied for sample splitting.

A second example of the versatility of the flow cell is sample switching. Here again only one control port needs to be active. This time the liquid is removed through the control port at a flow-rate that equals the flow-rate of the total flow of liquid. As a result the complete sheath flow including the sample liquid is switched (see Figure 3-14). When a coaxial sheath flow is used this is even possible without the sample liquid touching the wall of the channel.

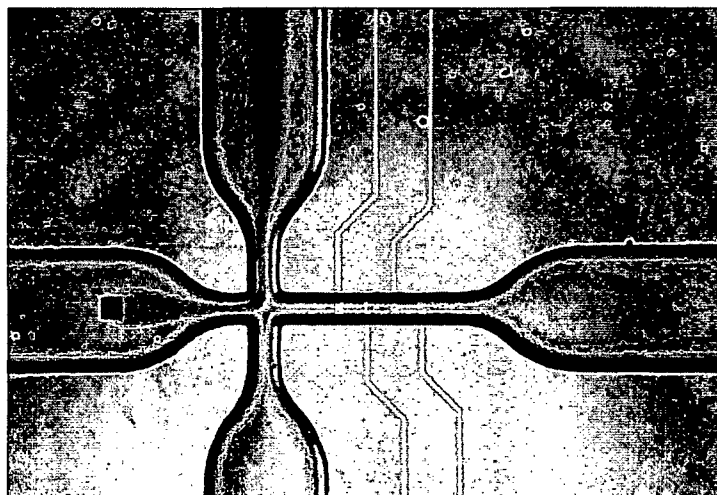


Figure 3-14. The flow cell applied for flow-switching.

3.8. Conclusions

Two new flow cells have been developed that are very versatile. The flow cells can generate both non-coaxial and coaxial sheath flows. Using an orthogonal control mechanism the flow cells allow dynamic control of the sample flow dimensions. With one additional vertical position inlet the sample flow can also be freely positioned inside the channel. The processing of the flow cells is very simple, and can be easily combined with the integration of sensors to form a complete integrated analysis system.

Experiments were carried out with one of the flow cells and a comparison of experimental results and simulation results show that the complicated flow behaviour of the device can be modelled very accurately. Also the influence of diffusion is realistically taken into account. The results on the horizontal and vertical control of the sample flow dimensions show that both mechanisms work well and that they can be predicted from simulation results. The control ports make the flow cells very versatile so that they can also be used for other applications such as sample splitting and flow switching.

3.9. References

- [1] O. Hofmann, P. Niedermann, and A. Manz, "Modular Approach to Fabrication of Three-Dimensional Microchannel Systems in PDMS - Application to Sheath Flow Microchips," *Lab on a Chip*, vol. 1, pp. 108-114, 2001.
- [2] M. Tidare, H. Roos, and U. Lindberg, "Hydrodynamic Addressing; A Flow Cell for Improved Signal Quality in Bioanalytical Systems," presented at Transducers '01, Munich, Germany, 2001.
- [3] U. D. Larsen, G. Blankenstein, and J. Branebjerg, "Microchip Coulter particle counter," presented at Transducers '97, Chicago, USA, 1997.
- [4] K. Roberts, M. Parameswaran, M. Moore, and R. S. Muller, "A Silicon Microfabricated Aperture for Counting Cells using the Aperture Impedance Technique," presented at IEEE Canadian Conference on Electrical and Computer Engineering, Edmonton, Alberta, Canada, 1999.
- [5] G. Lee, B. Hwei, and G. Huang, "Microfluidic Chips with MxN Continuous Sample Introduction Function Using Hydrodynamic Flow Switching," presented at Transducers '01, Munich, Germany, 2001.
- [6] R. Miyake, H. Ohki, I. Yamazaki, and R. Yabe, "A Development of Micro Sheath Flow Chamber," presented at MEMS '91, Nara, Japan, 1991.
- [7] D. Sobek, A. M. Young, M. L. Gray, and S. D. Senturia, "A microfabricated flow chamber for optical measurements in fluids," presented at MEMS '93, Fort Lauderdale, USA, 1993.
- [8] K. Tashiro, T. Sekiguchi, S. Shoji, T. Funatsu, W. Masumoto, and H. Sato, "Design and Simulation of Particles and Biomolecules Handling Micro Flow Cells with Three Dimensional Sheath Flow," presented at MicroTAS 2000, Enschede, The Netherlands, 2000.
- [9] A. Wolff, U. D. Larsen, P. Friis, and P. Telleman, "Chip-Integrated Microfluidic System for Cell Sorting and Cell Culturing," presented at Eurosensors XIV, Copenhagen, Denmark, 2000.
- [10] D. Huh, Y. Tung, H. Wei, J. B. Grotberg, S. J. Skerlos, K. Kurabayashi, and S. Takayama, "Use of Air-Liquid Two-Phase Flow in Hydrophobic Microfluidic Channels for Disposable Flow Cytometers," *Biomedical Microdevices*, vol. 4, pp. 121-149, 2002.

- [11] P. Gravesen, J. Branebjerg, and O. S. Jensen, "Microfluidics - A review," *Journal of Micromechanics and Microengineering*, vol. 3, pp. 168-182, 1993.
- [12] M. Koch, A. Evans, and A. Brunnschweiler, *Microfluidic Technology and Applications*, 1st ed. Baldock: Research Studies Press Ltd., 2000.
- [13] J. V. Watson, *Introduction to flow cytometry*, 1st ed. Cambridge: Cambridge University Press, 1991.

Chapter 4

Integrated Coulter counter

4.1. Introduction

In this chapter the development of an integrated Coulter counter is discussed. The Coulter counter is a well established instrument in the medical and industrial field to determine the size distribution of particles. It was invented by Wallace H. Coulter in 1949 [1]. In the classical Coulter counter a conductive medium suspending the particles to be analysed is pumped through a small aperture, the Coulter aperture, while the impedance over the aperture is monitored (see Figure 4-1). When a particle passes through the aperture some of the conductive liquid is displaced by the particle. This causes an increase in impedance over the aperture that is proportional to the volume of the particle.

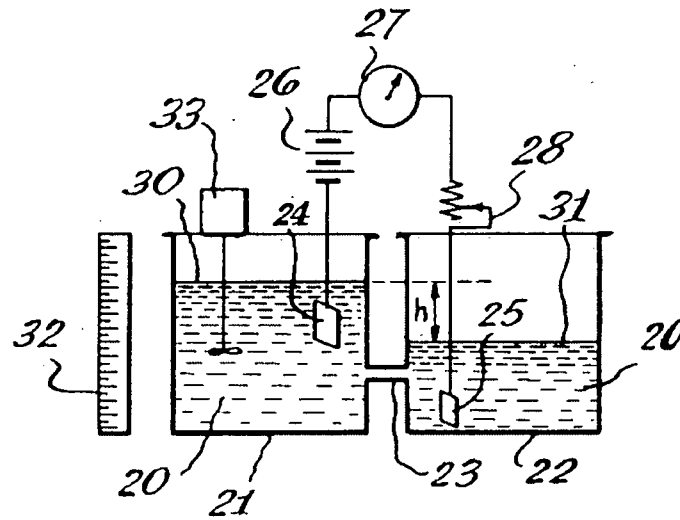


Figure 4-1. Schematic overview of the Coulter counter from the original patent US 2,656,508 (<http://www.uspto.gov>). A conductive liquid suspending the particles to be analysed (20) is moved through a small aperture (23) from one vessel (21) into the other (22) by different levels of liquid (30, 31). The impedance over the aperture is measured using two electrodes (24, 25) that are connected to a readout circuit, which consists of a battery (26), current meter (27) and a variable resistor (28). The instrument is equipped with an agitator (33) to keep the particles suspended and a graduated scale alongside the vessel (32) to measure the change of volume.

For many medical and scientific applications the diameter of the Coulter aperture ranges from approximately 30-200 μm . Because of the small dimensions involved, integrated circuit technology has been used to fabricate the Coulter aperture. In [2] a micro-machined Coulter aperture is discussed that was developed for somatic cell counts in dairy products. The aperture for this Coulter counter was fabricated by reactive ion etching a hole through a silicon membrane. A more advanced device is presented in [3]. Besides the Coulter aperture it also comprises a chamber with a channel on each side to form a sheath flow that focuses the particles through the middle of the aperture.

Not only parts of a Coulter counter, but also complete Coulter counters have been presented that were fabricated in IC-technology. The Coulter counter discussed in [4] has been fabricated from a sandwich of a silicon wafer and a glass wafer. It has a mechanical pre-filter structure that prevents the aperture from getting blocked. The electrodes to measure the impedance have been integrated in the aperture and are made of titanium, embedded between two layers of silicon nitride.

A Coulter counter that was fabricated using two glass wafers is discussed in [5]. The channels have been formed by isotropic etching and ultrasonic drilling was used to make through-holes that form the inlets for the liquid. The Coulter counter has a pair of platinum electrodes that were fabricated using a lift-off process. Resistive and reactive particle impedance measurements were performed based on multi-frequency measurements.

Another interesting example of an integrated Coulter counter is found in [6]. Here a Coulter counter is discussed for cell counting in haematology applications. The channel and the electrodes were realised on a glass substrate and a PDMS film was used to seal the channel. Impedance measurements were performed with a 3-electrode setup.

All of the devices discussed above use a classical Coulter setup with a fixed Coulter aperture. In these devices the size of the aperture is a trade-off between sensitivity and reliability: the smaller the aperture the higher the sensitivity, but at the same time the chance of clogging increases. Especially smaller apertures are easily blocked, requiring sample pre-treatment by sedimentation or wet-sieving to remove any larger particles [7]. Another limitation of the classical Coulter counter is that it is frequently necessary to physically exchange the apertures in between runs, since the operative size range is 3-40% of the diameter of the Coulter aperture [8].

In [9] it was proposed for the first time to make a Coulter aperture that can be adapted in one dimension, using a laminated flow profile that consists of a combination of organic and inorganic liquids. A drawback of this approach is that the interface between the liquids can be unstable due to surface tension forces between the liquids. Because of the applied laminated flow profile the aperture can only be adapted in one dimension, which limits the adaptivity of the sensitivity.

In this chapter an integrated Coulter counter chip will be discussed that has a liquid aperture that can be adapted in two dimensions. Problems with surface tensions between the sample liquid and the sheath liquid are avoided by using an aqueous liquid for both the sheath liquid and the sample liquid.

4.2. Aperture control

The basic assumption for the Coulter principle is the dependence of the electrical output on particle volume. Assuming that the particle in the capillary has an infinite resistivity, the change in impedance depends on the integral of the particle cross-section. For an ideal homogeneous electrical field and a spherical particle the change in resistance becomes [10]:

$$\Delta R = 2\rho_{liquid} \left(\arctan \left(\frac{r_{particle}}{\sqrt{\frac{A_{channel}}{\pi} - r_{particle}^2}} \right) \right) / \left(\pi \sqrt{\frac{A_{channel}}{\pi} - r_{particle}^2} - \frac{r_{particle}^2}{A_{channel}} \right) \quad (formula 4-1)$$

where ρ_{liquid} is the impedance of the sample liquid, $r_{particle}$ is the radius of the particle and $A_{channel}$ is the cross-sectional area of the aperture. The formula shows that the ratio between particle size and the area of the aperture determines the sensitivity of the instrument. In the derivation of this formula it was assumed that the length of the Coulter aperture equals the diameter of the particle. In practice the aperture length will typically be larger, which reduces the observed change in impedance.

The Coulter discussed in this chapter is based on the non-coaxial sheath flow cell described in the previous chapter. For the Coulter counter application the sheath flow consists of a conductive sample liquid that is surrounded on three sides by a non-conductive sheath liquid.

The electrical behaviour of the Coulter counter is only determined by the conductive liquid, so the Coulter aperture is defined by the dimensions of the sample flow. In the narrow section of the channel a pair of electrodes has been added to measure the impedance of the sample liquid (see Figure 4-2).

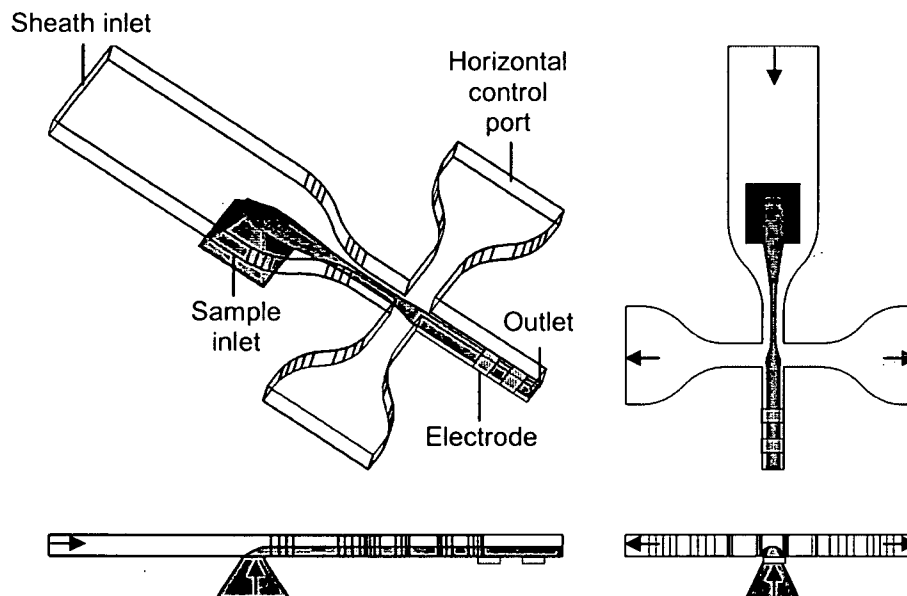


Figure 4-2. The Coulter aperture can be controlled in two dimensions by varying the relative flow-rates at the inlets; here the control inlets are used to widen the Coulter aperture.

The control mechanisms to adapt the dimensions of the sample flow that were discussed in the previous chapter can be used to adapt the dimensions of the Coulter aperture. This allows dynamically adapting the sensitivity of the Coulter counter, without the need to exchange parts. Besides the possibility to dynamically adapt its sensitivity, the liquid aperture has another advantage. The dimension of the Coulter aperture and the physical dimensions of the flow channel are decoupled. This means that the dimensions of the Coulter aperture do no longer determine the chance of clogging. Therefore, the liquid aperture allows working with a smaller Coulter aperture than would be possible with a fixed aperture, resulting in a higher sensitivity.

The applied sheath flow is non-coaxial, so that the liquid can be easily contacted by electrodes integrated in the bottom of the channel (see Figure 4-2). The resulting interrogation volume is very small, which reduces the chance of particle coincidence and allows analysing suspensions having a relatively high particle concentration.

A combination of a polar and a non-polar liquid to define the Coulter aperture seems attractive from an electrical point of view, where oil can be used as a non-conductive sheath liquid. However, as mentioned in the introduction, this may lead to unstable flow conditions due to surface tension effects at the liquid-liquid interface. Stable two-phase flows have been described in literature, where a guide structure is used to stabilise the flow [11]. Unfortunately the fixed geometry of the guide structures is not compatible with the adaptable Coulter aperture and therefore another solution is required.

The stability problems can also be prevented by using aqueous liquids for both the sheath liquid and the sample liquid; such a sheath flow is inherently stable. However, this introduces a new problem that has to be considered: the conductive ions of the sample liquid can now diffuse

from the sample liquid into the sheath liquid, thereby enlarging the dimensions of the Coulter aperture and affecting the sensitivity of the device.

4.3. Device simulation

To investigate the influence of diffusion the Coulter counter was modelled and finite element simulations were carried out with *Coventorware 2003.1*. In these simulations purified water was used as a sheath liquid and a NaCl-solution was used as sample liquid. In Figure 4-3 the concentration of the ions at a cross-section of the channel at the electrode location is depicted, which defines the dimensions of the Coulter aperture. These results show that the influence of diffusion on the dimensions of the Coulter aperture is limited for flow-rates higher than 0.5 $\mu\text{l/s}$. This flow-rate can be considered the lowest flow-rate at which the Coulter counter can be operated, without losing sensitivity.

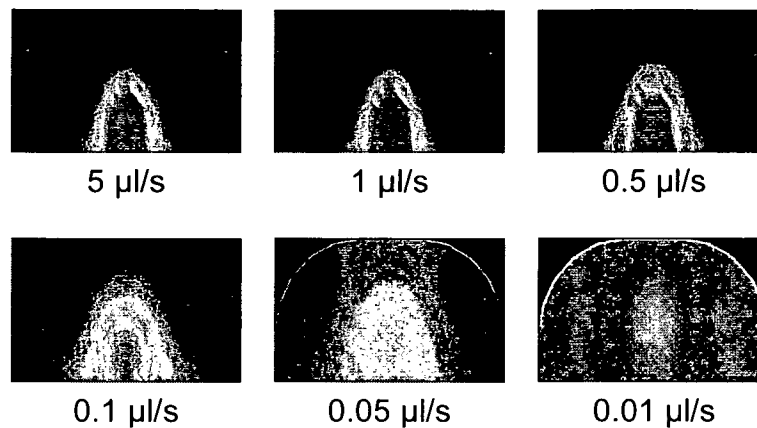


Figure 4-3. Simulation results of the influence by diffusion on the distribution of the Na^+ and Cl^- ions for different flow-rates for a cross-section of the channel at the electrode location.

To get repeatable measurement results, the electric field between the electrodes needs to be homogenous, so that the measured change in impedance does not depend on the position of the particle within the aperture. A homogeneous field is achieved when the spacing between the electrodes is sufficiently large with respect to the channel height. On the other hand the spacing between the electrodes should not be too large, because a larger spacing between the electrodes enlarges the interrogation volume, which increases the chance of particle coincidence. Furthermore, the relative change in impedance as a result of the presence of a particle decreases, since the total impedance between the electrodes goes up for larger electrode spacing.

Finite element simulations were carried to determine the minimum electrode spacing (see Figure 4-4). It was found that the current density varies less than 5% over the full aperture, when the electrode spacing is at least two times as large as the aperture height. The largest Coulter aperture that will be used measures 50 μm ; this leads to a minimum electrode spacing of 100 μm .

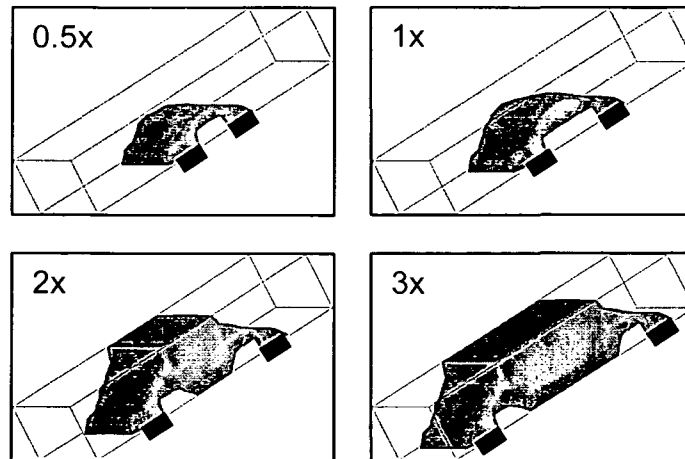


Figure 4-4. The current density distribution between 5% limits for an electrode spacing of 0.5, 1, 2 and 3 times the aperture height, respectively.

The pressure drop over the device has also been analysed, both analytically and based on finite element simulations. The results are depicted in Figure 4-5. From the graph it can be concluded that the main losses are viscous losses, since there is a linear dependency between pressure loss and flow-rate. The finite element results show a good match with the analytical results, demonstrating that the pressure drop over the device is limited to less than 40 kPa. At the highest flow-rates non-viscous (minor) losses start to appear in the simulation results, marked by a slightly steeper incline at the end of the curve.

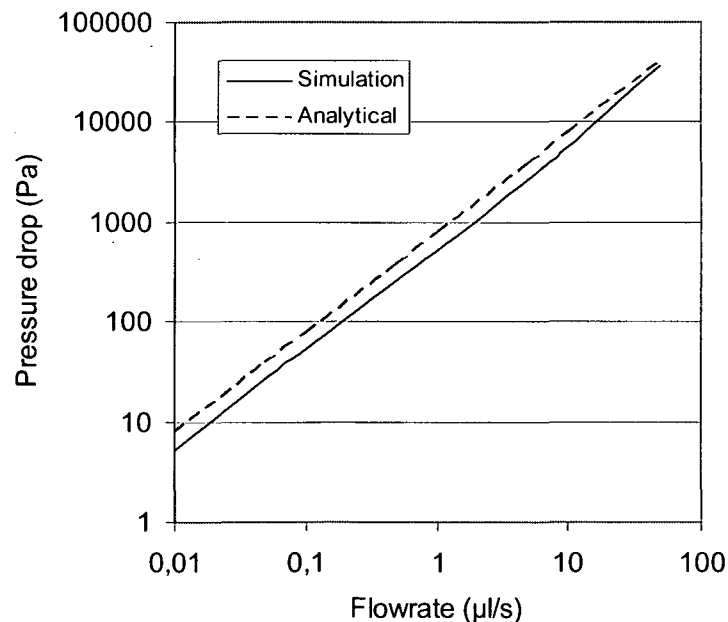


Figure 4-5. Analytical calculations (Analytical) and finite element simulations (Simulation) of the pressure drop over the Coulter counter as a function of flow-rate.

To investigate where minor-losses started to appear first, the model was divided into five sections and the relative pressure drop was extracted over each section. The results are shown in Figure 4-6.

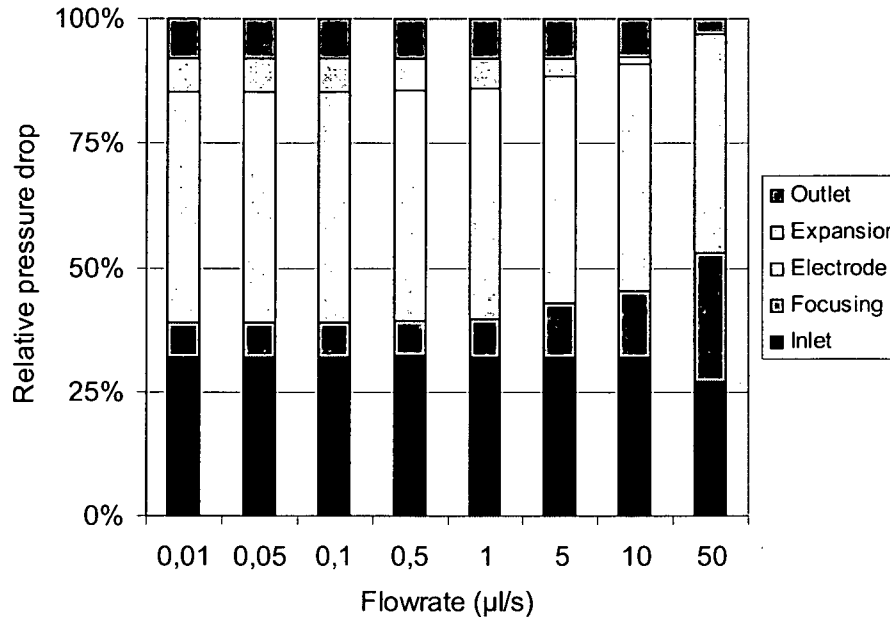


Figure 4-6. Finite element simulation results of the relative pressure drop over the different sections of the Coulter counter; at the highest flow-rates non-viscous losses start to become dominant.

At lower flow-rates the distribution of the pressure drop over the five sections is constant, but for flow-rates of 5 µl/s and up the relative pressure drop over the focusing section (the section between the sample inlet and the electrodes) increases and the pressure drop over the expansion section (the section between the electrodes and the outlet) almost disappears. The dominance of minor losses typically comes with the generation of vortices and other flow irregularities, so a flow-rate of 10 µl/s can be considered the upper boundary for the Coulter counter chip; this corresponds to a maximum liquid velocity of about 1 m/s in the section with the electrodes. Here one has to take into account that the particles travel at speeds lower than the maximum flow-speed of the liquid, because of the parabolic velocity-profile and the fact that the particles follow a trajectory close to the bottom wall.

The minimum flow-rate for the Coulter counter chip is thus determined by diffusion and the maximum flow-rate is restricted by the occurrence of non-smooth flow behaviour. This operation range can be shifted by changing the length of the focussing section between the sample inlet and the location of the electrodes. When this distance is decreased, the minimum flow-rate lowers, since the liquid would have to travel a shorter distance to the measurement area, thereby reducing the time for diffusion. Due to the more sudden contraction that would be present in this situation, non-laminar flow behaviour would start to occur at lower flow-rates thereby lowering the maximum flow-rate as well. When the focusing section is made longer the opposite situation occurs, shifting the operation range to higher flow-rates.

4.4. Device fabrication

The Coulter counter was fabricated based on the anodic bonding process described in Chapter 2. Therefore, only the processing of the silicon wafer will be discussed in detail here (see Figure 4-7). In the first step a dry-etching process is used to form trenches with a depth of $0.6\ \mu\text{m}$ in which later the electrodes will be positioned (I). Next an oxide layer is grown (II) with a thickness of $0.5\ \mu\text{m}$ to isolate the electrodes from the substrate. Subsequently gold electrodes (thickness $0.6\ \mu\text{m}$) are deposited by a lift-off technique (III) where chromium is used as an adhesion layer. Because the depth of the recess matches the thickness of the electrodes, the top of the electrodes is at the same level as the wafer surface. The processing of the silicon wafer is completed with an isotropic etching step from the back-side of the wafer that defines through-holes, which form the liquid inlets and outlet of the device (IV). The Coulter chips are finished by bonding the silicon wafer to a glass wafer that has a recess (V). A photograph of a Coulter chip is depicted in Figure 4-8.

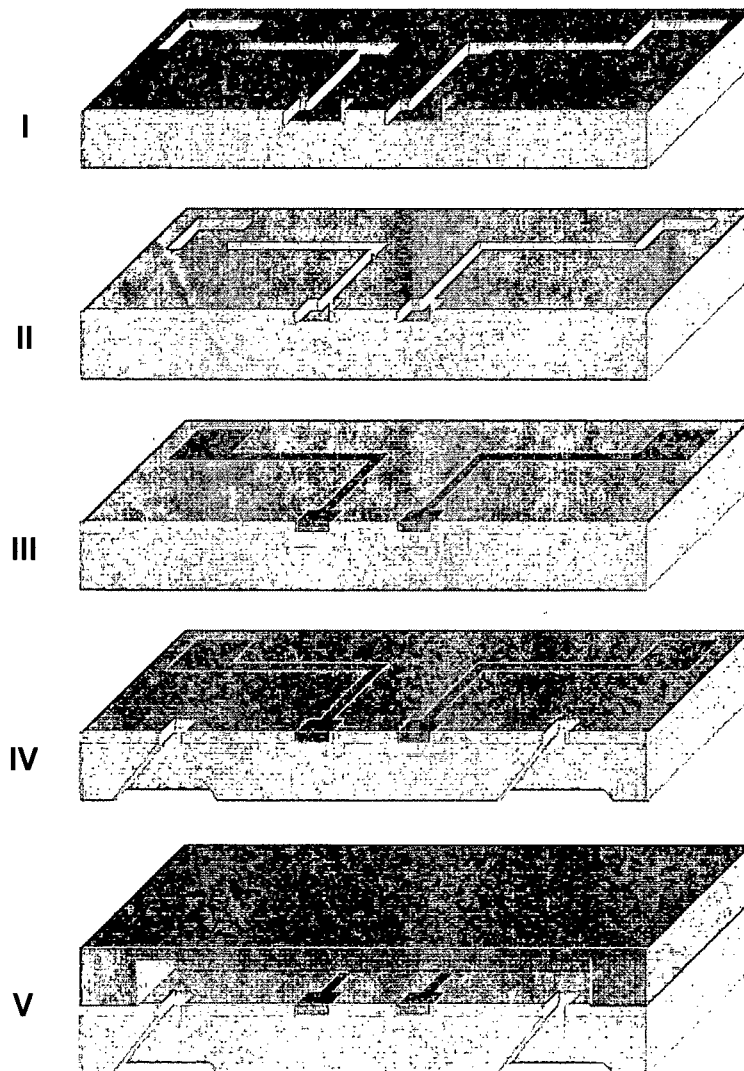


Figure 4-7. Schematic overview of the fabrication of the Coulter counter chip.

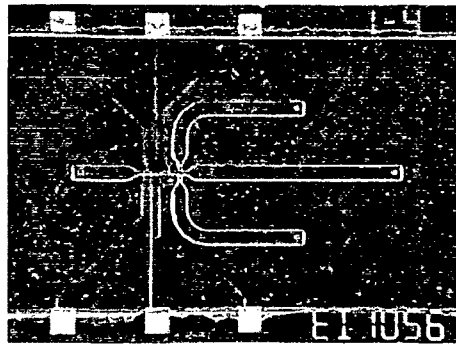


Figure 4-8. A photograph of the completed Coulter chip ($1.5 \times 2 \text{ cm}^2$).

4.5. Experimental

The impedance changes are measured by two gold electrodes located on the bottom of the channel. The electrodes have dimensions of $100 \times 150 \mu\text{m}^2$ with a spacing of $100 \mu\text{m}$. They are connected to large pads of $1 \times 1 \text{ mm}^2$ (see Figure 4-8) that are contacted with spring pins. A simplified electrical model of this configuration is shown in Figure 4-9, where R represents the resistance of the liquid (which is altered by the presence of a particle). C_{DL} is the double layer capacitance with a value of 3 nF (assuming $0.2 \text{ pF}/\mu\text{m}^2$ [12]) and C_{SUB} represents the parasitic coupling to the (grounded) silicon substrate with a value of 75 pF .

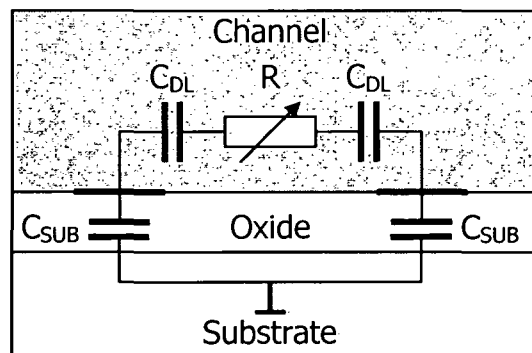


Figure 4-9. Simplified electrical model of the Coulter counter chip that comprises the impedance R (which is altered by the presence of a particle), the double layer capacitances C_{DL} and the substrate capacitances C_{SUB} .

The parasitic capacitances C_{SUB} are rather large because of the large size of the contact pads (required for the spring pins) and the thin isolating oxide (limited by the anodic bonding). As a consequence the measurement frequency has to be carefully selected depending on the channel impedance R . If the measurement frequency is too low the relative impedance change measured would be very small due to the high impedance of the double layer capacitances that are in series with R . But the frequency should also not be too high otherwise the main signal path would be through the substrate instead of through R , due to the low impedance of C_{SUB} , which would decrease the changes in the measured impedance due to the particles. Because of this tight balance the simplified model was extended to a model of the complete measurement set-up, including the trans-impedance amplifier and parasitic cable capacitances.

Based on simulations with this model the following measurement conditions were selected for an aperture of about $30 \times 35 \mu\text{m}^2$: a measurement frequency of 50 kHz and a 5% NaCl-solution with a conductivity of 7.8 S/m. These conditions lead to an impedance of about 5-10 k Ω .

The electrical signal path is as follows (see Figure 4-10): the built-in oscillator of the lock-in amplifier (Stanford Research SR830) generates an AC-voltage of 20 mV RMS. This is supplied to the Coulter chip by spring pins. When a particle passes through the Coulter aperture this AC signal is modulated. The modulated signal is then amplified with a trans-impedance amplifier based on a single opamp (National Semiconductor LF357) with feedback network. Subsequently the signal is demodulated and filtered by the lock-in amplifier and the resulting DC-signal is recorded with a digital memory oscilloscope (Tektronix TDS220).

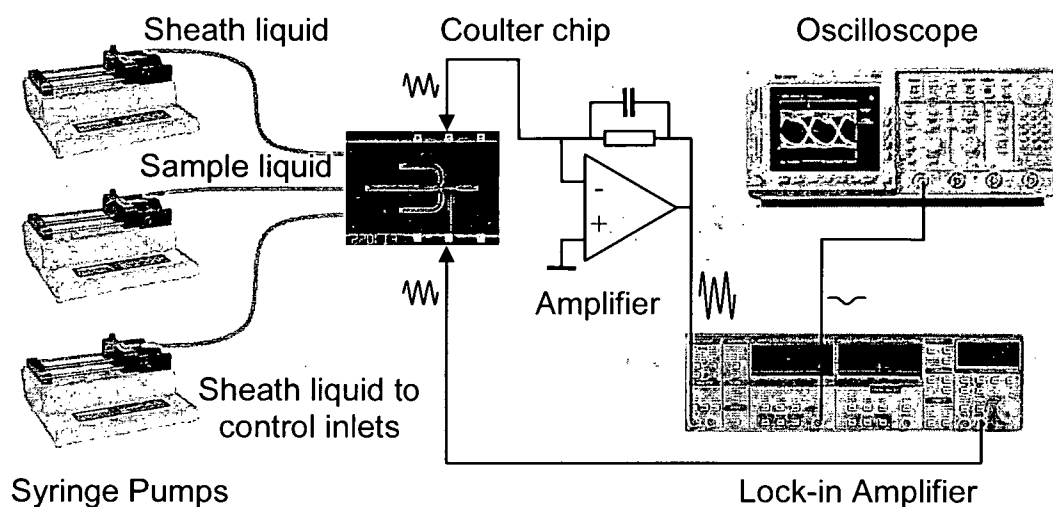


Figure 4-10. Schematic overview of the complete experimental setup with the fluidics part on the left and the electrical part on the right.

Three syringe pumps (kdScientific model 200 series) control the flow-rates of the sample liquid and sheath liquid. During the actual measurements a liquid aperture of approximately $30 \times 35 \mu\text{m}^2$ was used, by applying flow-rates of $0.67 \mu\text{l/s}$, $0.17 \mu\text{l/s}$ and $0.05 \mu\text{l/s}$ at the sheath inlet, control inlets and sample inlet respectively. The particles used are polymer particles (Duke Scientific) with a radius of $12 \mu\text{m}$. The sheath liquid consists of DI-water and at the measurement locations the physical channel has dimensions of $160 \mu\text{m} \times 100 \mu\text{m}$ (width x height).

A typical response is depicted in Figure 4-11, where a change in impedance of about 25% is observed. Without any liquid aperture, the impedance change of a passing particle would be only 0.5% for a channel with these dimensions and an aperture length of $100 \mu\text{m}$. This means 50 times higher sensitivity has been achieved with the same physical channel dimensions.

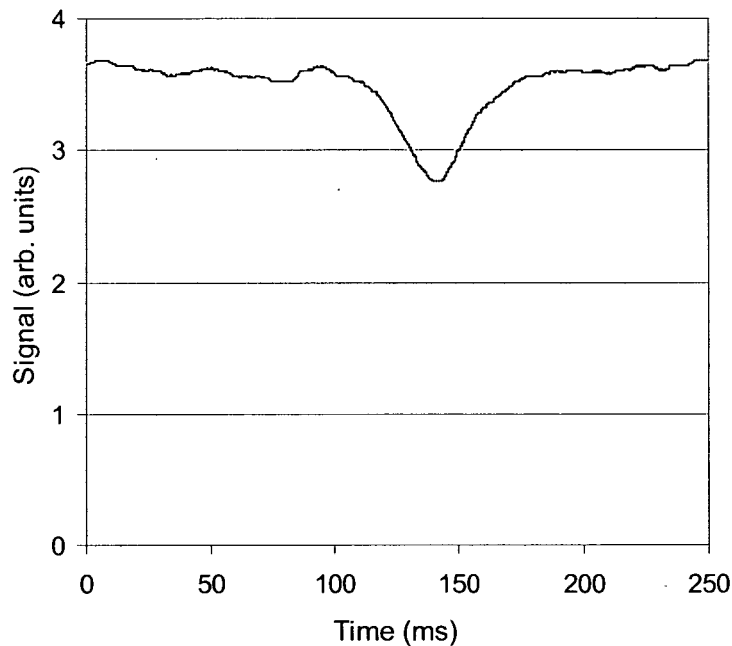


Figure 4-11. A typical response for a particle with a radius of $12 \mu\text{m}$ with an aperture of approximately $30 \times 35 \mu\text{m}^2$.

4.6. Improved Coulter counter

The result described in the previous paragraph marks an important milestone, since it is the first time a Coulter measurement has been performed with an adaptable aperture. Although this is of great relevance, the practical value of this result is limited by the difficulty that the measurement frequency and channel impedance have to be matched carefully to get any significant response from the device. Even with the matched frequency a significant amount of the signal is lost, causing a rather poor signal to noise ratio, which makes the Coulter counter in its current form not suitable for quantitative measurements.

The signal quality can be improved significantly when the substrate capacitance, C_{SUB} , is reduced. This can be achieved in a number of ways:

- by reducing the area of the parasitic capacities
- by changing the dielectric material
- by increasing the thickness of the insulation between the electrodes and the substrate

The surface area of the contact pads for the spring pins contributes significantly to the size of the substrate capacitance. It would be a possibility to put the chip on a carrier and then contact the carrier using the spring pins. This allows decreasing to size of the contact pads on the chip significantly. However, there are some drawbacks to this solution. The bonding wires would make the devices more fragile, it would be much more elaborate to fabricate the chips and the chips would no longer fit in the current test-setup. Since the insulating layer should not interfere with the anodic bonding process, changing the dielectric material or increasing the thickness of the insulating layer between the electrodes and the substrate has little potential for a reduction in parasitic capacity.

Based on the above considerations it was decided to use another bonding process, because the anodic bonding proved to be too much of a limitation. Fortunately a new adhesive bonding

process had become available [13] that is described in chapter 2. This process imposes no limitation on the thickness of the insulating layer, which solves the problem with the substrate capacity. Furthermore, the process is much more tolerant to surface roughness than anodic bonding, which means that it is no longer required to sink the electrodes into the surface of the wafer. This makes the fabrication process of the Coulter counter easier to integrate with other sensors and actuators.

The Coulter chips that were fabricated with the SU-8 adhesive bonding process have a channel height of 70 μm . The processing of the silicon remained the same. Measurements were performed with the new Coulter chip using two different kinds of particles:

- Plain polystyrene microspheres, radius 12 $\mu\text{m} \pm 2\%$ (Polymer Laboratories)
- Silver coated polystyrene microspheres, radius 10 $\mu\text{m} \pm 0.5\%$ (Microparticles GmbH)

Measurements with both kinds of particles showed an increase in impedance, so also for the conductive silver-coated particles the impedance goes up. This phenomenon is also observed in macro Coulter counters. It is explained by the formation of a layer of ions around the particle, which causes any kind of particle to increase the impedance, independent of its conductivity.

To analyse the quantitative performance of the Coulter counter a series of measurements was carried out. The size of the pulses was logged for 50 particles of each type. The statistical data for this measurement series is shown in Table 4-1 and a histogram of the measurements is depicted in Figure 4-12. The measurements demonstrate that the integrated Coulter counter can be used to discriminate between the two types of particles, since the measurement populations do not show any overlap. In the same graph the volume distribution of the particles as specified by the manufacturer is plotted around the average measurement values to illustrate the performance of the Coulter counter. The measured distribution matches the specification very well, which demonstrates the potential of the integrated Coulter as an instrument for quantitative particle analysis. It should be realised that although the specification for the particles is only 2% and 0.5% for the plain and the silver coated particles respectively, the variation in volume (which is measured by the Coulter counter) is about three times as high.

Table 4-1. Statistical data on series of 50 particles.

Particle radius	Mean signal peak	Standard deviation
10 μm	0.33	0.02
12 μm	0.81	0.11

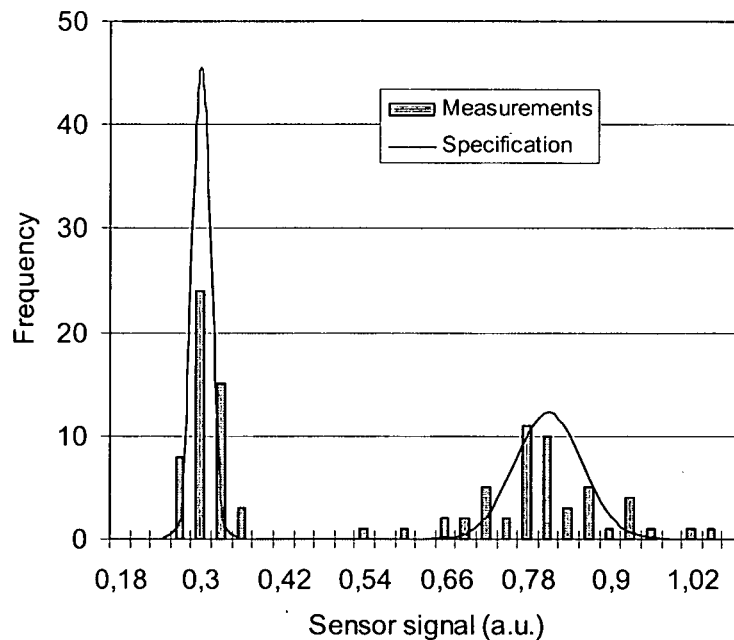


Figure 4-12. A histogram of 50 measurements with particles having a radius of 10 μm (left) and 12 μm (right); the measurements match the specification of the particles very well.

4.7. Discussion

During the measurements a noteworthy phenomenon was observed. Just after a particle had passed through the aperture a damped oscillation in the impedance could sometimes be seen, more often so with the larger particles. This is probably caused by a slight disruption of the sheath flow (see Figure 4-13) behind the particle. This could well be caused at the moment a particle is injected into the channel. The dimensions of the sample flow are stable under constant flow conditions, but when a rigid object is now injected into the sample flow it might cause a small pressure build-up that results in a slightly higher injection of sample liquid just after injection of the particle. However, the disruptions died out rather quickly (about two times the length of a measurement pulse) restoring stable flow conditions and a stable impedance level. This phenomenon did not seem to impact the accuracy of the measurements.

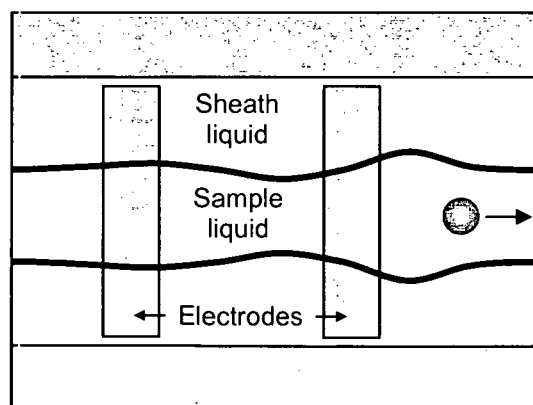


Figure 4-13. The measurements suggest a temporal distortion of the sheath flow just behind the particle, probably generated when the particle enters the channel.

4.8. Conclusions

A miniaturised version of the Coulter counter instrument has been realised on chip. The laminar flow properties resulting from the size reduction have been used to operate the Coulter counter with a liquid aperture. This liquid aperture has two major advantages over the traditional fixed Coulter aperture. Firstly, the trade-off between the device sensitivity and the reliability is circumvented since the electrical aperture can be much smaller than the physical aperture. Secondly, the liquid aperture also allows adapting the size of the Coulter aperture without the need to take the setup apart to exchange parts. As a result one and the same instrument can be used to size particles over a relatively large size range.

Particle sizing experiments have been performed with the integrated Coulter counter and the measurement results demonstrate that particles differing 20% in diameter can be clearly discriminated. The measurements show a distribution that is very similar to the specification of the particles, which demonstrates the potential of the instrument for quantitative particle analysis. Just like in the conventional Coulter counter both conductive and non-conductive particles can be detected.

4.9. References

- [1] W. H. Coulter, "Means for counting particles suspended in a fluid," 1953.
- [2] U. D. Larsen, H. Nørring, and P. Telleman, "Somatic Cell Counting with Silicon Apertures," presented at MicroTAS 2000, Enschede, The Netherlands, 2000.
- [3] K. Roberts, M. Parameswaran, M. Moore, and R. S. Muller, "A Silicon Microfabricated Aperture for Counting Cells using the Aperture Impedance Technique," presented at IEEE Canadian Conference on Electrical and Computer Engineering, Edmonton, Alberta, Canada, 1999.
- [4] M. Koch, A. G. R. Evans, and A. Brunnschweiler, "Design and fabrication of a micromachined Coulter counter," presented at Micromechanics Europe, Ulvik, Norway, 1998.
- [5] C. K. Fuller, J. Hamilton, H. Ackler, P. Krulevitch, B. Boser, A. Eldredge, F. Becker, J. Yang, and P. Gascoyne, "Microfabricated multi-frequency particle impedance characterization system," presented at MicroTAS, Enschede, The Netherlands, 2000.
- [6] S. Gawad, L. Schild, and P. Renaud, "Micromachined impedance spectroscopy flow cytometer for cell analysis and particle sizing," *Lab on a Chip*, vol. 1, pp. 76-82, 2001.
- [7] C. Washington, *Particle size analysis in pharmaceuticals and other industries*. Chichester: Ellis Horwood Limited, 1992.
- [8] B. H. Kaye, *Characterization of Powders and Aerosols*. Weinheim: WILEY-VCH Verlag GmbH, 1999.
- [9] U. D. Larsen, G. Blankenstein, and J. Branbjerg, "Microchip Coulter particle counter," presented at Transducers, Chicago, USA, 1997.
- [10] M. Koch, A. Evans, and A. Brunnschweiler, *Microfluidic Technology and Applications*, 1st ed. Baldock: Research Studies Press Ltd., 2000.
- [11] M. Tokeshi, T. Minagawa, K. Uchiyama, A. Hibara, K. Sato, H. Hisamoto, and T. Kitamori, "Integration of chemical processing on a chip," presented at MicroTAS 2001, Monterey, USA, 2001.
- [12] J. Bockris, B. E. Conway, and E. Yeager, *The double layer*, vol. 1. New York: Plenum Press, 1980.

- [13] P. Svasek, E. Svasek, B.Lendl, and M.Vellekoop, "Fabrication of miniaturized fluidic devices using SU-8 based lithography and low temperature wafer bonding," *Sensors and Actuators A*, vol. 115, pp. 591-599, 2004.

Chapter 5

Integrated projection cytometer

5.1. Introduction

Optical methods play a major role in the field of particle analysis. Many different techniques exist, mainly based on light-scattering, optical projection and fluorescence. A technique that is frequently applied for continuous optical analysis of small particles is cytometry [1]. In a typical cytometry setup the sample liquid is focused into a narrow stream by means of a sheath flow. This causes the particles to line-up so that they can be analysed individually. The particles are illuminated by a laser where the scattered light and fluorescence emission signals are registered by an optical detector. The drawback of cytometry is that typically only the far-field optical properties are registered, which means that some detailed information is lost and that an image of the particle is not readily available.

Another popular technique for the analysis of small particles is microscopy [2], which is based on optical projection. Microscopy yields very detailed information on the particles, such as shape, size and information on the internal properties of the particle, because the near-field properties of the optical field are registered. In microscopy the particles are confined to a thin layer, typically between two glass slides, and an advanced optical system is focused onto this layer to project the optical field onto an imaging system. The main drawback of microscopy is that it typically works on a batch basis, which is not suitable for in-line monitoring.

In this chapter a microsystem is developed that combines the advantages of cytometry and microscopy. The instrument is suitable for the continuous analysis of individual particles and yields detailed optical information obtained from the near-field of the optical projection. The instrument will be referred to as integrated projection cytometer.

The complex optical system used in microscopy setup is difficult to integrate onto a chip, but miniaturisation offers a unique possibility to obtain the near-field optical properties of the particle in another way. Very close to the particle the near-field properties of the optical field are still intact, hardly affected by diffraction. In the integrated projection cytometer this property of the optical field is exploited. The sensors are placed directly in the near-field of the optical projection, which eliminates the need for lenses or any other imaging optics; the result is a much smaller and far less expensive instrument.

Cytometers to image particles and cells have been presented in literature, e.g. in [3]. These instruments typically consist of a microscope that is built on top of a cytometer setup. This approach has the drawback that it yields rather bulky and very expensive instruments, mainly due to the complex optical systems required.

In literature several microsystems have been presented that comprise one or more components of a cytometer. The device described in [4] has a V-groove channel that was fabricated in micro-technology for application in blood component analysis. The analysis of the cells is based on light scattering, where the optical setup was realised using external components.

In [5] a microsystem is discussed that can be clipped onto a conventional capillary. The microsystem has waveguides that lead to the capillary and the optical signals are registered by integrated mesa photodiodes.

The integrated cytometer described in [6] is based on fluorescence. A semiconductor laser excites a high intensity leaky waveguide mode directly in the fluidic channel using prism coupling. The fluorescent signal is detected by a flip-chip bonded avalanche photodiode.

Another integrated cytometer based on fluorescence has been presented in [7]. A coaxial sheath flow focuses the particles into a narrow stream after which they pass through an optical interrogation zone. The light from an argon laser is coupled into the channel by an integrated wave guide and the fluorescent signal is detected using an external photomultiplier tube. Based on the optical signals an external valve is actuated to sort out particles of interest.

The micro-machined cytometer discussed in [8] is based on light scattering. In this device a laminated flow profile was used to focus the particles into a narrow stream. The particles are illuminated by an inserted optical fibre and the scattered light is detected by another optic fibre located on the opposing side of the channel.

The microsystems described above use fluorescence and light scattering to analyse the size of particles. The microsystem that is developed in this chapter differentiates itself because it is based on optical projection. The main difference is that optical projection yields near-field optical information about the particles. As a result additional properties such as particle shape or the optical properties of the particle can be measured.

5.2. Operation principle

The integrated projection cytometer consists of a transparent flow channel that is illuminated from the top (see Figure 5-1). A one-dimensional optical sensor has been integrated in the bottom of the channel, oriented perpendicular to the direction of flow. The particles that are to be analysed are pumped through the channel, suspended in a liquid. When a particle passes over the optical sensor it partially blocks the light, which is registered by the optical sensor. By repeatedly reading out the sensor as the particle moves over the sensor, a two-dimensional projection of the particle is obtained.

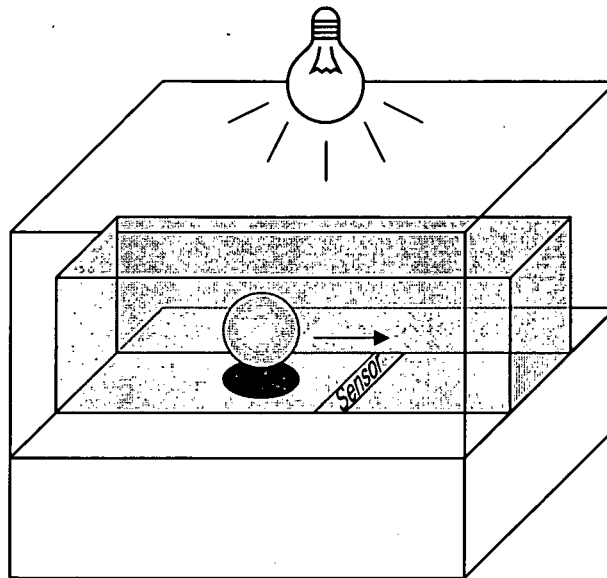


Figure 5-1. Schematic overview of the integrated cytometer.

5.3. Diffraction

The key in performing direct optical measurement results (without the application of any imaging optics) of such small objects is to have a very small projection distance. Only when the particles move very close over the sensor, their projection will not be severely distorted by diffraction of the light. To illustrate the influence of diffraction a series of simulations was performed using the *LightPipes 1.3* toolbox with *Matlab 6.1*. In Figure 5-2 the results are shown for the projection of a particle with a diameter of $15\ \mu\text{m}$ over a distance of $0\ \mu\text{m}$, $15\ \mu\text{m}$, $30\ \mu\text{m}$, $45\ \mu\text{m}$ and $60\ \mu\text{m}$, for monochromatic light at a wavelength of $500\ \text{nm}$. A

square particle was selected since this is a shape that deteriorates rapidly under the influence of diffraction.

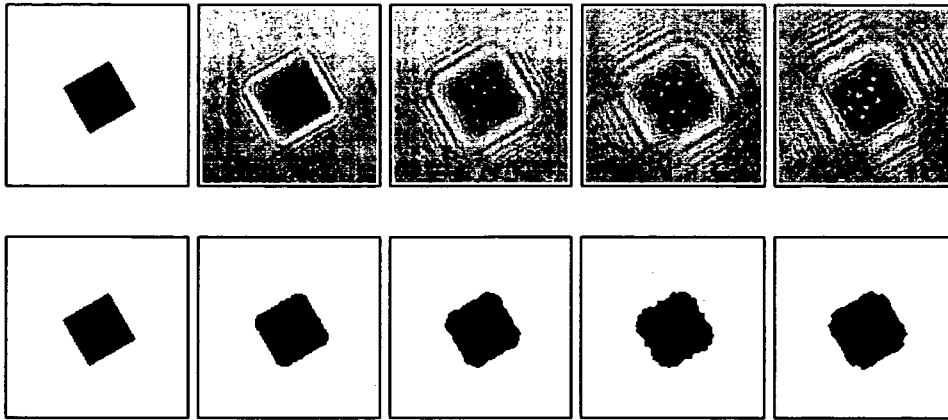


Figure 5-2. Simulated projection of 15 μm square particle over a distance of 0 μm , 15 μm , 30 μm , 45 μm and 60 μm (from left to right) using 500 nm monochromatic light (top) and the result after applying a threshold operation (bottom).

The simulation clearly shows that detail information is lost as the projection distance increases. For this reason it is only possible to do direct optical measurements with an integrated device, especially when even smaller particles are to be analysed. From the simulation data it could be derived that as a ‘rule of thumb’ a projection distance that is up to roughly two times the diameter of the particle still produces acceptable results for particles in this size range; for larger projection distances the distortion becomes too severe. The small projection distance is realised in the integrated cytometer by applying a non-coaxial sheath flow that focuses the particles closely over the optical sensor using the non-coaxial flow cell, described in chapter 3.

Although limited, some diffraction distortion will still be present. For some applications even this little distortion might be a problem. But since the diffraction of light is a deterministic process it is possible to reverse its effect, as long as all data is available. Unfortunately this is not the case here: the optical sensors that register the projected image transform the incident optical power into electrical power. This means that only the amplitude information of the optical field is registered and the phase information is lost. Furthermore, the optical sensors have a limited resolution, which causes an additional loss of information. An algorithm has been developed to reconstruct the non-diffracted image, based on back-propagation of the optical field with an estimation of the phase-information. A schematic overview of the algorithm is depicted in Figure 5-3.

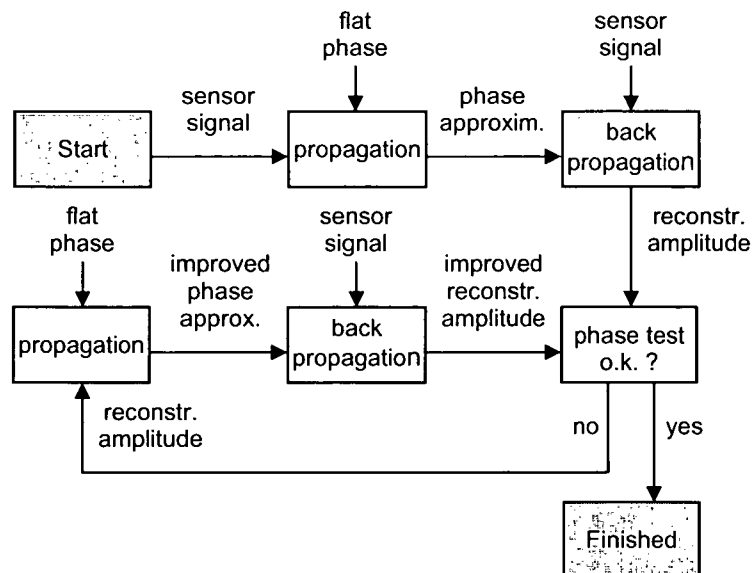


Figure 5-3. Schematic representation of the optical reconstruction algorithm.

The algorithm starts with a simulated propagation of the amplitude information of the sensor over the same distance as in the measurement setup. Since the propagation is performed in simulation the phase information after the propagation is available. This phase information is an approximation of the true phase information and it is used with the amplitude data from the measurement to perform a back-propagation. This yields a reconstruction of the amplitude information at the location of the object, with reduced distortion by diffraction. When the reconstruction is perfect, the reconstructed phase information would be flat. If the reconstructed phase is close enough to the flat phase of the incident light the algorithm ends. If the phase information shows too large a deviation the procedure is repeated using the reconstructed amplitude information to obtain a better approximation of the phase. The only requirement for this algorithm is that the light-source in the measurements has to produce coherent light, since the original phase information of the incident light needs to be known. Since a laser is a common light-source in the area of particle analysis, this is not a severe limitation.

The results that can be obtained with this algorithm are illustrated in Figure 5-4. Simulations were performed with data that can be obtained using a one-dimensional array of optical sensors with a pitch of $2.5 \mu\text{m}$. The first picture in Figure 5-4 shows the original particle ($15 \mu\text{m} \times 15 \mu\text{m}$). The second picture shows the diffracted image for a projection distance of $30 \mu\text{m}$ with 500 nm monochromatic light. The middle picture shows the image that is obtained if the second picture is scanned with a photodiode array having a pitch of $2.5 \mu\text{m}$. The result after applying the algorithm on the sensor signal is depicted in the fourth picture. The clear enhancement in shape when comparing the fourth picture with the second one can be explained by the fact that the algorithm also uses the information in the diffracted light when reconstructing the particle shape. The final picture shows the result after applying a threshold operation on the reconstructed image.

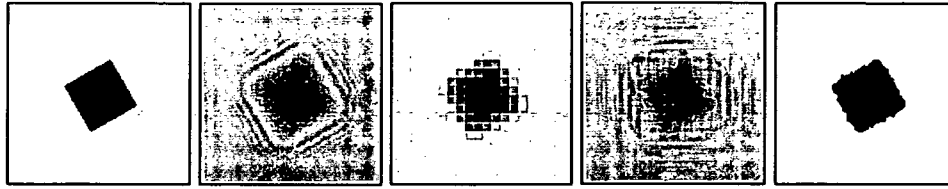


Figure 5-4. Simulation results showing from left to right: the original 15 μm particle, its projection over a 30 μm distance, the image as registered by an array of optical sensors with a 2.5 μm pitch, the image after applying the reconstruction algorithm and finally the reconstructed image after applying a threshold operation.

5.4. Sensor design

To acquire a two dimensional image it seems straight-forward to use a two-dimensional image sensor in stead of scanning the particle as it moves over the sensor using a one-dimensional image sensor. The decision to use the latter configuration is based on resolution and fill-rate.

In a one-dimensional optical sensor the wires that are necessary to electrically contact the sensing elements can be placed outside of the photo-sensitive area, which is not possible when using a two-dimensional sensor. This is important for two reasons. Firstly, the wires increase the pitch of the sensing elements in a two-dimensional sensor. Since no imaging optics is applied in the cytometer, the pitch of the optical sensor directly relates to the resolution of the acquired images. So, a two-dimensional optical sensor fabricated in the same technology as a one-dimensional sensor would result in images having a lower resolution. Secondly, since the optical elements in the sensor are very small, they do not generate large photocurrents. Therefore, it is essential to maximise the fill-rate of the optical sensors. The wiring of a two-dimensional sensor significantly reduces its fill-rate, resulting in smaller photocurrents. This leads to a worse signal-to-noise ratio for a two-dimensional sensor compared to a one-dimensional sensor.

A minor drawback of using a one-dimensional image sensor is that the aspect ratio of the obtained images is not readily available. In the direction orthogonal to the movement of the particles the size is well defined by the geometry of the sensor, but for size information along the direction of movement the speed of the particles has to be known. By using a second sensor at a known distance from the first one it is possible to calculate the speed of the particle. The velocity is obtained by dividing the distance between the two sensors by the time difference between the registrations of the particle at the two sensors. The velocity information can be used to calculate the correct aspect ratio.

Photodiodes were selected as the sensing elements, because they have some favourable properties. Photodiodes can be made in a standard IC-process, they are fast (response-time in the ns-range) and, most importantly, they can be made with very small dimensions. The photodiodes were designed with a shallow junction (0.25 μm) so that they have good sensitivity for light with a relatively short wavelength (450 nm), which shows minimal diffraction. Two different types of sensors were developed and both were made in the same standard 1 μm bipolar IC-process.

The first sensor consists of a double one-dimensional array of 40 tiny (2.5 x 2.5 μm^2) photodiodes. A photograph of the array sensor is depicted in Figure 5-5, where the small squares depict the photo-junction areas. The photodiodes of the second half of the array measure the light in between the pixels of the first half. The arrays have been designed such

that the pixels of the second half of the array have an offset of two pixels in the direction of flow. When the arrays are read-out at a frequency of which one period resembles a particle displacement of $2.5 \mu\text{m}$, the data of the two arrays are combined by simply delaying the signals of the first half of the array by two periods. This approach realises a one-dimensional sensor that has an effective pitch of $2.5 \mu\text{m}$ with a 100% fill-rate. The images obtained with this sensor have camera-like appearance that is built-up out of pixels.

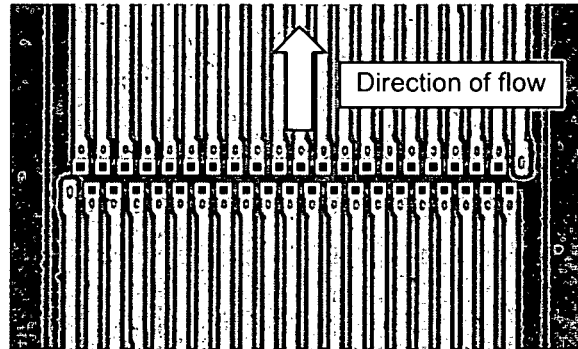


Figure 5-5. Photograph of the array sensor; the sensor consists of a double one-dimensional array of 40 tiny photodiodes ($2.5 \times 2.5 \mu\text{m}^2$); when the data from the two arrays is combined an effective pitch of only $2.5 \mu\text{m}$ is realised.

The second sensor consists of two elongated (strip) photodiodes, which have a junction that is $50 \mu\text{m}$ wide, with a length of $1 \mu\text{m}$. The junction areas are marked with the left and right rectangles in Figure 5-6. When a particle passes over the sensor the photocurrents will drop proportional to the width of the particle. So this sensor only registers the width of the particle for an individual image line, and not the spatial relationship of these widths to each other.

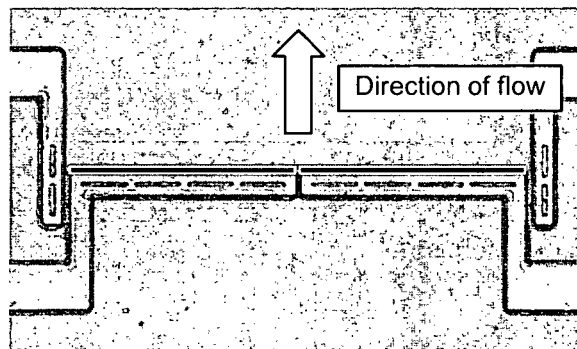


Figure 5-6. Photograph of the strip sensor; the sensor consists of 2 elongated photodiodes ($50 \mu\text{m} \times 1 \mu\text{m}$) that are separated by a $1 \mu\text{m}$ cut.

To uniquely reconstruct the original image from a strip-type sensor a reference is needed. Therefore, two photodiodes are used instead of one; this is illustrated in Figure 5-7. The reference point is only available as long as the particle passes over the cut in between the two photodiodes. In the integrated cytometer this is achieved using hydrodynamic focussing. The main advantage of the strip structure is that the resolution in the direction perpendicular to the flow is not limited by a pitch, but is determined by the signal-to-noise ratio of the photocurrent. In the experiments a signal to noise ratio of about 100 was obtained with the

strip sensor. Since the width of one photodiode in the strip sensor is $50\ \mu\text{m}$ the resolution of the strip sensor under these conditions can be approximated to be $0.5\ \mu\text{m}$ in the direction perpendicular to the flow.

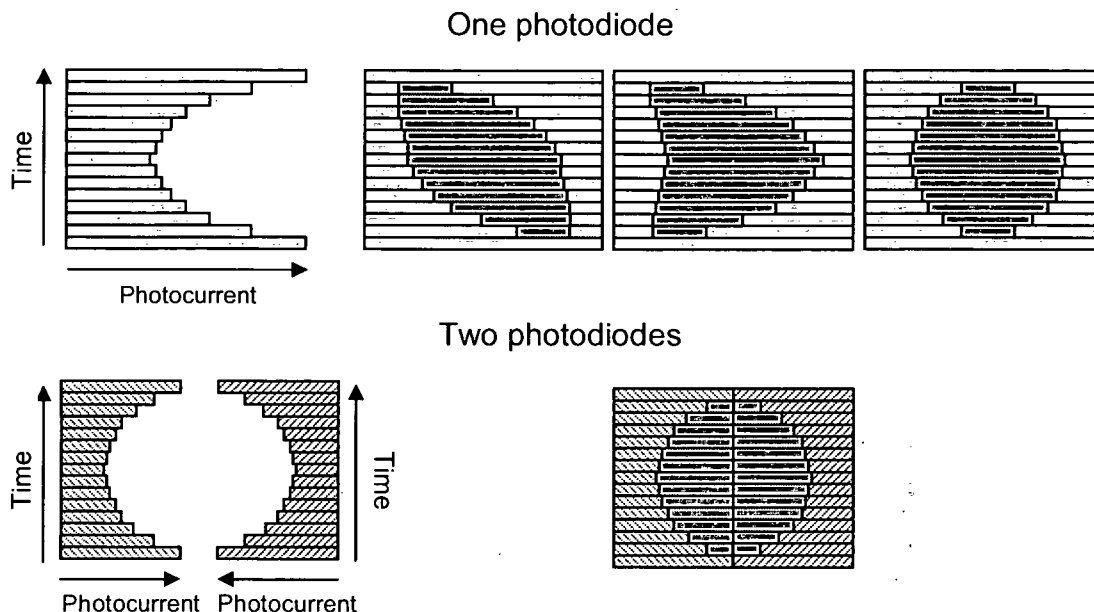


Figure 5-7. With only one photodiode the spatial relationship of the registered widths by the strip sensor is not known, which could lead to many different particle shapes (top); therefore the strip sensor consists of 2 photodiodes, where the cut in the middle is used as a reference (bottom).

In Table 5-1 the measurement capabilities of the two different sensors are compared. The main advantage of the array sensor is that it is the most versatile; it can be used for all kinds of particles. Besides non-transparent particles also semi-transparent and even non-uniform semi-transparent particles do not cause a problem; these will cause a smaller drop in photocurrent for the individual photodiodes but do not influence the geometrical information. The main drawback of the array sensor is that it generates a vast amount of data that needs to be processed in real-time.

Table 5-1. Comparison of the measurement capabilities of the 2 sensors.

Particle Property	Array sensor	Strip sensor
Non-transparent	✓	✓
Uniformly semi-transparent	✓	✓ ¹
Non-uniformly semitransparent	✓	-

¹Only possible after performing a calibration measurement

The strip sensing-element has the advantage that it only requires two readouts for every image line, and it has no fixed pitch limiting the resolution in the direction perpendicular to the flow. Furthermore, the photocurrents generated by the strip sensor are almost 10 times larger than those from the array sensor, which make them easier to read out. A disadvantage is that

without any a priori knowledge of the particles the strip sensor is only suitable for non-transparent particles.

When uniform semi-transparent particles pass the sensor, these will cause a smaller drop in photocurrent than if they were non-transparent. However, it is not possible to tell this from the measurements with the strip sensor. As a result the particles will be registered having a smaller width. This can be corrected for when first a calibration measurement is performed. When the particles are not only semi-transparent, but when the transparency also varies over the particle it is no longer possible to obtain the exact shape with the strip sensor, since the geometrical variations in transparency are integrated over the width of the sensor. This results in a pulse shape that no longer resembles the actual particle shape. Although in this case particle shape cannot be obtained, the pulse shape registered by the strip sensor can still be used to discriminate between different types of particles using correlation techniques.

5.5. Sensor characterisation

For the sensor characterisation the two different optical sensors were fabricated on a silicon chip without any flow channel. The first measurements were performed in a quasi-static manner, where images were obtained by moving a piece of bonding-wire (diameter 27 μm) with a bonding-ball (diameter 67 μm) over the sensors in small steps. For these measurements the light source consisted of a bright LED (Toshiba TLYH190P) that was switched to emit modulated light. The photocurrents were read out using a lock-in amplifier (Stanford Research SR830). A very low modulation frequency was necessary (< 1 Hz), since otherwise the current induced in the sensor as a result of the electric field emitted by the LED would be significant compared to the size of the generated photocurrents.

The results of this measurement are depicted in Figure 5-8, with on the left the measurement results from the array, in the middle a photograph of the bonding wire and on the right the measurement results with the strip. Both sensors recorded an accurate registration of the object, which is a first demonstration that the measurement principle works as predicted by theory. For a non-transparent object as used here the array sensor does not yield any additional information and the strip sensor is to be preferred.

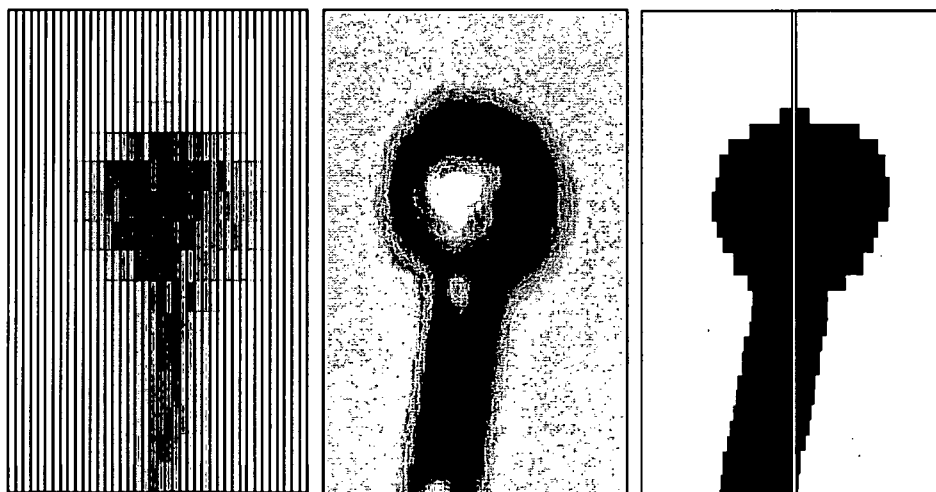


Figure 5-8. Image obtained with the array sensor (left), a photograph of the test object (middle,) and the image obtained using the strip sensor (right) in a quasi static measurement.

The coarse vertical resolution in both measurements is caused by the fact that in the used measurement setup the minimum vertical movement of the bonding wire was about 7 μm . The slight fuzziness in the measurement result obtained with the array sensor (Figure 5-8 left image) is probably caused by two factors. The first is the long time the measurement lasted, during which the bonding-wire might have moved slightly. The second factor is a non-ideal match of the movement of the bonding wire with the fixed pattern of the array: the steps in the movement did not match the off-set between the two lines of pixels and the movement of the bonding-wire might have been not perfectly aligned perpendicular to the array. As a result the signals from the diodes in the bottom half of the array do not exactly align with the signals of the top half of the array. When the array sensor is applied in the cytometer these two factors are not an issue; the particle movement will be aligned perfectly to the sensor by the channel and the sample frequency can be chosen arbitrarily to match the offset between the two parts of the array.

Next a series of dynamic measurements was performed. Since no electronics are integrated with the devices it would be difficult to measure the 40 tiny photocurrents of the array sensor in real-time using external components. Therefore, the dynamic measurements were only performed with the strip sensor. With this element just two photocurrents need to be monitored, which in addition are substantially larger than the photocurrents from the array sensor.

For the dynamic measurements the low modulation frequency of the light cannot be used. To still have a reasonable signal to noise ratio without modulation a 50 Watt halogen light source was used for this measurement, where an optical fibre was used to direct the light to the sensor orthogonal to the sensor-plane. The two photocurrents that were generated by the sensor were each amplified by a custom trans-impedance amplifier and then connected to a memory oscilloscope (Tektronix TDS220). The test objects for the dynamic measurements consisted of irregularly shaped PVC particles in the size range of 30 - 80 μm (see Figure 5-9).

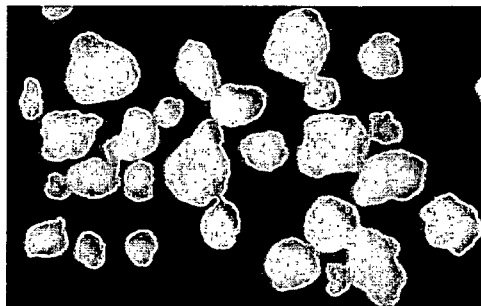


Figure 5-9. Photograph of the irregularly shaped PVC test-particles (30-80 μm).

The PVC particles were blown over the sensor with a speed of approximately 2 cm/s at a projection distance of about 30 μm (estimated from shadows). In the left part of Figure 5-10 the results of two particle shape measurements are depicted. The magnitudes of the photocurrents are plotted horizontally, with their maximum values directed towards the middle. The vertical axis is the time-axis. The combined decrease in photocurrent of the two photodiode strips defines the shape of the particles (black).

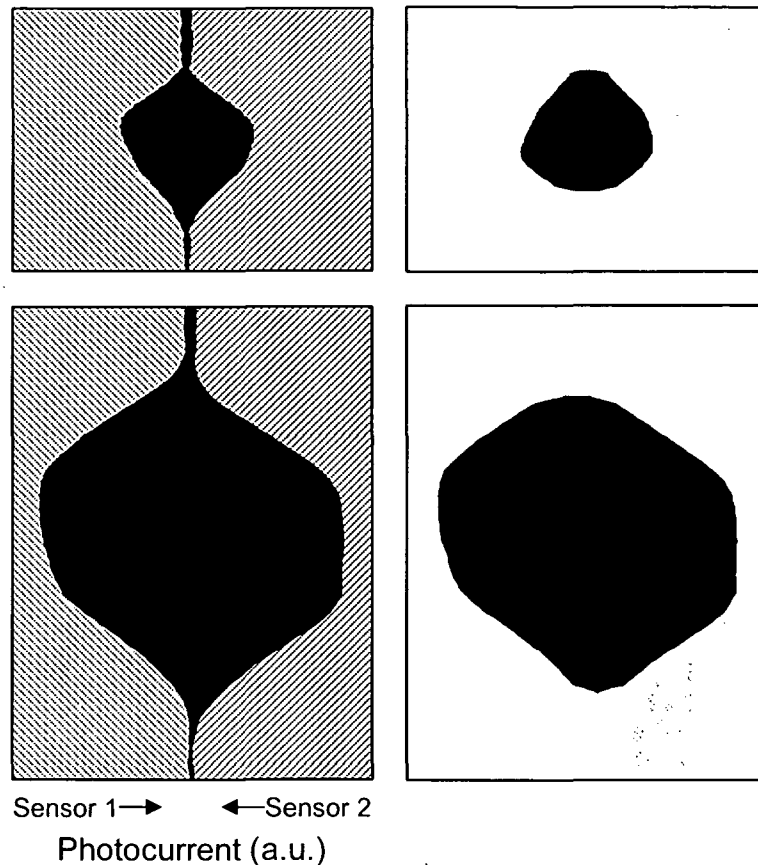


Figure 5-10. Dynamically measured particle shapes; raw data (left) and after applying additional data processing (right).

In the current measurement set-up it was not possible to capture the particles that had passed the sensor to study them under a microscope to verify their shape. It would still not have given conclusive information about the accuracy of the shape measurements, because the orientation of the particle when it passed the sensor is not known. Therefore, another approach was taken.

Just like in the quasi static measurements a piece of bonding wire with a bonding ball was used for the reference measurements. This time the bonding wire was moved over the sensor at a steady speed, just like the test particles. The measurement speed was just over 2 cm/s and the projection height was 30 μm (estimated from shadow). The results are depicted in Figure 5-11 along with a photograph of the piece of bonding-wire. As can be seen in this picture the shape is accurately registered by the sensor. Even the asymmetry of the bonding ball is clearly visible. This measurement illustrates the performance of the sensor.

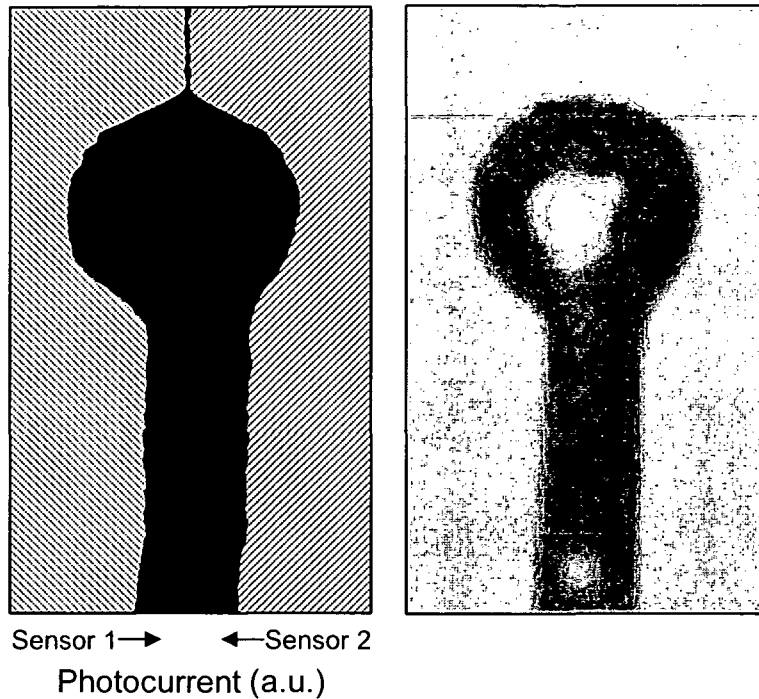


Figure 5-11. Dynamic measurement (left) and photograph (right) of a piece of bonding wire that served as reference object.

The dynamic measurements show that the photocurrents do not drop very suddenly, but they ramp down gradually when an object moves over the sensor. As a result the images show peaks at head and tail (see Figure 5-10 left and Figure 5-11 left). This effect occurs because the photosensitive area in the sensor is larger than the actual junction area dimensions (see Figure 5-12).

Instead of registering only a very narrow line of the projection the weighted average over larger area of the projection is now registered. This causes a moving-average effect on the image, which is not desirable, since it causes the aforementioned distortion and loss of detail. In the next generation of the sensor this effect can be avoided by shielding the area directly around the photodiode area with metal.

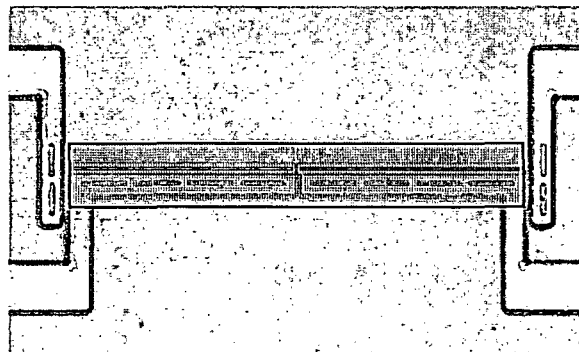


Figure 5-12. An area substantially larger than the junction area (shaded) turned out to be photosensitive.

An iterative algorithm has been developed to get an estimate of the original shape, without the distortion. The idea behind the algorithm is that it constructs an approximation of the undistorted image that results in the distorted image (as registered by the sensor) when the moving average effect is applied. It should be noted that there is not one unique image that would lead to the distorted image, because information is lost during the distortion process. However this estimate is an improvement over the images with peaks at head and tail as can be seen in the right part of Figure 5-10.

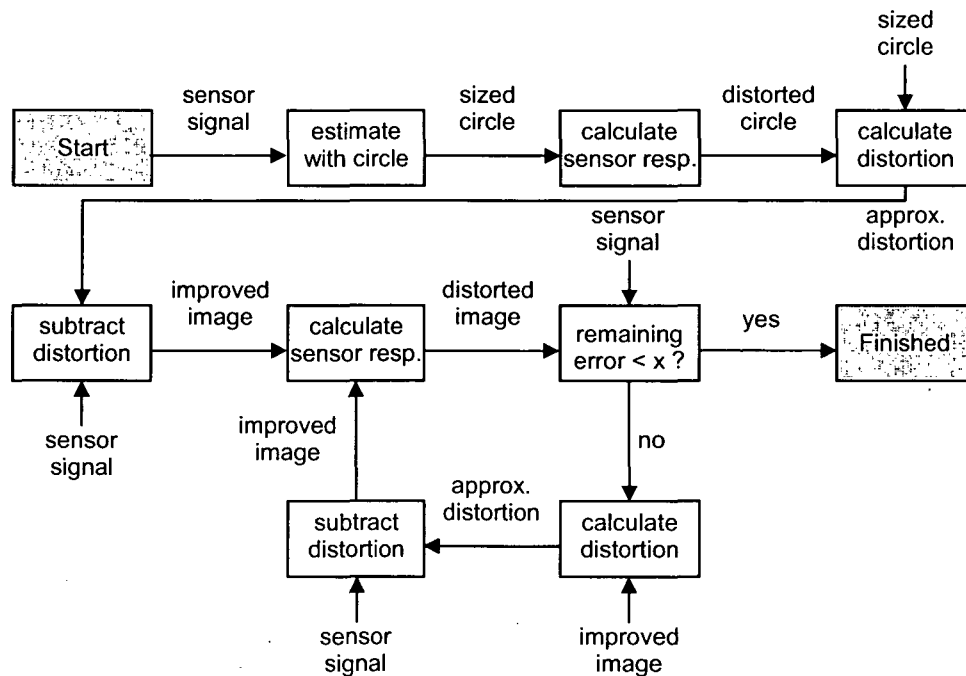


Figure 5-13. Schematic representation of the algorithm to reduce the distortion by the too wide sensitive area.

5.6. Integrated cytometer

The integrated cytometer is formed by combining the integrated flow cell (described in chapter 3) and the optical strip sensor in a single device. The fabrication of the cytometer is based on the anodic process flow described in chapter 2. The design of the strip sensor was not modified, apart from applying optical shielding around the junction area of the photodiode to improve the resolution. The optical shield consists of a metal frame that has two openings of $2 \times 50 \mu\text{m}^2$. The metal layer in the optical shield has a thickness of 300 nm, which completely blocks the light.

The optical sensors were fabricated in a standard bipolar IC-process. As a post-processing step the second dielectric layer was removed in locations where the silicon wafer has to form an anodic bond with the glass wafer. The surface of the silicon wafer shows some roughness due to the IC-processing, in particular at the locations of the wiring. To prevent these protrusions from hindering the anodic bonding process, shallow recesses were designed in the glass wafer that fit exactly over the wires (see Figure 5-14).

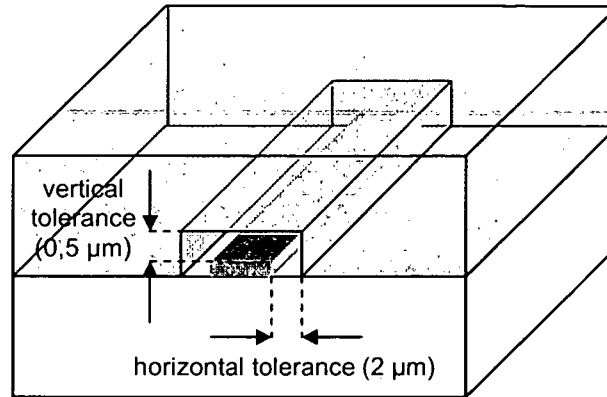


Figure 5-14. Recesses need to be defined in the glass wafer to prevent the metal tracks from hindering the anodic bonding process.

There is a trade-off in the design of these recesses. When the recesses are too large liquid will leak through the recess from the channel into other areas of the chip, possibly causing a short circuit. When the recesses are too small they do not fit over the wiring, which might prevent the wafers from forming a reliable bond.

Even when the size of the recesses is just right a small miss-alignment between the two wafers can cause the wafers not to bond. So the design of the recesses is very critical. It should be realised that a small gap around the wiring is still allowed, since the surface tension will prevent the liquid to get into very narrow holes. Based on the wafer-to-wafer alignment accuracy the recesses were designed to be $0.5 \mu\text{m}$ deeper and $2 \mu\text{m}$ wider than the metal wires. A photograph of a completed device is depicted in Figure 5-15.

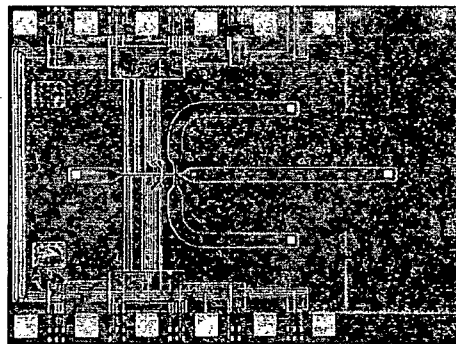


Figure 5-15. A photograph of the integrated cytometer ($2 \times 1.5 \text{ cm}^2$).

The measurement setup was comparable to the one that was used for the dynamic characterisation of the sensors. Before any measurements with particles were carried out a reference measurement was performed, where only sheath liquid (without any particles) was pumped through the device using syringe pumps (kdScientific model 200 series). The light-intensity of the source was increased in steps to verify reliable operation of the sensor over a wide range of light intensities and to check the photodiode matching. The photodiodes were connected in photovoltaic mode. Figure 5-16 depicts the results from this reference measurement.

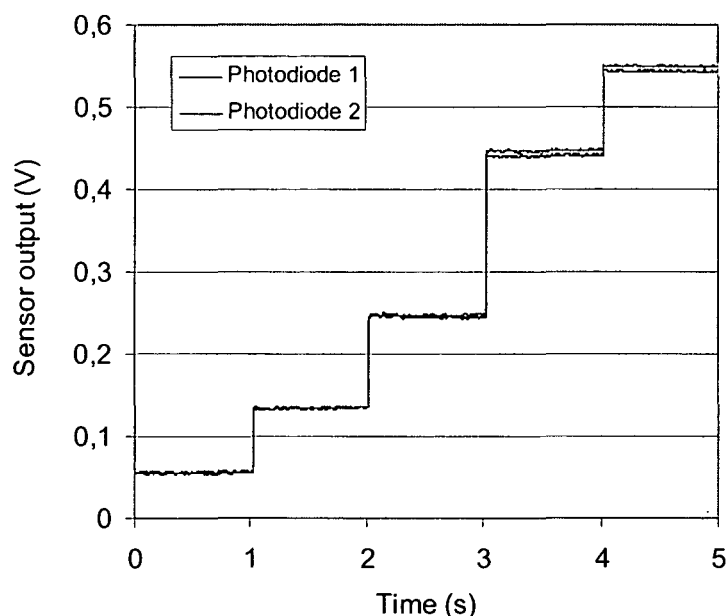


Figure 5-16. Output voltages generated by the photodiodes in photovoltaic mode for stepwise increasing light intensity.

The graph shows that the two photodiodes match well. The output voltage clips at 0.55 V, where the PN-junctions of the photodiodes come into forward bias. Based on this result a light intensity was selected that results in an output voltage near the maximum. This leads to the best signal to noise ratio, without any masking of the signals by clipping.

Next a sheath flow was formed with a sample liquid suspending spherical polystyrene microspheres with a radius of 12 μm (Polymer Laboratories). Some typical measurements are depicted in Figure 5-17. The measurements show that the particles can be clearly detected when they pass the sensor and that the shape of the signals is quite consistent.

The difference in the reduction of photocurrent between the two photodiodes of the sensor indicates that particles do not pass over the middle of the sensor (off-set about 6 μm). This is due to a geometrical asymmetry caused by a rather significant misalignment between the glass-wafer and the silicon wafer, which resulted in the sensors being located off of the middle of the channel. Although the flow cell can compensate for misalignments by directing the sample-flow more to one side of the channel, the misalignment was too large to be fully corrected.

Another consequence of the misalignment is that the recesses in the glass did not coincide with the metal wires on the silicon wafer. As a result the device had leakage problems and typically after about 10 minutes of operation some liquid protruded along the metal wires causing a short-circuit. After drying the devices they could be used again, but the leakages severely hindered the measurements.

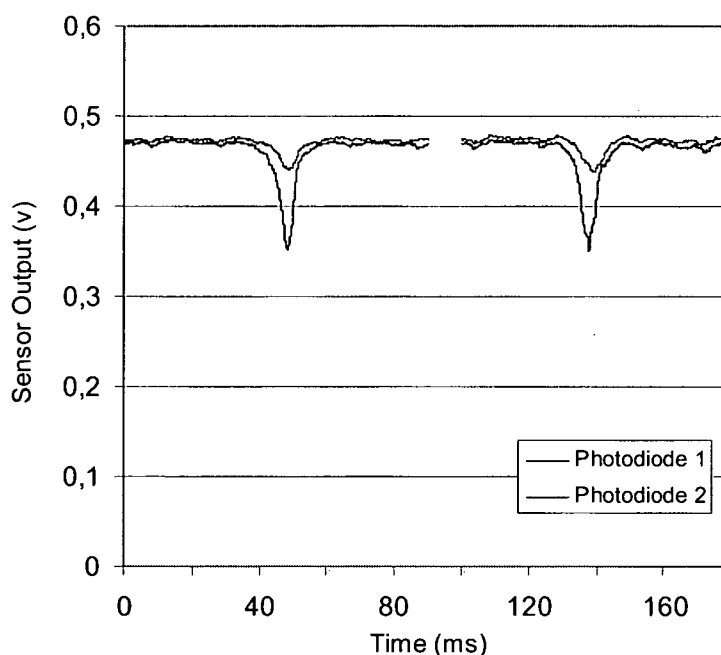


Figure 5-17. Sensor response in photovoltaic mode for two consecutive particles.

The pulses registered by the sensor do not resemble the shape of the particles very well. This is probably caused by the rounded shape of the channel, caused by the wet-etching of the glass, which causes some refraction of the light rays at the glass-liquid interface. As a consequence the light-rays are no longer parallel and can create internal reflections which distort the projection.

Although the first cytometer devices did not perform optimally some important results were obtained. The particles could be clearly detected using an integrated device that includes both the flow cell and the optical sensors. The results show that very consistent signals were obtained demonstrating great promise to obtain highly repeatable results with such a system. However, the measurements also demonstrated that the optical system needs improvement to get more detailed information on the particles.

5.7. SU-8 based cytometer

The main problems with the first version of the device were related to leakage and the optical qualities of the channel. Both problems were solved by changing the fabrication technology. For the second version of the integrated projection cytometer the two-step SU-8 process [9] was used that is discussed in chapter 2. The liquid SU-8 between the double rigid channel outline seals the holes around the metal tracks eliminating any leakage problems. The square channel cross-section that is obtained using the SU-8 process is very suitable to make an optical projection, since it will not cause any refraction of the light. The silicon part of the device remained unchanged. A photograph of an integrated cytometer device based on SU-8 technology is depicted in Figure 5-18.

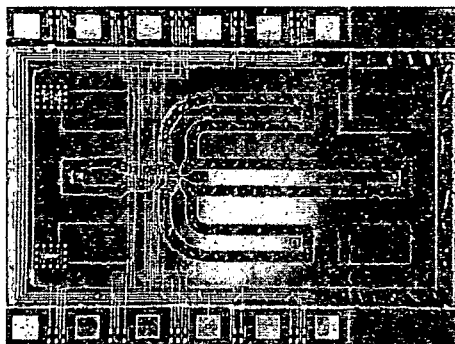


Figure 5-18. A photograph of the integrated cytometer ($2 \times 1.5 \text{ cm}^2$), based on SU-8 technology.

The measurement setup was also adapted to further improve the quality of the signals. To make the device insensitive to environmental light and to increase the signal to noise-ratio it was decided to use modulated light. A diode laser (Roithner Lasertechnik GLMC1-10, wavelength 532 nm) was selected as a light-source, since it can be easily modulated. Another advantage of using a laser is that it can be placed relatively far away from the chip, eliminating any electrical cross-talk, and still maintain a well focused spot (diameter $< 1.5 \text{ mm}$) to selectively illuminate the sensing area. A lock-in amplifier (Stanford Research SR830) was used to modulate the laser and to demodulate the photocurrent from the photodiodes. The signals were recorded using a memory oscilloscope (Tektronix TDS220). A photograph of a measurement in progress is depicted in Figure 5-19.

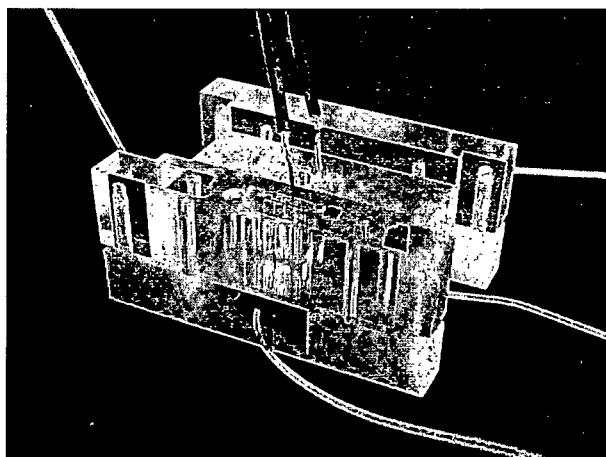


Figure 5-19. Measurement in progress with the cytometer chip in a custom holder illuminated with the green diode laser.

Measurements were performed with two different types of particles:

- Plain polystyrene microspheres, radius $12 \mu\text{m} \pm 2\%$ (Polymer Laboratories)
- Silver coated polystyrene microspheres, radius $10 \mu\text{m} \pm 0.5\%$ (Microparticles GmbH)

Measurements showed that the particles could be focused exactly over the reference of the photodiode strip (see Figure 5-20).

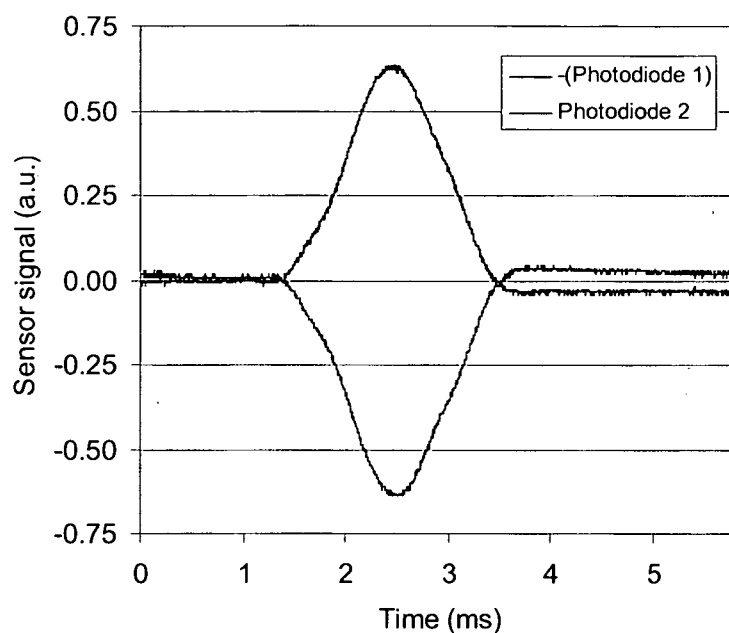


Figure 5-20. With the SU-8 based cytometer the particle can be focused exactly over the middle of the reference of the photodiode sensor.

However, since the test particles are completely symmetrical, focusing the particles over the reference does not add any additional information. Due to the 'blind spot' between the two photodiode even some signal is lost. Therefore, the sheath flow was focused so that the particles only pass over one of the photodiodes in the strip sensor. Ten consecutive measurement pulses with each type of particles are shown in Figure 5-21.

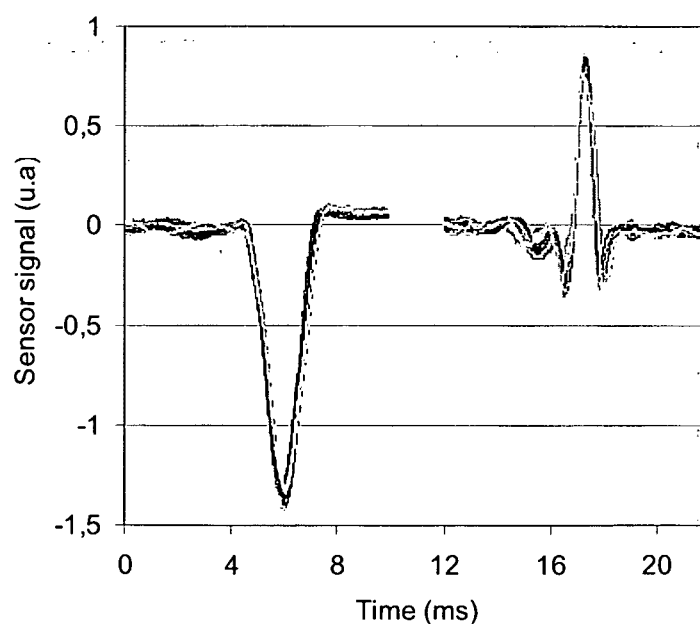


Figure 5-21. Ten measurements printed on top of each other for 10 μm radius silver coated particles (left) and 12 μm radius plain particles (right) demonstrate very good repeatability.

The measurements show very good repeatability, with respect to the size of the peaks and to the shape of the sensor pulses. This repeatability can be mainly attributed to application of the sheath flow, which causes all particles to pass the sensor in exactly the same way. Statistical data on the measurements for 50 particles of each kind is shown in Table 5-2.

Table 5-2. Statistical data for 50 pulses with both kinds of particles.

Type of particle	Mean signal peak	Standard deviation
Silver coated	-1.41	0.06
Plain	+0.82	0.07

5.8. Discussion

The measurements show that both kinds of particles can be clearly detected. Due to their optical properties the two types of particles caused very different signal shapes. The (opaque) silver coated particles cause a simple pulse with a relative steep drop in the measurement signal, as expected. The signal shape obtained with the transparent microspheres was more interesting. First the photocurrent dropped somewhat and then it went up above the baseline followed by a second small dip. This pulse shape can be explained by a lens-effect (see Figure 5-22), caused by the higher refractive index of polystyrene (1.58) compared to the glycerol water mixture (approx. 1.4). This phenomenon can also be observed when looking at transparent particles through a microscope, where the particles are visible as bright spots surrounded by dark rings.

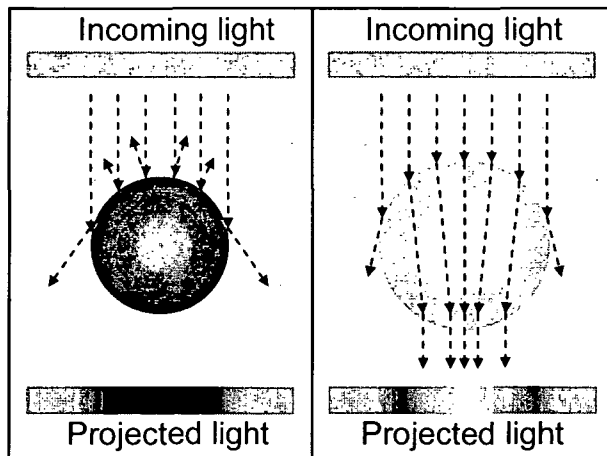


Figure 5-22. The different pulse shapes obtained with the silver coated particle (left) and the plain, transparent particle (right) can be explained by their optical properties.

5.9. Conclusions

In this chapter an integrated cytometer was developed that is based on optical projection. The miniaturisation allows registering an image of the particles without the need for lenses or any other optical components due to the small projection distance that can be achieved. This has major advantages related to size and cost of the instrument compared to the macro instruments.

Two different sensors, an array sensor and a strip sensor, have been introduced that differ in versatility and ease of use. Quasi-static measurements have been performed with both sensors that prove that an image of a small object (27-67 μm) is accurately obtained. An integrated cytometer device has been fabricated based on the strip sensor. Measurements with two different kinds of particles of comparable size demonstrate that they can be clearly distinguished. The measurement signals show optical details of the particles and demonstrate very good repeatability.

5.10. References

- [1] J. V. Watson, *Introduction to flow cytometry*, 1st ed. ed. Cambridge: Cambridge University Press, 1991.
- [2] T. Allen, *Particle size measurement.*, vol. 1. Powder sampling and particle size measurement, 5th ed. London: Chapman and Hall, 1997.
- [3] J. Wietzorrek, M. Stadler, and V. Kachel, "Flow Cytometric Imaging - a novel tool for identification of marine organisms," presented at OCEANS '94, Brest, France, 1994.
- [4] E. Altendorf, D. Zebert, M. Holl, and P. Yager, "Differential blood cell counts obtained using a microchannel based flow cytometer," presented at Transducers '97, Chicago, 1997.
- [5] O. Leistiko and P. F. Jensen, "Integrated bio/chemical microsystems employing optical detection: the clip-on," *J. Micromech. Microeng.*, vol. 8, pp. 148-150, 1998.
- [6] J. Krüger, K. Singh, A. O'Neill, C. Jackson, A. Morrison, and P. O'Brien, "Development of a microfluidic device for fluorescence activated cell sorting," *J. Micromech. Microeng.*, pp. 486-494, 2002.
- [7] A. Wolff, I. R. Perch-Nielsen, U. D. Larsen, P. Friis, G. Goranovic, C. R. Poulsen, J. P. Kutter, and P. Telleman, "Integrating advanced functionality in a microfabricated high-throughput fluorescent-activated cell sorter," *Lab Chip*, vol. 3, pp. 22-27, 2003.
- [8] C. H. Lin and G. B. Lee, "Micromachined flow cytometers with embedded etched optic fibers for optical detection," *J. Micromech. Microeng.*, vol. 13, pp. 447-453, 2003.
- [9] P. Svasek, E. Svasek, B. Lendl, and M. Vellekoop, "SU-8-Based Fluidic Devices," presented at Eurosensors XVII, Guimarães, Portugal, 2003.

Chapter 6

Particle sorter

6.1. Introduction

In the previous chapters various microsystems were discussed for the analysis of particles. The functionality of such analytic instruments could be greatly extended by adding an actuator to actively sort the particles, based on the reading of the sensors. In literature a variety of integrated particle sorters has been presented based on different actuation principles. Sorters have been presented that use thermal actuation, where local heating causes an increase (based on a sol-gel process [1]) or decrease [2] in viscosity of the liquid in one of the branches of a channel junction; this controls the flow distribution between the two branches. Magnetic actuation has been applied for the sorting of particles, where a strong magnetic field pulls the magnetic [3] or magnetically labelled [4] particles into the desired output channel. Many sorters have been presented, based on mechanic actuation applying either internal [5] or external valves [4, 6-10] to switch the flow to the desired channel branch. Electric actuation has also been extensively used to sort particles [11-22]. Finally, a sorter using optical tweezers has been demonstrated [23].

The sorters developed in this chapter will be based on dielectrophoresis, a form of electric actuation. Dielectrophoresis is defined as the lateral motion imparted on uncharged particles as a result of polarisation induced by non-uniform electric fields. It is an attractive actuation principle for microfluidics because it requires no moving parts, no labelling of the sample and no high voltages. Furthermore, the actuators are simple electrodes, which make dielectrophoretic based particle sorters suitable for integration with other components into larger systems. Although for most macro-systems the forces generated by dielectrophoresis are not significant, the situation is different for microsystems. IC-technology enables the fabrication of very small electrode geometries with dimensions comparable to those of the particles. With these micro-electrodes very strong field gradients can be realised to create sufficiently large dielectrophoretic forces.

Different types of dielectrophoretic particle sorting can be distinguished. The first type is two-dimensional spatial separation of a binary mixture of particles, which has been demonstrated in many forms and for all kinds of particles, down to particles in the sub-micron range e.g. [11-15]. Another interesting approach is found in [16] where particles are analysed and sorted by temporarily trapping them using a trapezoidal arrangement of electrodes.

The type of sorter that is the focus of this chapter is a so-called flow-through particle sorter. In contrast to the dielectrophoretic sorter types mentioned before, there is no accumulation of particles in a flow-through configuration. A flow-through sorter works like a switch that sends the particles either to one or the other branch of a channel junction (see Figure 6-1). In literature a number of flow-through sorters have been presented [17-22], but these typically operate at relatively low flow-speeds compared to the sorters found in (macro) cytometry.

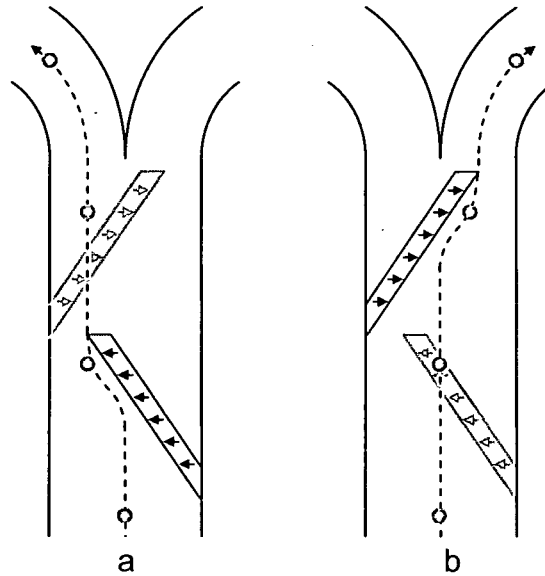


Figure 6-1. Schematic representation of the operation principle of a flow-through particle sorter based on negative dielectrophoresis; it allows sending the particles either into the left branch (a) or into the right branch (b) of the outlet channel.

In this chapter dielectrophoretic flow-through particle sorters will be analysed, to design a sorter that is suitable for high flow-speeds. During the analysis most variables influencing sorter performance are discussed, but the main focus is on the design of the electrodes, where the configuration, shape and topology of the electrodes will be optimised for high-speed.

6.2. Theory

The force on a particle generated by the non-uniform electric field can be calculated with the following formula [24]:

$$F_{DEP} = 2\pi\epsilon_l r^3 \text{Re}(K_{CM}) \nabla E_0^2 \quad (\text{Formula 6-1})$$

where ϵ_l is the permittivity of the liquid, r is the radius of the particle, $\text{Re}(K_{CM})$ is the real part of the Clausius-Mossotti function and E_0 is the electric field. In the lossless case K_{CM} can be written as:

$$K_{CM} = \frac{\epsilon_p - \epsilon_l}{\epsilon_p + 2\epsilon_l} \quad (\text{Formula 6-2})$$

where ϵ_p is the permittivity of the particle. To analyse the dynamic behaviour of a particle also the drag force is important, which is related to the particle speed, size, shape and surface characteristics. For a smooth sphere the Stokes approximation for this force is:

$$F_{DRAG} = 6\pi\eta r \vec{v} \quad (\text{Formula 6-3})$$

where η is the viscosity of the fluid and v is the speed of the particle. The final force considered here is the buoyancy force:

$$F_B = \frac{4}{3}\pi r^3 (\rho_l - \rho_p) \bar{g} \quad (\text{Formula 6-4})$$

where ρ_l and ρ_p are the densities of the liquid and the particle respectively and g is the gravitational constant. When these forces are constant a steady state will be reached (after an initial transient period) where the settling speed of the particle is given by:

$$v_{\text{settle}} = \frac{\epsilon_l r^2 K_{CM} \bar{\nabla} E_0^2}{3\eta} + \frac{2r^2 (\rho_l - \rho_p) \bar{g}}{9\eta} \quad (\text{Formula 6-5})$$

The first part of this equation is caused by F_{DEP} and the second part is determined by F_B . Of course F_B only plays a role in the vertical direction. The time constant for this process is:

$$\tau = \frac{2\rho_p r^2}{9\eta} \quad (\text{Formula 6-6})$$

In this chapter we analyse the dielectrophoretic force on polystyrene particles with a radius of 12 μm in purified water. For this situation the time constant is only 32 μs . Because of this short time-constant the particles can be considered to travel at settling-speed constantly, as long as there are no sudden changes in the electric field. With the gradually sloping sorter configurations analysed here this seems justified.

6.3. Critical flow speed

The goal of flow-through dielectrophoretic sorters is to move particles in the horizontal plane as they move through the micro-channel, so that they end up in the proper outlet (see Figure 6-1). Many of the flow-through sorters found in literature show a straight dielectrophoretic element that is placed inside the flow-channel at an angle with flow-direction of the liquid. The elongated shape that results makes sense, because it maximises the time a particle is exposed to the sorter. As a result the required force on the particle does not need to be very large to still allow for successful sorting.

Increasing the flow-speed of the sample liquid reduces the time that the particles are exposed to the dielectrophoretic actuator and therefore the displacement that can be achieved reduces as well. At a certain flow speed the dielectrophoretic force (in the region with the maximum field gradient) is just sufficient to push the particles sideways far enough to make them follow the outline of the electrodes. This is the critical flow speed of the sorter, the highest flow speed for which the sorting still works properly.

At flow speeds higher than the critical flow-speed the particle will break through the barrier formed by the maximum electric field gradient and will no longer follow the outline of the sorter electrodes. At these flow speeds sorting is no longer possible. To increase the critical flow speed of the sorter, either the maximum horizontal velocity that the sorter can generate has to be increased, or the required horizontal displacement has to be lowered. Both methods will be investigated in this chapter by optimising the configuration and the topology of the electrodes.

6.4. Design variables

Besides the design of the electrodes there are many other variables that also have significant influence on the sorter performance. Before the influence of the sorter electrodes is thoroughly studied, these other factors are briefly discussed below.

Firstly, there are the channel dimensions. The height of the channel has a strong influence on the maximum force that can be generated. When electrodes are applied both on top of the channel and on the bottom of the channel the maximum field strength is inversely proportional to the height of the channel, and therefore the dielectrophoretic force is inversely proportional to the square of the channel height (see Formula 6-1). When electrodes are applied only on the bottom of the channel the maximum force also changes with the channel height but now the relation is more complicated and depends on the electrode geometry. However, in both cases the following is clear: the smaller the channel height the larger the maximum attainable forces. The minimum channel height is typically governed by clogging problems for relatively small channel dimensions. So, there is a trade-off between performance and reliability.

The width of the channel has in first order not much influence on the performance when the flow-rate is kept constant, because the two main effects from widening the channel play a compensating role. When the channel is wider a particle has to travel a longer distance from one side of the channel to the other side. At the same time, the flow speed of the liquid suspending the particle goes down proportional to the width-increase of the channel. When buoyancy effects are neglected these effects exactly balance out. A small performance increase for wider channels might be observed as a consequence of a change in the velocity profile. The flow profile becomes less parabolic and more uniform for large aspect ratio channels, which reduces the relative liquid velocity maximum in the centre of the channel somewhat.

The length of the sorter element is directly proportional to the maximum flow-speed the sorter can handle. When the sorter element is longer (and the angle of the electrode with the direction of flow is less) the particles will experience a force from the dielectrophoretic element for a longer period of time. Therefore, less displacement per unit time is required for successful sorting operation in a longer sorter, so the flow-speed can be higher. However, this does not improve the sorting speed. To be able to sort out individual particles, only one particle can be present at an electrode at the same time. So, although the flow-speed is higher, the time that a particle is exposed to an electrode remains constant, since the horizontal speed that causes the required displacement (see Formula 6-5) does not change.

Beside the geometry of the channel also the size of the particles and electrical properties of the particles and liquid have influence on the performance of the sorter. The dielectrophoretic force is proportional to the third power of the particle radius (see formula 6-1), while the drag force is proportional to the radius (see Formula 6-3). As a consequence the sorting speed increases with the square of the particle radius (see Formula 6-5), so larger particles can be sorted faster than smaller ones. The combination of the liquid and the particles should be chosen such that their permittivity is quite different, which results in a Clausius-Mossotti factor close to -0.5 (the strongest negative dielectrophoretic effect, see Formula 6-2). Using a liquid with a low viscosity also improves performance, since it reduces the drag force on the particle (see Formula 6-3).

Finally, the applied voltage has direct influence on the sorter performance: the electric field strength increases proportional to the voltage, which leads to a square increase in the dielectrophoretic force (see Formula 6-1). However, the voltage is limited by Joule heating effects [18, 25-28]. Joule heating may lead to a temperature rise that influences the sample,

especially in highly conductive media this can be an issue. The Joule heating also causes temperature gradients in the liquid and therefore gradients in density, permittivity and conductivity. The changes in density result in liquid flows due to natural convection and the gradients in permittivity and conductivity cause interactions with the electrical field. The latter interactions lead to electric forces on the liquid. At frequencies below 0.5 MHz AC electro-osmosis at the electrode surface has been observed [26].

6.5. Electrode configuration

The electrode configuration has significant influence on the sorter performance. It makes sense to improve the sorter performance by optimising the electrodes, because most of the variables discussed in the previous paragraph are typically dictated by the application. The optimisation starts with a qualitative analysis of four electrode configurations in a cross-sectional plane of the sorter. The four electrode configurations can be split in two groups. The first two configurations only have electrodes located on the bottom of the channel, while the other two configurations have electrodes both at the top and on the bottom of the channel. Configuration I has two equally sized electrodes, located on the bottom of the channel. The electrodes have a width of 25 μm and a spacing of 70 μm . Configuration II is comparable to configuration I, but now the electrodes extend to the side-walls of the channel. In configuration III the electrodes have the same dimensions as in configuration I, but here they are located on the bottom and at the top of the channel. In configuration IV the electrodes on top and bottom of the channel extend from the middle of the channel to the side-wall on one side (see Figure 6-2).

Finite element simulations have been performed to calculate the electric field distribution for each electrode configuration in a 2D plane, using the *NetFlow* module of the finite element simulation package *Coventorware 2003.1*. The models consist of about 10,000 elements and represent a channel with a height of 70 μm and a width of 1 mm. In the left column of Figure 6-2 the logarithm of the electric field intensity squared is plotted for each electrode configuration (for clarity only the middle section of the channel is shown; the vertical dimensions of the plots have been stretched).

Based on the numerical data of the electric field simulation the steady state velocity vectors for a particle with respect to the liquid were analytically calculated for a cross-section of the sorter module using Formula 6-5. This calculation was performed in *Matlab 6.1*. The direction vectors for the resulting vector field are plotted in the middle column of Figure 6-2. The calculations were performed for polystyrene particles with a radius of 12 μm in a watery liquid with a voltage difference between the electrodes of 9.1 V_{RMS} (to match experimental conditions). The direction vectors illustrate the qualitative behaviour of the particles in the plane orthogonal to the direction of flow. They show that the particle behaviour near the electrodes is dominated by the dielectrophoretic force and that the buoyancy force (pulling the particles downward) plays a role near the sides of the channel.

To illustrate the quantitative values for this sort of devices, the maximum horizontal (sorting) velocity that can be obtained with each electrode configuration as a function of the channel height is plotted in the right column of Figure 6-2. Next, these three series of graphs will be discussed in more detail for each electrode configuration.

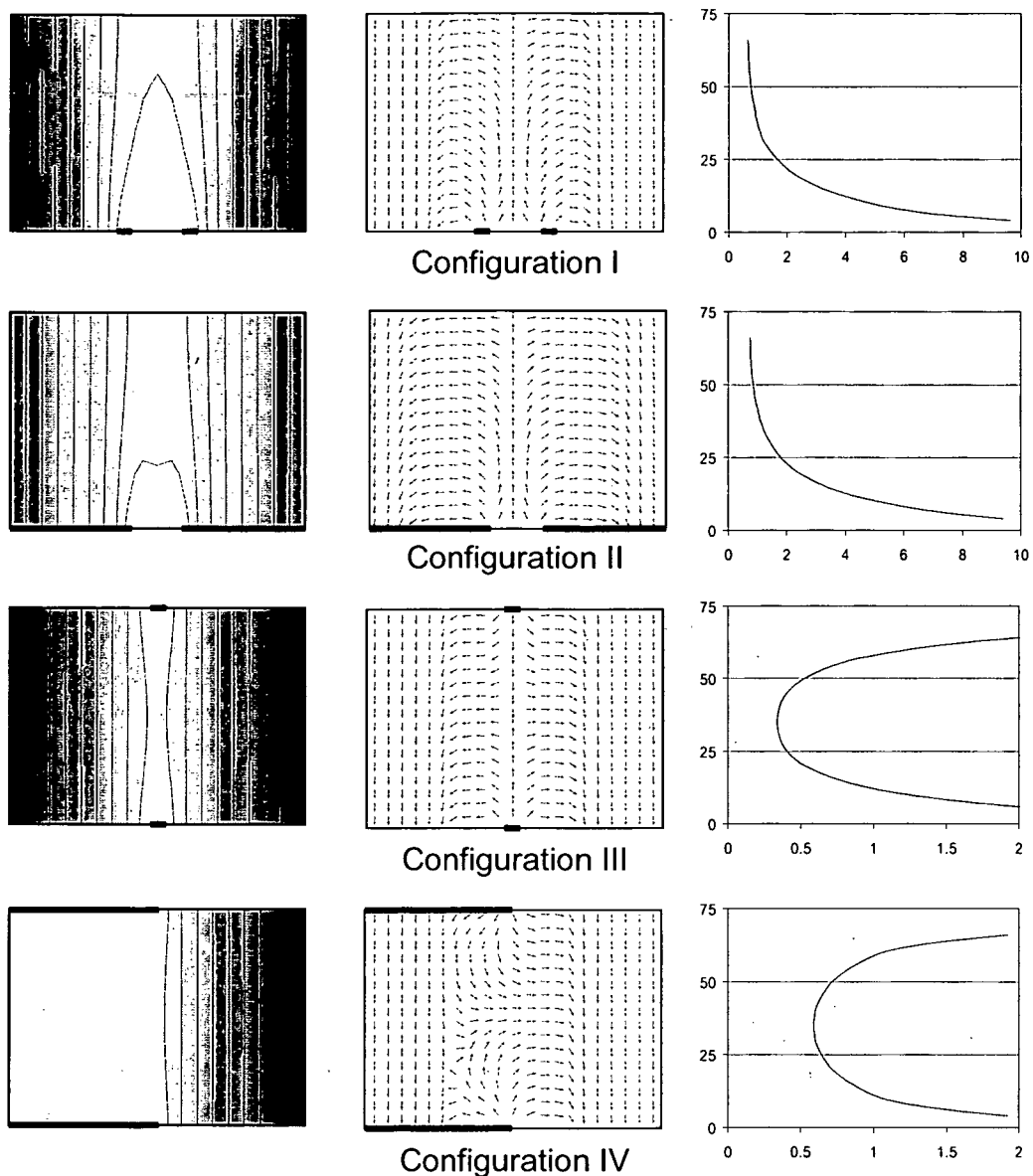


Figure 6-2. The distributions of the electric field (left) and the velocity vector field (middle) for a cross-section of the channel (for clarity only the middle section of the channel is shown and the vertical dimensions of the plots were stretched); in the right graphs the maximum horizontal speed generated by the actuator (horizontal axis in mm/s) versus the position in the channel (vertical axis in μm) are displayed for the four electrode configurations analysed (from top to bottom).

6.5.1. Configuration I

The main part of the electric field distribution of configuration I is concentrated in the area around the electrodes and drops rapidly in all other directions. This means that there is a large field gradient, which generates a strong force in this area, but in the rest of the channel cross-section a particle will only experience a weak force.

From the plot of the direction vectors it becomes clear that besides the wanted horizontal motion there also is a vertical component that pushes the particle upwards as it moves along the actuator, into the region where the electric field intensity is less strong. Near the sides of the channel the vertical gradient in the electrical field squared is so weak that the particles tend to sediment to the bottom of the channel in these regions.

In the right graph that depicts the maximum horizontal speed that can be realised with this actuator, it can be seen that the maximum achievable horizontal speed drops dramatically at larger heights. While at a height of 10 μm a speed of almost 6 mm/s can still be achieved, the maximum speed at a height of 30 μm is already 4 times less.

6.5.2. Configuration II

In configuration II both electrodes extend to the side-walls of the channel. In the electric field plot it can be seen that as a consequence the electric field is stronger in the higher parts of the channel (marked by the lighter colour). The plot of the direction vectors for this configuration shows that the electric field gradient is distributed over a larger area in the horizontal plane. The maximum velocity plot reflects the observations that were made in the previous two plots. Although for this configuration there still is a large drop in the maximum velocity higher in the channel, the absolute value at the top of the channel is still somewhat higher than in configuration I. The distribution of the electric field gradient over a larger horizontal area leads to a somewhat lower sorting speeds at smaller heights. This, however, is not an issue since the overall sorter speed is constrained by its (substantially lower) performance at higher vertical positions.

6.5.3. Configuration III

For configuration III the electric field distribution looks very different. The electrodes at top and bottom create an electric field that is concentrated (in the horizontal plane) around the middle of channel and that is relatively constant over the channel height. Such a field distribution is very suitable to push a particle sideways, because in the horizontal direction there is a strong horizontal field gradient over the full height of the channel.

The maximum obtainable horizontal flow-speeds are quite different for a configuration with electrodes on both top and bottom of the channel. The maximum velocity plot shows a substantially smaller drop, with its minimum at the middle of the channel. This minimum is much larger than for the configurations with electrodes located on only the bottom of the channel (note that a different scale is used for configurations III and IV for this graph).

6.5.4. Configuration IV

In configuration IV the electrodes on top and bottom of the channel extend to the left side wall. In the plot of the electric field distribution two effects can be observed. Firstly, on the left side of the channel a strong electric field is present. Secondly, and more of interest, the horizontal gradient in the electric field has increased at the right side of the channel. This means that a particle can be pushed sideways more strongly.

In the plot of the direction vectors the non-symmetrical behaviour of this configuration is very clear: particles can only be pushed efficiently to one side with this configuration. On the left side the electric field has become so uniform that there is practically no electric field gradient left and therefore the buoyancy forces dominate the behaviour there. The maximum horizontal velocity graph shows the result of the increased gradient most clearly by an increase in the speeds that can be achieved at the middle of the channel. Configuration IV shows the highest minimum in the velocity graph, so this configuration is expected to perform best.

6.6. Simulation of electrode configuration

In the previous paragraph the qualitative flow behaviour was deduced from a 2D analysis. To analyse the performance of the different configurations in a quantitative way, the simulation model will now be extended to 3 dimensions. The method applied here is based on the orthogonality of the dielectrophoretic force and buoyancy force in a cross-sectional plane of the flow-channel with respect to the velocity of the liquid in a direction along the flow-channel.

The velocity profile of the liquid under pressure driven actuation was calculated for the flow-channel using the *MemCFD* module of the finite element simulation package *Coventorware 2003.1*. By adding the velocity vector components of the liquid itself to the vectors that describe the particle motion with respect to the liquid, the 3D vectors are obtained that describe the 3D particle motion for a single plane of the device. By repeating this procedure with a small horizontal offset for the electric field, the 3D particle velocity vector field for the sloped sorter layout is obtained. This can be used to calculate particle trajectories, which are essentially the streamlines in the velocity vector field. The *stream3* routine in the mathematics software package *Matlab 6.1* was used to calculate these streamlines.

The 3D simulation model that has been constructed by stacking 2D simulation has a length, width and height of 1.5 mm, 1 mm and 70 μm respectively. As a particle moves along the channel it experiences a maximum displacement of 750 μm (when it started near the wall on the 'wrong' side of the channel). The particle trajectories start evenly distributed over the whole channel cross-section and should all end within the left part of the channel. The maximum average flow speed (since the flow speed is not uniform across the channel) of the liquid for which the particles could be sorted (or in other words where the trajectories remained on the proper side of the actuator) was determined for each electrode configuration. Simulations were performed for polystyrene spheres with a radius of 12 μm in a watery solution. A voltage of 9.1 V_{RMS} is applied between the two electrodes to match experiments.

The simulation results for the four sorter configurations are depicted in Figure 6-3. The most striking about the results is the variation in critical flow speed: the performance varies by almost a factor 3, only as a result of changes to the electrode arrangement. Furthermore, as predicted in the qualitative analysis, there is a large performance difference between the single-sided configuration with electrodes only on the bottom of the channel (I, II) compared to configurations with electrodes on both top and bottom of the channel (III and IV). This has to do with the much lower electric field density of the single-sided electrode configurations near the top of the channel. Since the overall maximum flow speed that can be handled is determined by the minimum performance anywhere along the cross-section of the channel, this causes the single sided configurations to perform substantially less.

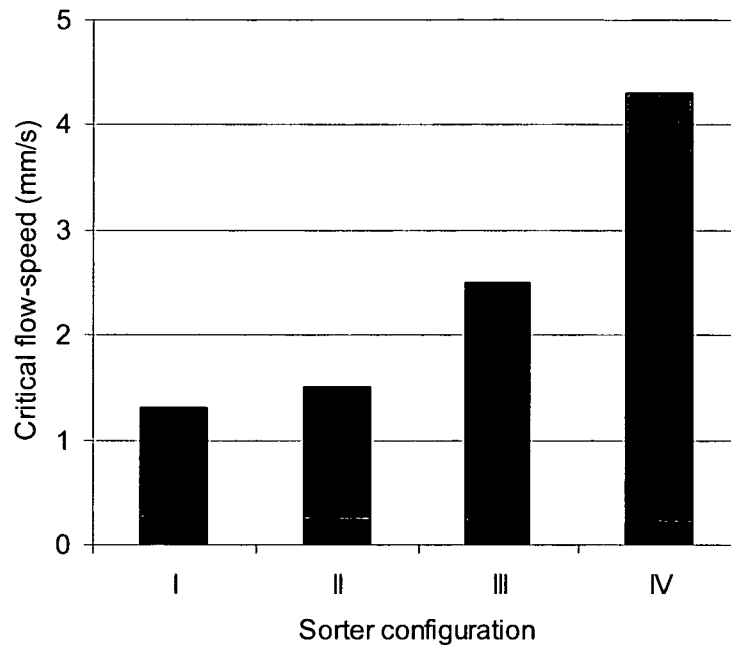


Figure 6-3. Simulation results of the critical flow-speed for the four sorter configurations based on the stacked simulation model.

For the single-sided electrode configurations extending the electrodes to the channel side walls in configuration II improved the electric field intensity near the top of the channel somewhat. The simulation results show an overall performance increase of 15% for configuration II compared to configuration I. Although the performance obtained with these configurations is considerably lower than with the double sided electrode configurations their performance is still very usable. Furthermore they have the advantage that they are easier to fabricate than the double-sided configurations. So if in a certain application performance is not critical these configurations can be the right choice.

Under the same conditions the double-sided configurations III and IV show much higher performance. This can be understood when one considers that for the double sided electrode configurations the electric field intensity fans out over only half the channel height after which it increases again thanks to the opposite electrode. The higher performance of configuration IV with respect to configuration III can also be explained. Configuration IV has a higher maximum horizontal field gradient, which is located near the edge of the electrodes where the relatively uniform field on the left side goes over into the more non-uniform field on the right side (see Figure 6-2 bottom left). Because the performance increases with the square of the electric field intensity, moderate changes in the electric field can result in substantial performance differences. Besides the higher complexity, another drawback of the double-sided electrode configurations is that the electrodes partially block the view inside the channel when common electrode materials (gold, platinum) are used. This can be solved, by using a top electrode that is made of a transparent conducting material, such as for example Indium Tin Oxide (ITO).

Two assumptions have been made in this method that allow for the relatively fast and easy simulations. The first assumption made is that the particles travel at settling speed all the time. This approximation is very safe since the time constant for the particles to reach settling speed is more than four orders of magnitude faster than the time it takes for a particle to flow past the sorter.

The second approximation made is that the dielectrophoretic forces can be considered orthogonal to the velocity of the liquid. This is only justified for structures that have an elongated appearance such as the gradual sloped sorters considered here. The errors that are introduced with this approximation emanate from the fact that there are also dielectrophoretic forces along the direction of flow. However, these forces are rather small compared to the drag force by the flowing liquid. The effect of the dielectrophoretic forces along the direction of flow would lead to a minor slowing down of the particles. Taking this into account should result in slightly higher maximum performance.

6.7. Electrode shape

In the previous paragraphs the configuration of the electrodes in a cross-sectional plane of the sorter has been studied. In the following sections the layout of the electrodes in the top and bottom plane will be analysed, starting with the shape of the electrodes.

For a pressure driven flow the velocity-profile of the liquid is not flat over a cross-section of the channel. A channel having almost equal width and height has a flow-profile that is not only parabolic in the vertical plane, but also along the horizontal plane, where the sorting has to take place. It is clear that the optimal sorter shape is not straight in this situation. Near the walls a particle moves slower along the direction of flow than in the middle of the channel, therefore near the walls the angle of the sorter element with the direction of flow can be larger than in the middle of the channel. The primitive function of the velocity distribution along the width of the channel is the optimal shape for the electrodes, since in this situation the required horizontal velocity is constant. For a parabolic flow-profile this results in S-shaped electrodes. However, in most practical micro-channels the width is much larger than the height, causing the flow profile to be almost flat along the horizontal plane. This means that the optimal shape of the electrodes is less curved for relatively wide channels. In Figure 6-4 it is shown how much performance can be gained with curved electrodes in comparison to straight electrodes as a function of channel width. The data for this figure was obtained by running a series of finite element simulations with *Coventorware 2003.1* to calculate the velocity profile for channels having different aspect ratios. The graph clearly shows that for channels with an aspect ratio of about 10 or larger (most practical channels) the performance gain with curved electrode is marginal. So, only for channels having an almost equal height and width the curved electrodes will result in a significant performance increase (up to 50%). For all other channels straight electrodes would be almost as good.

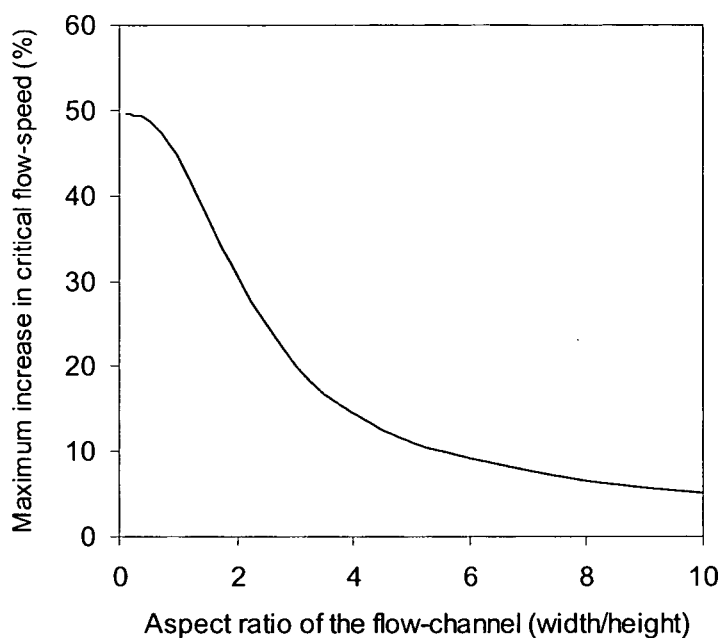


Figure 6-4. The theoretical increase in critical flow-speed that can be realised by applying curved electrodes in stead of straight electrodes as a function of the aspect-ratio of the flow channel.

6.8. Sorter topology

Besides optimising the shape of the sorter elements, the arrangement of the sorter elements can also be improved. Different criteria can be used to optimise a sorter for high speed. The first criterion considered here is the maximum flow-rate. Based on this criterion the sorter should be optimised for a maximum through-put of sample liquid. The second criterion that will be discussed is that of maximum switching speed..Here the sorter is optimised to handle a flow with a minimal distance between the individual particles.

6.8.1. Switching electrode topology

As previously discussed the critical flow speed of the sorter depends on the horizontal speed that can be generated. However, the critical flow speed can be increased at the same horizontal speed when the angle of the electrodes with the direction of flow is reduced. For a sorter with a fixed length this means that the horizontal displacement is reduced. Successful sorting with a smaller horizontal displacement can still be achieved by increasing the number of outlet channels (see Figure 6-5). In a sorter with two outlets, a particle would have to travel a maximum distance of half the channel width (if it starts near the wall on the 'wrong' side of the channel) at each sorter element. By adding more outlets the maximum distance that a particle needs to be moved becomes less, since an appropriate outlet is nearer. The outlets near the wall of the channel should have half the width of an outlet that is located in the middle of the channel to keep the required displacement at a minimum. Using this outlet arrangement, the required displacement reduces to only one quarter of the width of the channel for three outlets, to one sixth for four outlets, etc. In contrast to elongating the entire sorter (which also reduces the angle between the electrodes and the direction of flow) this solution actually increases the sorting speed. The length of the electrodes remains unchanged,

while the particles move faster. This means that a particle is exposed to an electrode for a smaller amount of time, which allows handling more particles per unit time.

However, there is a price to be paid for the increase in sorter performance. As the number of outlets increases, the width of each outlet decreases. This means that the tolerance on the particle placement gets smaller; for a very large number of outlets this could lead to decreased sorting accuracy. The accuracy could be restored by keeping the width of the individual outlets the same, while increasing the number of outlets. This, however, would lead to (much) larger sorter geometries. So there is a trade-off between speed, reliability and size.

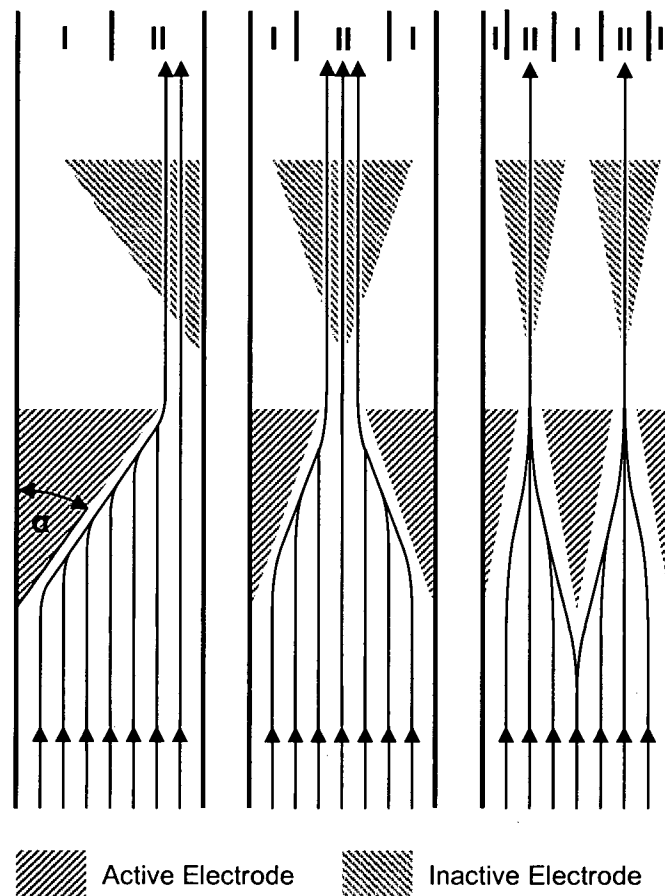


Figure 6-5. Increasing the number of outlets reduces the required displacement; this allows reducing the angle of the sorter elements (a) with the direction of flow, which increases the critical flow-rate.

6.8.2. Focusing electrode topology

The maximum switching-speed of a sorter depends on the size of the sorter elements. This can be easily seen: to direct successive particles to different outlets, the actuation of different sorter elements is required. A sorting element can only be switched after the current particle has completely passed the element, so only one particle can be guided by a single sorter element at the same time. In order to maximise the switching-speed, the time a particle spends at a sorting element should be minimised, which means that the displacement induced by this element will also be minimised. Thus a sorter topology is required where the switching sorter elements should be as small as possible. This is achieved by the focusing sorter topology depicted in Figure 6-6. It consists of two parts: a static part with large focussing elements and

a dynamic part with small switching elements. The focusing electrodes are continuously activated and concentrate all particles into narrow streams that are in line with the boundaries between the outlets. The small switching elements only need to give a particle its final push into one or the other outlet depending on the type of particle. The advantage of this geometry is that the distance between the particles is only determined by the length of the switching elements, instead of the larger elements of the previous topology.

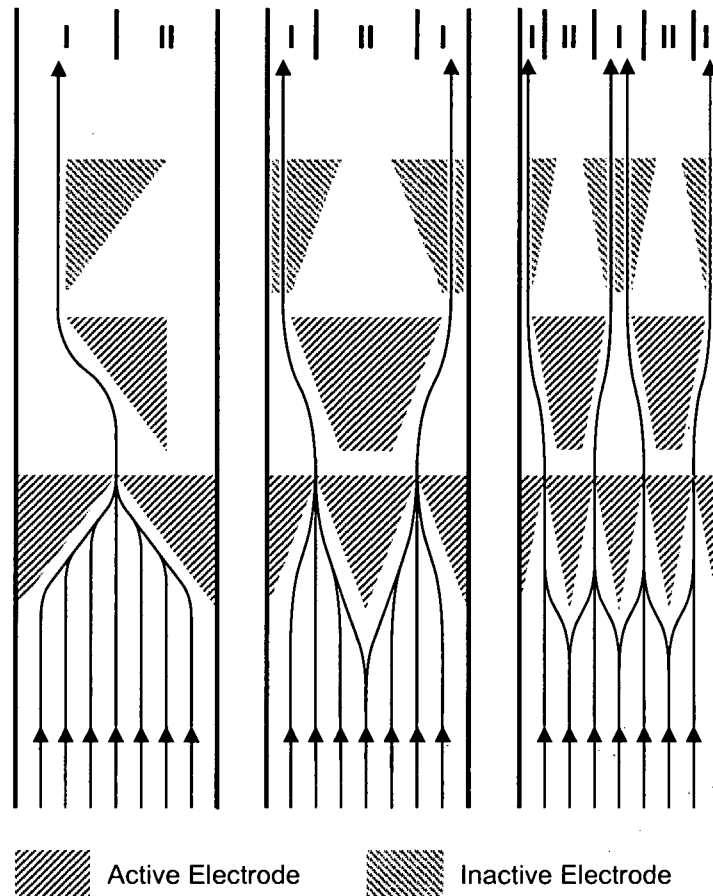


Figure 6-6. In the focusing electrode topology all particles are first focused to streams that are in line with the boundaries between the outlets; the switching elements only need to give a particle its final push into one or the other outlet, which maximises the switching speed.

6.8.3. Sorter selection

When selecting the topology for a sorter the following practical consideration should be taken into account. For a sorter with less than four outlets it is possible to recombine the different outlets to two outlets on a chip-level, without the need to cross any flow-channels. For four or more outlets crossing flow-channels is inevitable to recombine them at the chip-level. In case it is decided to recombine the outlets off-chip rather than on-chip, more than two outlet connections are required. In the first situation the chip will require an additional layer and in the second situation the chip will typically have to be larger to make space for additional connectors. So, using four or more outlets comes at a price.

6.9. Simulation of electrode topology

Based on a theoretical analysis of the configuration, shape and topology of the electrodes several performance enhancements were proposed. To verify how these theoretical improvements translate into real-life gains four sorter configurations were designed that implement these enhancements step by step (see Figure 6-7). Based on the simulations with the stacked 2D model in paragraph 6.6, only sorters with electrodes on the bottom and at the top of the channel will be considered.

The first two sorter configurations are the ones that performed best in the cross-sectional analysis. To avoid confusion the same numbers as in the previous analysis will be used and therefore they will be referred to as sorter configuration III and IV. Configuration III is the configuration often used in literature and it serves as a reference model. Configuration IV is of interest since it should bring a major improvement in sorter performance, at relatively minor changes. Sorter configurations V and VI have three outlets in stead of two, to further increase the performance. One geometry (V) is based on the switching electrode topology, where the other (VI) has the focusing electrode topology.

The four sorter configurations were designed with straight electrodes, since the velocity profile of the liquid in the horizontal plane is almost flat because a channel is used that is much wider (1 mm) than it is high (70 μm). In this situation the performance that could be gained with curved electrodes would have been less than 5% (see Figure 6-4).

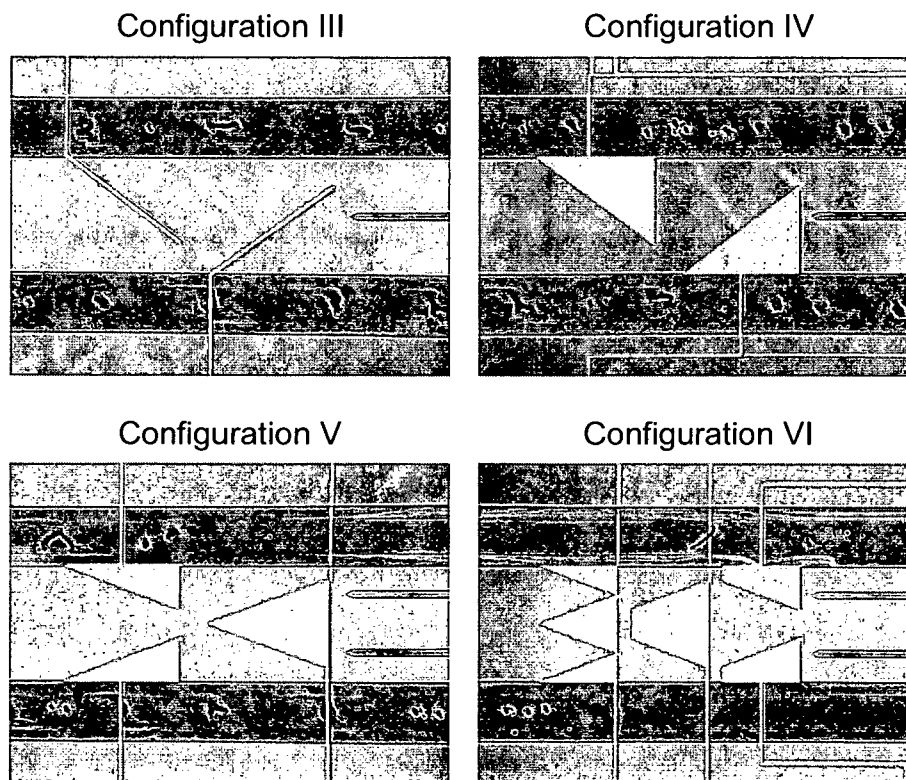


Figure 6-7. Photographs of the four sorter configurations that will be further analysed; strip electrode (III), plane electrode (IV), switching electrodes with 3 outlets (V) and focusing topology with 3 outlets (VI).

The four final sorter structures were analysed by simulation. The simulation procedure is comparable to the one described in paragraph 6, but now all simulation have been carried out in 3D. This is necessary to accommodate topologies V and VI. As a consequence the number of elements of a complete 3D model is substantially less than in the stacked models, since the electric field distributions had to be simulated for the whole model at once. However, in contrast to the simulations performed with the stacked model, the 3D simulations performed here do allow taking the dielectrophoretic effect into account in all three dimensions (so also along the direction of flow). Figure 6-8 shows the simulations results for a sorter of configuration IV for both sorting states (for clarity only a few trajectories at the middle of the channel are depicted). The results of the 3D simulations are summarised in Figure 6-9 and will be discussed in detail in paragraph 6.11.

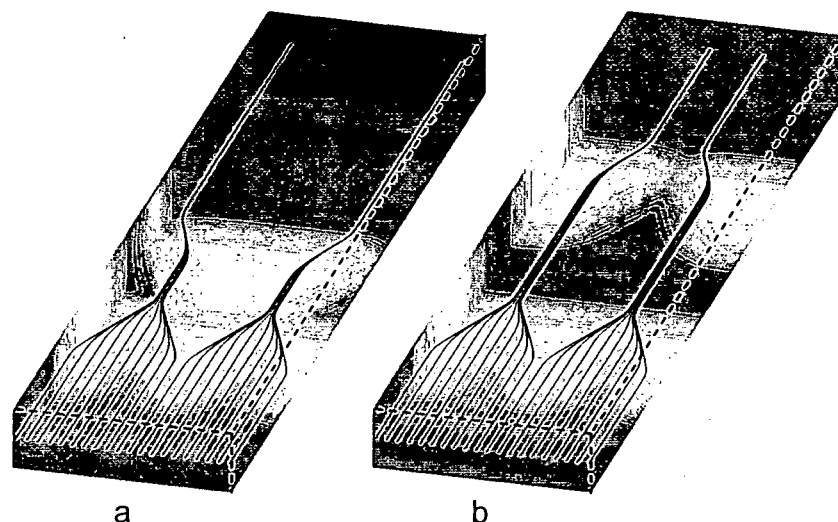


Figure 6-8. Simulation of particle streamlines with the 3D simulation model for sorters of configuration VI; the particles are either switched to the outlets near the walls of the channel (left) or to the outlet in the middle of the channel (right).

6.10. Sorter experiments

The four sorter configurations described in the previous paragraph were fabricated based on the SU-8 process described in chapter 2. On a silicon wafer gold electrodes (300 nm) were defined using a lift-off process with chromium as an adhesion layer. Inlets for the liquid were defined by anisotropic etching from the back. On a glass a second set of gold electrodes were applied. SU-8 was used to define a 70 μm deep and 1 mm wide channel and was also used to bond the two wafers together.

The chips were placed in a custom-made holder, where the liquid contacts were sealed by O-rings and the electrical contacts were formed by spring-pins (see paragraph 2.6). A 1 MHz AC-Voltage of 9.1 V_{RMS} was applied to the electrodes. A dilute suspension of polystyrene microspheres with a radius of 12 μm (Duke Scientific) was pumped through the chips using syringe pumps (kdScientific model 200 series). The flow-rate was increased in small steps until the particles could no longer follow the outline of the electrodes. The experiments were performed for both sorting states (activating either one or the other set of sorting electrodes) and the average results are plotted in Figure 6-9.

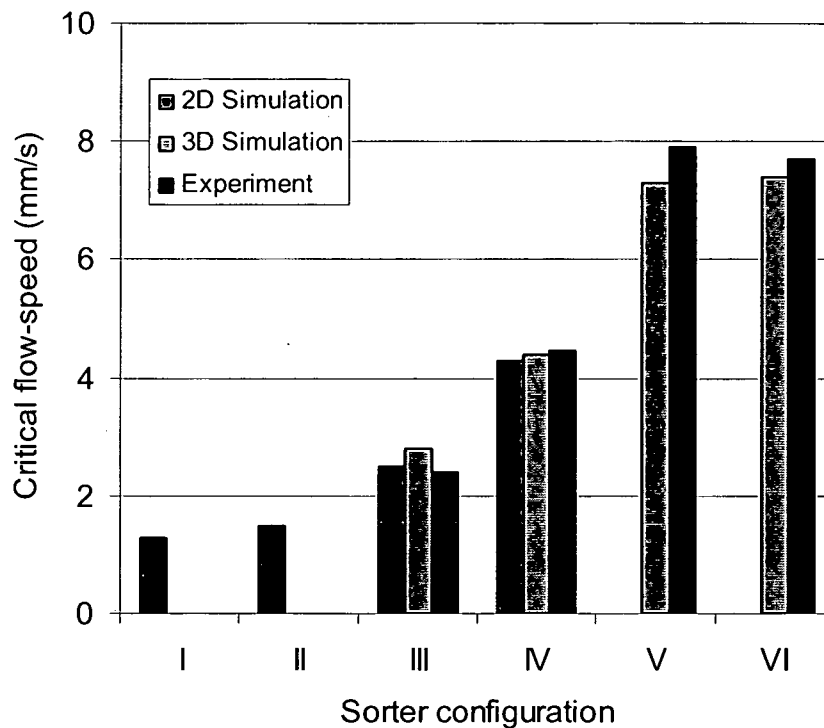


Figure 6-9. An overview of the performance of the sorter configuration based on the stacked 2D simulation model, the 3D simulation model and the experiments.

6.11. Results and discussion

Both experimental results and simulations demonstrate that with the optimised sorter configurations high performance gains can be achieved. The best sorter designs show a performance increase of more than 200% compared to the sorter with strip electrodes on top and bottom (Configuration III) known from literature. During the experiments a very accurate placement of the particles in the middle of the outlets was observed (see Figure 6-10), indicating that by increasing the number of outlets the critical flow-speed can be raised even more, without sacrificing sorter accuracy.

A comparison between the experimental results and the simulations shows a very good match. The simulations with the stacked 2D model and with the 3D model also show good agreement. This means that the simplification was allowed not to take into account the dielectrophoretic forces along the direction of flow in the stacked 2D model. Actually, the stacked 2D model shows better agreement with the experimental results for configuration III than the 3D model. This probably has to do with the number of the elements, which was significantly higher in the stacked 2D model. The diagonal sorter shape had to be approximated with square meshes, where the effects of the discrete approximations are expected to be most severe for relative narrow structures such as the line electrodes

In the simulations the redistribution of particle due to hydrodynamic forces has not been taken into account, based on previous experiments [16]. During the sorting experiments no notable influence of hydrodynamic forces was observed. After the particles had followed the outline of the active electrodes they followed a straight trajectory to the outlet (see Figure 6-10). So, these experimental observations and the good match between simulation and experiment seem to justify this decision.

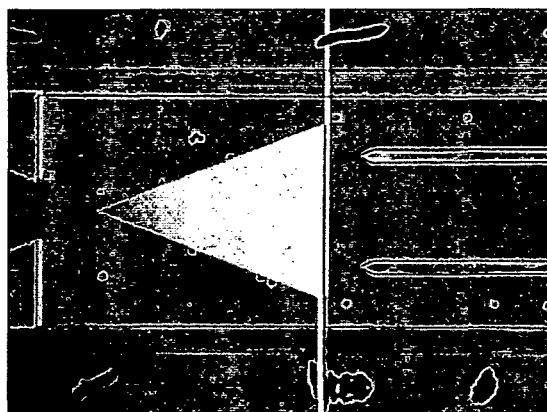


Figure 6-10. A photograph of the sorter chip in action; the particles follow the outline of the electrodes and continue with a straight trajectory into the outer outlets (note: for clarity a higher particle concentration is used)

The focus of the optimisation has been on the critical flow speed of the sorters, which is the area that is mainly responsible for the limited usability of dielectrophoretic sorters; other properties such as the optimal frequency of the AC-signal or the time required to switch an electrode have not been investigated. These values, however, can be assumed to be similar to the values for sorter found in literature [17-22], since the basic actuation principle has remained the same.

6.12. Joule heating

One aspect that has not yet been discussed up till now is heating. The potential difference applied between the electrodes causes a current, which results in Joule heating. Especially in biological applications the temperature increase of the liquid is of importance, since it could interfere with the sample. The amount of heat generated depends on a number of parameters [8, 17, 18]. Based on Ohm's law the following factors can be identified:

- potential difference between the electrodes (quadratic dependency)
- distance between the electrodes (linear dependency)
- conductivity of the liquid (linear dependency)
- electrode area (linear dependency)

The temperature rise that occurs as a consequence of the heating depends on the flow-rate of the liquid. At a higher flow-rate the same amount of heating power is applied to a larger volume of liquid. As a result the temperature rise is inversely proportional to the flow-rate. Finally, the geometry of the electrodes also plays a role in the maximum occurring temperatures.

To investigate the amount of Joule heating for the four sorter configurations, finite element simulations were performed with Coventorware 2003.1. The model consists of the flow-channel with electrodes at top and bottom. A voltage of 9.1 V is applied between the electrodes (to match the experimental conditions). A watery liquid with a conductivity of 10 mS/m is pumped through the channel at the critical rate of each sorter, which ranges from 2.4-7.9 mm/s, depending on the configuration. It was decided to convey all the heat from the device by the liquid and not to take into account any heat transport through the substrate, since this would depend very much on the materials used. As a result the simulations depict a worst-case situation. The simulation results are summarised in Table 6-1.

Table 6-1. The temperature rise in each of the sorter configurations operated at the critical flow-rate (2.4-7.8 mm/s) for a voltage of 9.1 V and a conductivity of 10 mS/m.

Configuration	I	II	III	IV
? T_{\max} (K)	1.4	3.0	2.1	3.6
? T_{avg} (K)	1.2	1.8	1.8	3.3

Configurations II and III do show about 50% more temperature rise than the default strip electrode of configuration I. Although more heat is generated due to the larger electrode area, this is partially compensated by the higher flow-speeds at which these configurations can be operated. Configuration IV causes a significantly larger rise in temperature, which mainly has to do with the larger electrode area compared to configuration III, while operating at the same flow-speeds.

It should be noted that the maximum temperatures are generated at locations between the electrodes, where the particles should not be present under normal operation conditions. Therefore, the average temperature rise, after the heat has spread evenly is of most importance. An interesting consequence of the scaling laws for this system is that higher flow-speeds can be achieved without an increase in temperature rise, since both the critical flow-speed and the amount of heat generation increase with the second power of the voltage between the electrodes. If in a certain application the temperature rise is a critical factor or when highly conductive liquids are required, it is also possible to realise the switching electrode topology or the focusing electrode topology with line electrodes instead of plane electrodes.

6.13. Conclusions

In this chapter the design of dielectrophoretic flow-through sorters has been analysed in detail. It was found that sorters with electrodes both on top and on the bottom of the flow channel show significantly higher performance than electrode configurations that have electrodes only located on the bottom of the flow channel. A large improvement in sorter performance (+80%) has been realised by replacing the classical line electrode with plane electrodes.

For channels with an almost equal width and height applying curved electrodes results in a significant performance gain (+50%). However, for channels having a much larger width than height, straight electrodes should perform almost as well, since the flow profile in the horizontal plane is almost flat for sorters having a large aspect ratio.

Two new electrode topologies have been presented, the 'switching electrode topology' and the 'focusing electrode topology', optimised for a general increase in flow-rate or to maximise switching speed, respectively. By increasing the number of channel outlets the performance can be further increased significantly. This has been experimentally verified for a topology with three outlets, which showed a performance increase of 80%. The experiments show a very high accuracy in the particle placement, which indicates that the performance can be further enhanced by increasing the number of outlets, without sacrificing sorter accuracy.

The optimised sorter designs developed in this chapter show a performance gain of more than 200% compared to the line electrodes found in literature, with the potential for a further increase. Simulations on the thermal behaviour predict an increase in temperature rise for the high speed sorters.

6.14. References

- [1] K. Tashiro, S. Ikeda, T. Sekiguchi, S. Shoji, H. Makazu, T. Funatsu, and S. Tsukita, "A particles and biomolecules sorting micro flow system using thermal gelation of methyl cellulose solution," presented at MicroTAS, Monterey, California, USA, 2001.
- [2] T. Schulz, S. Poser, E. Ermantraut, J. McCaskill, H. Mathis, and J. M. Köhler, "Miniaturized electrocaloric flow controller for analyte multiplexing and cell/particle sorting," presented at MicroTAS, Banff, Alberta, Canada, 1998.
- [3] N. Chronis, W. Lam, and L. Lee, "A microfabricated bio-magnetic separator based on continuous hydrodynamic parallel flow," presented at MicroTAS, Monterey, California, USA, 2001.
- [4] P. Telleman, U. D. Larsen, J. Philip, G. Blankenstein, and A. Wolff, "Cell sorting in microfluidic systems," presented at MicroTAS, Banff, Alberta, Canada, 1998.
- [5] A. Fu, C. Spence, A. Scherer, F. Arnold, and S. Quake, "A microfabricated fluorescence-activated cell sorter," *Nat. Biotechnol.*, vol. 17, pp. 1109-1111, 1999.
- [6] G. Blankenstein and U. D. Larsen, "Modular concept of a laboratory on a chip for chemical and biochemical analysis," *Biosensors & Bioelectronics*, vol. 13, pp. 427-438, 1998.
- [7] A. Fu, C. Spence, A. Scherer, F. Arnold, and S. Quake, "A microfabricated fluorescence-activated cell sorter," *Nat. Biotechnol.*, vol. 17, pp. 1109-1111, 1999.
- [8] A. Tripathi, J. Wolk, R. Sandberg, A. Chow, M. Kerby, R. L. Chien, and G. Wada, "Development of an on-chip cell sorting system designed for cloning mammalian cells with functional, heterologously expressed surface receptors," presented at MicroTAS 2001, Monterey, California, USA, 2001.
- [9] J. Krüger, P. Porta, A. Morrison, K. Singh, A. O'Neill, and P. O'Brien, "Micro-optical laser induced fluorescence detection on a miniaturised flow cytometry device," presented at MicroTAS, Nara, Japan, 2002.
- [10] J. Wolk, A. Tripathi, R. Sandberg, Y. Suo, and G. Wada, "A Labchip® cell sorting and deposition system based on a rapid functional response to stimulation of purinoceptors," presented at MicroTAS, Nara, Japan, 2002.
- [11] M. Washizu, S. Suzuki, O. Kurosawa, T. Nishizaka, and T. Shinohara, "Molecular dielectrophoresis of biopolymers," *IEEE Transactions on Industry Applications*, vol. 30, pp. 835-843, 1994.
- [12] H. Morgan, M. P. Hughes, and N. G. Green, "Separation of Submicron Bioparticles by Dielectrophoresis," *Biophysical Journal*, vol. 77, pp. 516-525, 1999.
- [13] F. Fernandez-Morales, J. Samitier, O. Ruiz, J. Bausells, and E. Abdelhamid, "Design and simulation of didelectrophoretic-based microsystem for bioparticle handling," presented at 1st Annual International IEEE-EMBS Special Topic conference on Microtechnologies in Medicine & Biology, Lyon, France, 2000.
- [14] L. Cui, D. Holmes, and H. Morgan, "The dielectrophoretic levitation and separation of latex beads in microchips," *Electrophoresis*, vol. 22, pp. 3893-3901, 2001.
- [15] H. Li and R. Bashir, "Dielectrophoretic separation and manipulation of live and heat-treated cells of *Listeria* on microfabricated devices with interdigitated electrodes," *Sensors and Actuators B*, vol. 86, pp. 215-221, 2002.
- [16] J. Voldman, M. L. Gray, M. Toner, and M. A. Schmidt, "A Microfabrication-Based Dynamic Array Cytometer," *Anal. Chem.*, vol. 74, pp. 3984-3990, 2002.
- [17] S. Fiedler, S. Shirley, T. Schnelle, and G. Fuhr, "Dielectrophoretic sorting of particles and cells in a microsystem," *Anal. Chem.*, vol. 70, pp. 1909-1915, 1998.

-
- [18] T. Schnelle, T. Müller, G. Gradl, S. G. Shirley, and G. Fuhr, "Paired microelectrode system: dielectrophoretic particle sorting and force calibration," *Journal of Electrostatics*, vol. 47, pp. 121-132, 1999.
- [19] M. Dürr, T. Schnelle, T. Müller, and M. Stezle, "Dielectrophoretic separation and accumulation of (bio)particles in micro-fabricated continuous flow systems," presented at MicroTAS, Monterey, California, USA, 2001.
- [20] S. Gawad, P. Batard, U. Seger, S. Metz, and P. Renaud, "Leukocytes discrimination by impedance spectroscopy flow cytometry," presented at MicroTAS, Nara, Japan, 2002.
- [21] T. Hara, T. Ichiki, Y. Horiike, and K. Yasuda, "Fabrication of on-chip sorter devices with sub-micrometer scale channels and self-aligned microelectrodes," presented at MicroTAS 2002, Nara, Japan, 2002.
- [22] D. Holmes, N. G. Green, and H. Morgan, "Microdevices for Dielectrophoretic Flow-Through Cell Separation," *IEEE Engineering in Medicine and Biology Magazine*, vol. 22, pp. 85-90, 2003.
- [23] K. Hirano and Y. Baba, "Optical recovery of particles on a chip toward cell sorting and bead-bed detection," presented at MicroTAS, Nara, Japan, 2002.
- [24] T. B. Jones, *Electromechanics of Particles*. Cambridge: Cambridge University Press, 1995.
- [25] T. Schnelle, T. Müller, A. Voigt, K. Reimer, B. Wagner, and G. Fuhr, "Adhesion-Inhibited Surfaces. Coated and Uncoated Interdigitated Electrode Arrays in the Micrometer and Submicrometer Range," *Langmuir*, vol. 12, pp. 801-809, 1996.
- [26] A. Ramos, H. Morgan, N. G. Green, and A. Castellanos, "Ac electrokinetics: a review of forces in microelectrode structures," *J. Phys. D: Appl. Phys.*, vol. 31, pp. 2338-2353, 1998.
- [27] N. G. Green, A. Ramos, and H. Morgan, "Ac electrokinetics: a survey of sub-micrometre particle dynamics," *J. Phys. D: Appl. Phys.*, vol. 33, pp. 632-641, 2000.
- [28] T. Müller, A. Pfennig, P. Klein, G. Gradl, M. Jäger, and T. Schnelle, "The Potential of Dielectrophoresis for Single-Cell Experiments," *IEEE Engineering in Medicine and Biology Magazine*, vol. 22, pp. 51-61, 2003.

Chapter 7

Outlook

7.1. Introduction

In the previous chapters several microsystems have been presented for particle analysis. These microsystems were developed to a level that the operation principle could be univocally demonstrated and at which the measurement results could be explained by theory and/or modelling. Towards commercial application further characterisation is needed with a range of well defined samples. The results obtained up till now show great potential to enhance the performance of the currently available instrumentation.

The microsystems were developed as general instruments, not tailored to any specific application. Therefore, there are many ways in which these microsystems can be further developed. In this chapter some of the most promising ideas for future research are briefly discussed.

7.2. Flow cell

It would be interesting to find out how small a sample flow can be generated. With the current flow cell, that has a width of 160 μm , sample flows with dimension smaller than 10 μm could be easily achieved. This suggests that based on a smaller channel the formation of a sub-micron sample flow could be feasible. For such a small sample flow the effect of diffusion is more severe, because the relative broadening of the sample flow matters. When the narrow dimensions of the sample stream are achieved by stronger hydrodynamic focusing it will cause the flow-speed to go up. This partially counteracts the higher sensitivity to diffusion, because it reduces the diffusion time.

The main challenge will probably be to keep the sheath flow smooth and stable at high speeds. Using multiple focusing stages in series to reduce the dimensions of the sample flow (see Figure 7-1) might be a way to accomplish this. Such a very small sample flow could be applied in a Coulter counter for the measurement of sub-micron particles.

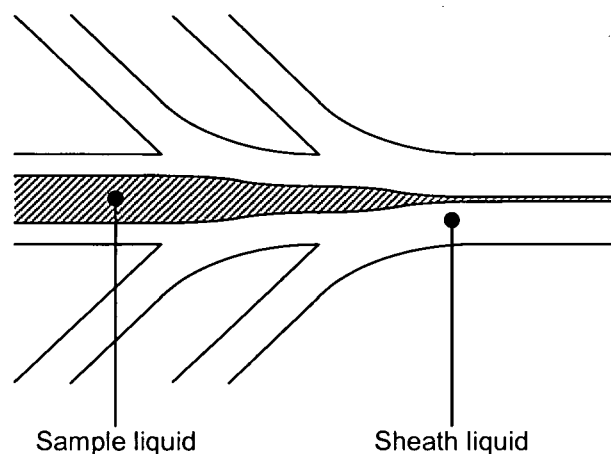


Figure 7-1. Two focusing stages in series to form a very narrow sample flow.

7.3. Coulter counter

It could be very useful to measure the impedance at several frequencies simultaneously instead of measuring the Coulter impedance at a single frequency. In [1] a simulation is presented that demonstrates that it should be possible to extract three important cell parameters, using impedance measurements at different frequencies. With properly

dimensioned electrodes measurements between 10 and 100 kHz relate to cell size, a frequency at around 1 MHz gives a value for the cell membrane capacitance and above 10 MHz the change in impedance is related to the cytoplasmic higher resistivity. When a Coulter counter is developed that measures impedance at these three frequencies simultaneously, it would be possible to discriminate between cells of comparable size that differ only in some of the other electrical properties. The developments that are required to realise this are mainly in the development of sophisticated read-out electronics.

7.4. Integrated projection cytometer

The integrated projection cytometer is a highly integrated system, but still an external light source is used. For application in a handheld device it could be helpful if the light-source could also be integrated. However, the material properties of silicon are not favourable to fabricate a light-source that emits in the visible range. Furthermore, the light-source should ideally be located on the top of the channel, on the glass-side of the device. Therefore, the easiest solution would be to put a very small light-source on top of the channel. Vertical Cavity Surface Emitting Lasers (VCSELs) seem to be an attractive option, because these lasers are very small and they emit light perpendicular to their surface. Gluing a VCSEL on top of the cytometer device and connecting it to the bond-pads on the silicon substrate would be a very fast way to explore the possibilities.

7.5. Particle sorter

The particle sorters have so far been fabricated on separate chips. It would be very interesting to integrate the particle sorters on a single device with one or more microsystems for particle analysis. Such a device can be used to actively sort out rare particles based on the readings of the sensors for applications such as sample enrichment. Since the fabrication process of the particle sorters is fully compatible with the fabrication process of the other microsystems, making such a device should be no problem. The real challenge is to develop signal processing that is fast enough for real-time processing of the sensor data to activate the sorter in time. With a dedicated DSP this should be feasible.

7.6. Low-cost version

The microsystems described in this thesis were developed in glass-silicon technology, which proved to be an ideal basis for prototyping. However, to make a commercial product the silicon-glass technology is likely to be too expensive, especially when such large devices ($1.5 \times 2 \text{ cm}^2$) are made. Of course the chips could be made substantially smaller, but still the chips would be relatively expensive. The trend is towards disposable devices because contamination can be a serious problem, especially when dealing with biological samples.

The plastics technologies briefly mentioned in chapter 2 could very well be used to reduce the costs. The flow cell, the Coulter counter and the particle sorters can be realised in plastics technology without many problems, since these microsystems only require channels, through holes and electrodes. The optical sensor cannot be easily integrated in such technology and is by far the most complicated component to fabricate; therefore it would be good if this component could be re-used, while the other parts are disposable.

Based on the above consideration a low-cost instrument that combines the microsystems could look like the chip depicted in Figure 7-2. All components except for the optical system could be realised in a cheap disposable plastic device. The optical sensor could be located in the holder, where it fits into a recess at the bottom of the chip. By placing the optical sensor

underneath an optically transparent membrane, it is placed very close to, but not inside the microchannel. Therefore, the relatively expensive optical system could be used many times, since it would not come into contact with any of the liquids. The other parts do get in contact with the liquids and can be easily replaced, since they are fabricated on a cheap substrate.

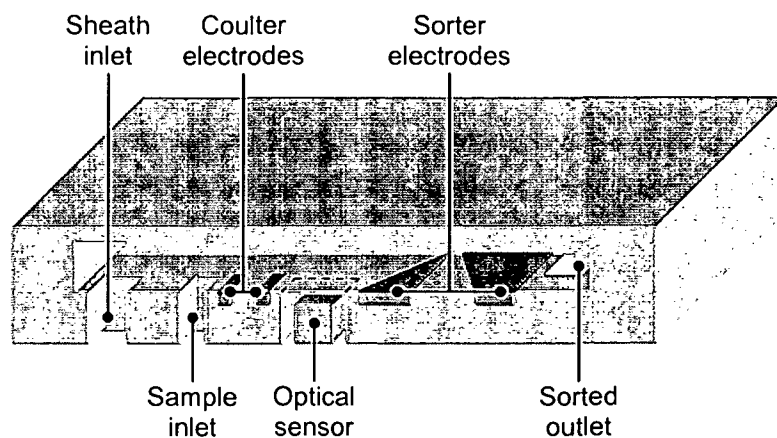


Figure 7-2. Cross-section on what a low-cost instrument could look that includes the functionality of all microsystems.

Instead of using a moulded cavity to form a thin transparent window on the bottom of the flow channel it is also possible to use a thin slide of transparent plastic to form the bottom half of the device. For very small particles, however, it will still be required to integrate the optical sensors into the channel wall, since the allowed projection distance decreases with particle size.

7.7. References

- [1] S. Gawad, L. Schild, and P. Renaud, "Micromachined impedance spectroscopy flow cytometer for cell analysis and particle sizing," *Lab on a Chip*, vol. 1, pp. 76-82, 2001.

Acknowledgements

A PhD thesis is often contributed to a single person, but it requires the support of many people. I would like to express my gratitude to everybody who has contributed, directly or indirectly, to this thesis.

I thank my supervisor Michiel Vellekoop for inspiring me to start a PhD and for the fruitful relationship we had over the past years. I appreciate the freedom he gave me to explore, while he was always available for feedback and advice.

I would like to thank my colleagues at the group for Industrial Sensor Systems for the pleasant working atmosphere and the way they made me feel at home, away from home. In particular I would like to thank to my room-mates Jochen Kuntner and Daniel Rocha for their friendship and for the great time we had at the office and outside of the office. Other persons that I would like to mention are Franz Kohl for his advice and help during the measurements and Artur Jachimowicz and Peter Svasek for the fabrication of the chips that were made in Vienna.

I am grateful to the members of the Delft Institute for Microelectronics and Submicron-technology at the Delft University of Technology for making me feel so welcome on my visits to Delft. In particular Andre Bossche and Peter Turmezei for the cooperation during the project, Lina Sarro for her technological advice and her help in coordinating the fabrication the chips at the DIMES and Jeroen Bastemeijer for designing the chip holder and all his other help.

Many of the chips presented in this thesis were fabricated in the DIMES clean room of the Delft University of Technology with funding from the Technologiestichting STW (project DPC.5521), which is greatly acknowledged for the financial support.

Finally, but foremost, I would like to thank my family for their understanding and for their support during the last couple of years.

Publications

1. J. H. Nieuwenhuis, G. W. Lubking, A. Berthold, P. M. Sarro, and M. J. Vellekoop, "Integrated Shape Sensor for Particles and Cells based on Optical Projection," presented at Eurosensors XIV, Copenhagen, Denmark, 2000.
2. J. H. Nieuwenhuis, S. S. Lee, J. Bastemeijer, and M. J. Vellekoop, "Particle-shape Sensing-elements for Integrated Cytometer," presented at MicroTAS 2001, Monterey, California, USA, 2001.
3. J. H. Nieuwenhuis, J. Bastemeijer, A. Bossche, and M. J. Vellekoop, "Dynamic Particle-Shape Measurements Using a Near-Field Optical Sensor," presented at IEEE Sensors Conference, Orlando, Florida, USA, 2002.
4. J. H. Nieuwenhuis, J. Bastemeijer, P. M. Sarro, and M. J. Vellekoop, "Integrated Coulter Counter with Non-coaxial Sheath-flow and Dynamic Aperture Control," presented at Eurosensors XVI, Prague, Czech Republic, 2002.
5. J. H. Nieuwenhuis, J. Bastemeijer, P. M. Sarro, and M. J. Vellekoop, "Virtual Flow Channel: A Novel Micro-fluidics System with Orthogonal, Dynamic Control of Sample Flow Dimensions," presented at MicroTAS 2002, Nara, Japan, 2002.
6. J. H. Nieuwenhuis and M. J. Vellekoop, "FEM study of Coulter Counter with Water-Based Adaptable Aperture," presented at MicroTAS 2002, Nara, Japan, 2002.
7. J. H. Nieuwenhuis, J. Bastemeijer, A. Bossche, and M. J. Vellekoop, "Near-Field Optical Particle-Shape Sensors for Application in an Integrated Cytometer," *IEEE Sensors Journal*, vol. 3, pp. 646-651, 2003.
8. J. H. Nieuwenhuis, J. Bastemeijer, P. M. Sarro, and M. J. Vellekoop, "First Measurement Results with an Integrated Projection Cytometer," presented at MicroTAS 2003, Squaw Valley, California, USA, 2003.
9. J. H. Nieuwenhuis, J. Bastemeijer, P. M. Sarro, and M. J. Vellekoop, "Integrated Flow-Cells for Novel Adjustable Sheath Flows," *Lab on a Chip*, vol. 3, pp. 56-61, 2003.
10. J. H. Nieuwenhuis, F. Kohl, J. Bastemeijer, and M. J. Vellekoop, "First Particle Measurements With An Integrated Coulter Counter Based On 2-Dimensional Aperture Control," presented at Transducers '03, Boston, Massachusetts, USA, 2003.
11. J. H. Nieuwenhuis and M. J. Vellekoop, "Performance Comparison of Dielectrophoretic Particle Sorters based on a Novel Analysis Method," presented at Eurosensors XVII, Guimarães, Portugal, 2003.

12. J. H. Nieuwenhuis and M. J. Vellekoop, "Improved Dielectrophoretic Particle Actuators For Microfluidics," presented at IEEE Sensors Conference, Toronto, Canada, 2003.
13. S. Kostner, J. H. Nieuwenhuis, P. Svasek, A. Jachimowicz, and M. J. Vellekoop, "Continuous Particle Separator Based on Periodical DEP Elements," presented at MicroTAS 2004, Malmö, Sweden, 2004.
14. J. H. Nieuwenhuis, A. Jachimowicz, P. Svasek, and M. J. Vellekoop, "High-Speed Integrated Particle Sorters based on Dielectrophoresis," presented at IEEE Sensors Conference, Vienna, Austria, 2004.
15. J. H. Nieuwenhuis, F. Kohl, J. Bastemeijer, P. M. Sarro, and M. J. Vellekoop, "Integrated Coulter Counter based on 2-Dimensional Liquid Aperture Control," *Sensors and Actuators B*, vol. 102, pp. 44-50, 2004.
16. J. H. Nieuwenhuis, P. Svasek, P. M. Sarro, and M. J. Vellekoop, "Particle Size Discrimination with a Liquid Aperture Coulter Counter," presented at Eurosensors XVII, Rome, Italy, 2004.
17. J. H. Nieuwenhuis, P. Svasek, P. M. Sarro, and M. J. Vellekoop, "Particle Discrimination with an Improved Projection Cytometer," presented at MicroTAS 2004, Malmö, Sweden, 2004.
18. J. H. Nieuwenhuis and M. J. Vellekoop, "Simulation Study of Dielectrophoretic Particle Sorters," *Sensors and Actuators B*, vol. 103, pp. 331-338, 2004.
19. J. H. Nieuwenhuis, A. Jachimowicz, P. Svasek, and M. J. Vellekoop, "Optimisation of Microfluidic Particle Sorters based on Dielectrophoresis," *IEEE Sensors Journal*, pp. in press, 2005.

About the author

Jeroen Nieuwenhuis was born in Bergen op Zoom, the Netherlands in 1977. In 2000 he received the M.S. degree in electrical engineering (cum laude) from the Delft University of Technology, the Netherlands, for his thesis on the development of an integrated particle shape sensor.

After finishing his studies he spent seven months at IC-Sensors, Milpitas, California USA, where he worked at the Research and Development department. During this period he mainly worked on solid-state accelerometers and pressure sensors.

He started working towards a Ph.D. degree in electrical engineering in January 2001 at the Delft University of Technology and in September 2001 he moved to Austria where he continued his studies at the Vienna University of Technology. His research has been focused on the development of integrated microsystems for particle analysis, which is described in this thesis.

In 2004 he staid four months at the Bosch Research and Technology Center North America, Pittsburgh, PA USA. In close cooperation with the Carnegie-Mellon University he worked on the development of a new micro-acoustic sensor, where his main contribution was in the modelling of the sensor.